ESD-TR-65-3

A PHYSICAL MODEL FOR THE PREDICTION OF LARGE-SCALE LOW CLOUDINESS

Joseph P. Gerrity, Jr.

February 1965

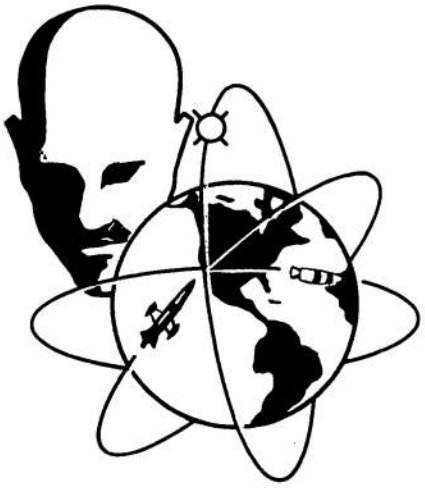

433L SYSTEMS PROGRAM OFFICE
ELECTRONICS SYSTEMS DIVISION
AIR FORCE SYSTEMS COMMAND
UNITED STATES AIR FORCE
L. G. Hanscom Field, Bedford, Mass.

Qualified users may obtain copies of this report from the Defense Documentation Center.

When U. S. Government drawings, specifications, or other data are used for any purpose other than a definitely related Government procurement operation, the Government thereby incurs no responsibility nor any obligation whatsoever, and the fact that the Government may have formulated, furnished, or in any way supplied the said drawings, specifications, or other data, is not to be regarded by implication or therwise, or in any manner licensing the holder or any other person or corporation, or conveying any rights or permission to manufacture, use, or sell any patented invention that may in any way be related thereto.

ERRATA

ESD-TR-65-3

A PHYSICAL MODEL FOR THE PREDICTION OF LARGE-SCALE LOW CLOUDINESS

February 1965
7463-150

433L Systems Program Office
Electronics Systems Division
Air Force Systems Command
United States Air Force
L. G. Hanscom Field, Bedford, Mass.

Joseph P. Gerrity, Jr.
The Travelers Research Center, Inc.
250 Constitution Plaza
Hartford, Conn. 06103

Location	Error	Correction
P. 8, Equation	$w = -\int_h^z \left(\frac{\partial u}{\partial x} \quad \frac{\partial v}{\partial y} \right) dz$	$w = -\int_h^z \left(\frac{\partial u}{\partial x} + \frac{\partial v}{\partial y} \right) dz$ [add plus sign]
P. 10 Equation (III-17)	$\frac{\kappa T}{p} \frac{dp}{dt} + \frac{\partial}{\partial z}\left[K_H \frac{\partial T}{\partial z} + \frac{g}{c_p} \right] + \cdots$	$\frac{\kappa T}{p} \frac{dp}{dt} + \frac{\partial}{\partial z}\left[K_H \left(\frac{\partial T}{\partial z} + \frac{g}{c_p} \right) \right] + \cdots$ [add parentheses]
P. 11 Equation (III-19)	$\cdots + \frac{\partial}{\partial z}\left[K_H \frac{\partial T}{\partial z} + \frac{g}{c_p} \right] + \cdots$	$\cdots + \frac{\partial}{\partial z}\left[K_H \left(\frac{\partial T}{\partial z} + \frac{g}{c_p} \right) \right] + \cdots$ [add parentheses]
P. 45, Figure 2 Title	... roughness coefficient (m).	... roughness coefficient (cm).
P. 51, Figure 5 Title	...; Experiment no. 2 forecast; ...	...; Experiment no. 2 (complete model) forecast; ...
P. 54, 2nd full ¶, 5th line	maximum shading in Figure 10.	maximum shading in Figure 8.
P. 55, Figure 8 Title	...; Experiment no. 2 forecast;	...; Experiment no. 2 (complete model) forecast; ...
P. 55, Figure 8 Legend	RH ≥ 100%; RH ≥ 93%; RH ≥ 77%; RH < 77%	RH < 77%; 77% ≤ RH < 93%; 93% ≤ RH < 100%; RH ≥ 100%
P. 59, Figure 10 Title	...; Experiment no. 5 Forecast; ...	...; Experiment no. 5 ($\hat{w} = 0$) forecast; ...

Location	Error	Correction
P. 59, Figure 10, Legend	RH $\geq$ 100%; RH $\geq$ 93%; RH $\geq$ 77%; RH < 77%	RH < 77%; 77% $\leq$ RH < 93%; 93% $\leq$ RH < 100%; RH $\geq$ 100%
P. 68, last ¶, 1st line	Figures 8, 9, and 11 display ...	Figures 8, 9, and 10 display ...
P. 72, Figure 11, Title	...; Experiment no. 5 forecast; ...	...; Experiment no. 5 ($\hat{w} = 0$) forecast; ...
P. 75, Table XVI, Title	DISTRIBUTION OF (cm sec^{-1}) ...	DISTRIBUTION OF w (cm sec^{-1}) ...
P. 76, Figure 12, Title	...; Experiment no. 7 forecast; ...	...; Experiment no. 7 (K = constant) forecast; ...

ESD-TR-65-3

A PHYSICAL MODEL FOR THE PREDICTION OF LARGE-SCALE LOW CLOUDINESS

Joseph P. Gerrity, Jr.

February 1965

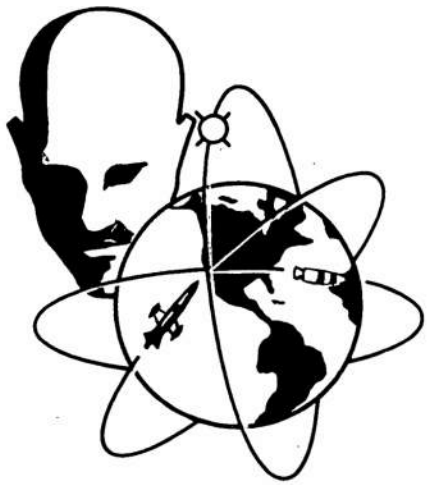

433L SYSTEMS PROGRAM OFFICE
ELECTRONICS SYSTEMS DIVISION
AIR FORCE SYSTEMS COMMAND
UNITED STATES AIR FORCE
L. G. Hanscom Field, Bedford, Mass.

FOREWORD

System 433L; project 1.0; task 1.2. This TR has been prepared for United Aircraft Corporation, East Hartford, Conn., under Subcontract no. 15107 to Contract no. AF 19(628)-3437, by The Travelers Research Center, Inc. The Research Center's publication number is 7463-150. Robert L. Houghten, Lt. Colonel, USAF, is Acting System Program Director. Submitted for approval on 2 January, 1965.

ABSTRACT

This paper is a report on a continuing effort to develop a physical-numerical model suitable for use in predicting large-scale fields of low cloudiness.

The need to incorporate, within such a model, those physical processes which are characteristic of the atmospheric boundary layer has been noted in several recent studies. That the inclusion of such processes be effected without imposing a requirement for non-standard, observational data has been adopted as a restriction in the design of the prediction model. A further design specification is that the model will be used in conjunction with a fine-mesh, free-air prediction model. This specification relieves us from the need to consider the prediction of dynamical developments within the bulk of the atmosphere.

Included in this paper are a derivation of a basic prediction model and the results of a test series of 12-hr forecasts made with various versions of the model using synoptic data for the period: 12Z, 6 Feb.—00Z, 7 Feb. 1964. The tests were designed to assess the characteristics of the model and to indicate areas in which more study is required.

The model tested differs broadly from previous boundary layer models in its use of all three space dimensions, a horizontal space mesh of 150 km, and a time step of 15 min. The model incorporates the computation of: eddy fluxes of heat and vapor, the transport of heat, vapor, etc. by ageostrophic horizontal winds, the influence of terrain- and friction-induced vertical motion, and the heat and mass exchanges involved in water-substance phase changes.

REVIEW AND APPROVAL

Publication of this technical documentary report does not constitute Air Force approval of the report's findings or conclusions. It is published only for the exchange and stimulation of ideas.

Robert L. Houghten
Lt. Colonel, USAF
Acting System Program Director

TABLE OF CONTENTS

Section	Title	Page
I	INTRODUCTION	1
II	PREVIOUS WORK	2
1.	Cloud Prediction Technique	2
2.	Boundary-layer Models	3
3.	Approach Used in Modeling	3
III	TRANSITION-LAYER PREDICTION EQUATIONS	5
4.	Introduction	5
5.	Wind Specification	6
6.	The Specification of Mixing Coefficients	8
7.	The Heat Transfer Equation	10
8.	Water Substance Prediction	11
9.	Computation of Water Phase Changes and Diabatic Heating	12
10.	Cloud Specification	17
11.	Radiative-heat Flux and Precipitation	18
IV	THE CONTACT-LAYER EQUATIONS	20
12.	Introduction	20
13.	The Contact-layer Hypotheses	21
14.	The Empirical Formulas	25
15.	Eddy Flux Evaluation	27
16.	Formulas for the Horizontal Wind Components and Mixing Coefficients	31
17.	Contact-layer Boundary Conditions	33
V	COMPUTATIONAL FORMULATION OF MODEL	35
18.	The Difference Equations	36
19.	Analysis of Computational Stability	37
20.	Specification of Boundary Conditions	40
VI	EXPERIMENTAL BACKGROUND	41
21.	Preliminary Experiments	41

Section	Title	Page
22.	The Analysis of Initial-temperature and Humidity Data	41
23.	The Analysis of the Geostrophic Wind	42
24.	Terrain Height and Surface Roughness	43
VII	EXPERIMENTAL RESULTS	46
25.	The Synoptic Case and the Experiments Conducted	46
26.	The Basic Experiment and its Verification	49
27.	Influence of the Time Step Used	64
28.	Influence of the Roughness-coefficient Variation	68
29.	Influence of the Terrain-induced Vertical Velocity	
30.	Influence of the Variation in the Mixing Coefficient	74
31.	Influence of Lateral-boundary Conditions	74
APPENDICES		
I	COORDINATE SYSTEM	83
II	UPWIND ADVECTION APPROXIMATION	89
III	THE DIFFERENCE APPROXIMATION FOR THE HEAT-DIFFUSION EQUATION	91
IV	THE DIFFERENCE APPROXIMATION FOR THE VAPOR-DIFFUSION EQUATION	93
V	DIFFERENCE APPROXIMATION TO THE MOISTURE DIFFUSION EQUATION	95
VI	DEFINITION OF COEFFICIENTS IN EQUATION V-3	97
REFERENCES		99

LIST OF ILLUSTRATIONS

Figure	Title	Page
1	Distribution of terrain height (m)	44
2	Distribution of surface-roughness coefficient (cm)	45
3	Synoptic chart; 1200Z, 6 Feb. 1964	47
4	Synoptic chart; 0000Z, 7 Feb. 1964	48
5	Constant level analysis (z = 1500 m); Ex. No. 2 Forecast; 0000Z, 7 Feb. 1964	51
6	Constant level analysis (z = 1500 m); 1200Z, 6 Feb. 1964	52
7	Constant level analysis (z = 1500 m); 0000Z, 7 Feb. 1964	53
8	Vertical cross section (M = 6); Ex. No. 2 Forecast; 0000Z, 7 Feb. 1964	55
9	Vertical cross section (M = 6); observed; 0000Z, 7 Feb. 1964	56
10	Constant level analysis (z = 1500 m); Ex. No. 5 Forecast; 0000Z, 7 Feb. 1964	59
11	Vertical cross section (M = 6); Ex. No. 5 Forecast; 0000Z, 7 Feb. 1964	72
12	Constant level analysis (z = 1500 m); Ex. No. 7 Forecast; 0000Z, 7 Feb. 1964	76

LIST OF TABLES

Table	Title	Page
I	Richardson's number	30
II	Synopsis of experiments conducted	50
III	Distribution of w(cm sec^{-1}) from experiment no. 2 (frictionally induced) at z = 1000m above msl	57
IV	Distribution of $\hat{w}$ (cm sec^{-1}) from experiment no. 2 (terrain induced) at z = 1000m above msl	58
V	Distribution of error (observed less forecast) in temperature predicted in experiment no. 2 over the 100 grid points at three levels in the vertical (measured above local terrain), and observed temperature changes (persistence)	60
VI	Experiment no. 2 temperature error (observed less forecast) at z = 500m in °C	61
VII	Experiment no. 2 temperature error (observed less forecast) at z = 1150m in °C	62
VIII	Experiment no. 2 temperature error (observed less forecast) at z = 1550m in °C	63
IX	Observed temperature change at z = 500m in °C	65
X	Observed temperature change at z = 1150m in °C	66
XI	Observed temperature change at z = 1550m in °C	67
XII	Distribution of w(cm sec^{-1}) from experiment no. 4 at z = 1000m above msl	69
XIII	Friction velocity (cm sec^{-1}) computed for 00Z, 7 Feb. 1964 by experiment no. 2 (lower values) and experiment no. 4 (upper values)	70
XIV	Heat flux (millical cm^{-2} min^{-1}, where positive value indicates downward heat transport) computed for 00Z, 7 Feb. 1964 in experiment no. 2 (lower values) and experiment no. 4 (upper values)	71
XV	Grid point values (°C) of vertically averaged absolute value of of the difference in temperature predicted in experiment no. 2 and experiment no. 5	73
XVI	Distribution of w(cm sec^{-1}) from experiment no. 7 (frictionally induced) at z = 1000m above msl	75
XVII	Grid point values (°C) of vertically averaged absolute value of the difference in temperature predicted in experiment no. 2 and experiment no. 7	77

Table	Title	Page
XVIII	Grid point values (°C) of vertically averaged absolute value of the difference in temperature predicted in experiment no. 2 and experiment no. 6	78
XIX	Grid point values (°C) of vertically averaged absolute value of the difference in temperature predicted in experiment no. 2 and experiment no. 8	79
XX	Grid point values (°C) of vertically averaged absolute value of the difference in temperature predicted in experiment no. 2 and experiment no. 9	80

I

INTRODUCTION

This report documents the status of our effort to develop a physical model which is to be used in the prediction of large-scale fields of low cloudiness. A previous report [1] points out the apparent significance of those physical processes associated with the structure of the atmospheric boundary layer for low-cloud prediction. Our initial assessment of the feasibility of incorporating these processes in a physical-prediction model has been discussed previously [17]. This paper reports on the base-prediction model which has been developed and presents the results of a series of tests of this model made with data from one synoptic situation.

It should be differentiated from the sub-synoptic scale boundary-layer models discussed in subsection 2. The model presented here has been designed to be used in conjunction with a free-air prediction model developed by Air Weather Service,[1] and for use with routine meteorological observations. Our model is still in the formative stage and further modification and testing are planned during the coming year. The experimental results reported here are incompletely documented because they are intended to indicate only the general characteristics of the model and areas in which further work is needed.

---

[1] We refer to the fine-mesh model under development by Maj. J. Howcroft, 1210th Weather Squadron, Suitland, Md.

II

PREVIOUS WORK

1. Cloud Prediction Techniques

Other tasks involved in cloud prediction or specification under Project 1 of the 433L Meteorological Technique Program have employed an empirical approach to the problem of low-cloud prediction. Numerical-analysis techniques, based on synoptic reasoning, have been used to relate the occurrence, amount, and height of cloudiness to a large number of meteorological quantities. A relatively recent summary of this work has been reported by Cooley, et al. [6].

Another approach to the problem is based on the numerical integration of simplified conservation equations for atmospheric humidity variables. This approach makes use of air trajectories computed from the wind components which are forecasted by large-scale, free-atmosphere, dynamical models [1, 22, 24].

Yet another approach is that spelled out by Smagorinsky [37] in which an internally consistent, free air, dynamical prediction model which includes the condensation process is employed to predict the entire behavior of a model atmosphere. This approach was initiated by Smagorinsky and Collins [38] some ten years ago. The methods discussed above have been developed largely because it did not prove profitable to employ the full dynamical approach in routine forecasting operations.

All three techniques discussed above have a common weakness — their use of data at only the standard pressure levels. It can be seen from even a cursory examination of atmospheric soundings that such data are insufficient to describe the distribution of humidity in the atmosphere. Further, the use in these techniques of geostrophic or balanced wind fields to compute the low level transport of atmospheric humidity cannot be regarded as sound. These factors, together with the neglect of other boundary-layer processes, may in part explain the relative lack of success of these techniques in the prediction of low cloudiness.

2. Boundary-layer Models

Fisher [14] and Estoque [12], in continuation of some initial work by Pearce [31], approached the problem of numerical prediction of the local, sea-breeze circulation. Their treatment of this phenomenon led naturally to rudimentary modeling of certain boundary layer processes. Subsequently, they embarked on studies [13, 15] of boundary-layer processes without the complication of local circulations in the wind field.

More recently, Pandolfo [30, 31] has undertaken the formulation of a boundary-layer prediction model for use in predicting short-period changes in cloudiness, visibility, and wind velocity. His model is intended for use with data from specially designed observation networks.

In the work of Estoque, Fisher, and Pandolfo, it has been assumed that the boundary-layer processes are confined to the region within some two kilometers of the ground. The dependence of the boundary-layer phenomena upon developments in the free air above that level is accounted for by ascribing the task of providing upper-boundary conditions for the boundary-layer model to an independent, free-air prediction model.

Additionally, Estoque and Pandolfo employ the hypothesis that through a shallow layer in proximity with the ground, the eddy fluxes of momentum, heat, and vapor are constant with respect to height. This constant-flux hypothesis is discussed in the book by Lumley and Panofsky [25].

3. Approach Used in Modeling

The low-cloud forecasting problem being studied in this work involves regarding clouds as susceptible to adequate specification if the humidity and temperature fields are provided on a horizontal grid-point network with characteristic spacing of 150 km. This horizontal-length scale and the characteristic, forecast-time interval of one-half day differentiate our formulation of the problem from that undertaken in the work discussed in Subsection 2. We do model the vertical structure of the lower atmosphere in the fashion of Estoque and Pandolfo.

This is done to permit adequate vertical resolution for the computation of the boundary-layer process of eddy diffusion. Such emphasis on boundary-layer processes has not been given in the other techniques discussed in subsection 1.

Our model has been designed to require only routine observational data for its implementation. Because of this design requirement, we did not choose to attempt the integration of the time-dependent, horizontal-momentum equation. The horizontal-wind components are computed from the diagnostic equations, which result if one assumes an instantaneous adjustment of the wind to create a balance among the pressure gradient, Coriolis, and frictional forces.

Consequent upon this scheme for computing the wind field is our use of empirical relationships between the geostrophic wind and the friction velocity. Additionally, it was necessary to use simple formulations for the distribution of the mixing coefficient throughout the transition layer.[2]

The large-scale character of the model has also required our omission of the interface energy balance technique [13] for computing the surface temperature. We propose instead to employ an empirical approach to the specification of this boundary value.

---

[2]The boundary layer is divided into a layer of constant flux (contact layer) and a transition layer.

III

TRANSITION-LAYER PREDICTION EQUATIONS

4. Introduction

The coordinate system used for expressing the model's governing equations is a modification of the quasi-Cartesian system [19]. Because the pertinent physical boundary is the surface of the ground or ocean, and not a fictitious mean sea level we choose as the vertical coordinate a parameter, z, which takes on the value zero at the ground level. Thus, if ξ, with value zero at mean sea level, is the customary vertical coordinate of the quasi-Cartesian system and if $E(x, y)$ is a function giving the elevation of the ground above mean sea level at a point with horizontal coordinates, (x, y), then z is given in terms of ξ and E by

$$z = \xi - E(x, y). \tag{III-1}$$

A detailed derivation of the form of the various differential operators in the modified coordinate system is given in Appendix I (note the difference in the definition of E).

In accordance with the assumptions regarding the structure of the boundary layer outlined earlier, the top and bottom of the transition layer are the coordinate surfaces,

$$z = H\,(2\text{ km}) \text{ and } z = h\,(50\text{m}), \tag{III-2}$$

respectively. In the formulation of the prediction equations, we will call for the specification of boundary conditions on these coordinate surfaces. In the case of the upper surface, the boundary conditions will be taken as prescribed by means of predictions made with an independent, free air model. This is a temporary solution to the ultimate problem of designing an internally consistent, physical model for the entire troposphere. The required lower boundary conditions will be obtained through the use of the equations applicable to the contact layer.

Additional boundary conditions will be required on the open lateral boundaries of the region to which the model is applied. These conditions require specification of the horizontal advection of the various quantities into the region. This

information cannot be given in realistic applications of the model to synoptic data; thus, one is forced to provide some approximation for these quantities and to accept the inward propagation of error. The propagation speed of such errors will be the speed of the local wind, and the errors will not rapidly corrupt the forecasts in the interior of a sufficiently large region.

The wind velocity and mixing coefficients appear in the equations derived below. These quantities will be determined through a series of relations which are both theoretical and empirical. They will not be governed by simple prediction equations.

5. Wind Specification

The horizontal wind components, u and v, are taken to be the solutions of the following simplified equations of motion:

$$\frac{d^2u}{dz^2} = -\frac{f}{K}(v - v_g), \tag{III-3a}$$

$$\frac{d^2v}{dz^2} = \frac{f}{K}(u - u_g), \tag{III-3b}$$

where f is the coriolis parameter and K is the momentum mixing coefficient which is assumed to be independent of z. The geostrophic wind components, u_g and v_g, are assumed to be linear functions of height,

$$u_g = u_g^H - \frac{(H - z)}{H}(u_g^H - u_g^0), \tag{III-4a}$$

$$v_g = v_g^H - \frac{(H - z)}{H}(v_g^H - v_g^0), \tag{III-4b}$$

where u_g^H and v_g^H are the geostrophic wind components at z = H, and u_g^0 and v_g^0 are the geostrophic wind components at z = 0.

The solution of Eqs. III-3a and 3b is specified by requiring that

$$u \to u_g \quad \text{as} \quad z \to \infty, \tag{III-5a}$$

$$v \to v_g \quad \text{as} \quad z \to \infty, \tag{III-5b}$$

and that

$$u = U(x, y, t) = U \qquad \text{at} \qquad z = h, \tag{III-6a}$$

$$v = V(x, y, t) = V \qquad \text{at} \qquad z = h. \tag{III-6b}$$

One may verify that the appropriate solution to the given system is

$$u = u_g + e^{-\alpha(z - h)} \{(U - u_g^h) \cos [\alpha(z - h)] + (V - v_g^h) \sin [\alpha(z - h)]\} \tag{III-7a}$$

and

$$v = v_g + e^{-\alpha(z - h)} \{(V - v_g^h) \cos [\alpha(z - h)] - (U - u_g^h) \sin [\alpha(z - h)]\} \tag{III-7b}$$

where u_g^h and v_g^h are the values of u_g and v_g at $z = h$, and α is given by

$$\alpha = \left[\frac{f}{2K}\right]^{1/2} \tag{III-8}$$

The boundary conditions at $z = h$ are prescribed through the appropriate contact layer formulas given later. If one were to take u_g and v_g as constants, and $U = V = 0$ at $z = h = 0$, the solution would reduce to an Ekman spiral. The simple linear dependence of the geostrophic wind upon height allows the superposition of a thermal shear upon the spiral. The specification of boundary conditions, U and V, at $z = h$, imposes a more realistic shear between the ground and $z = h$ than would result from an Ekman spiral solution. This may be attributed to the marked variation of the mixing coefficient with height in the contact layer. The value of the mixing coefficient used in evaluating the wind components varies with horizontal position and time, in accordance with the formulas subsequently derived for the contact layer.

The vertical wind in the transition layer has been divided into two components in accordance with the structure of the coordinate system being employed (see Appendix I). A frictionally-induced component is obtained from mass continuity considerations if we neglect the individual change in particle density (a reasonable approximation [21]) in the continuity equation.

This wind component is assumed to vanish at $z = h$ and is, therefore, given

by the relation

$$w = -\int_{h}^{z} \left(\frac{\partial u}{\partial x} + \frac{\partial v}{\partial y} \right) dz , \qquad \text{(III-9)}$$

where u and v are the horizontal wind components derived earlier. Although the horizontal winds are distributed in a more complex fashion than that given by an Ekman spiral solution, one may still qualitatively associate upward currents with low pressure centers and downward flow with high pressure centers.

The second component of the vertical-wind velocity is related to the variation of the ground elevation from mean sea level. We define the terrain-induced velocity, $\hat{w}$, as,

$$\hat{w} = u\frac{\partial E}{\partial x} + v\frac{\partial E}{\partial y} , \qquad \text{(III-10)}$$

where u and v are functions of x, y, z, and t, which are given by Eqs. III-7a and 7b. This velocity will vary with height due to the height dependence of u and v. Because of the coordinate system being employed, this component of the wind will appear explicitly only in the thermodynamic energy equation, in which it is associated with adiabatic temperature changes.

6. The Specification of Mixing Coefficients

By definition, the transition layer is a region in which the direct influence of the ground on atmospheric properties gradually diminishes. This layer can be taken to be of fixed depth only with respect to certain scales of atmospheric phenomena. We regard the large-scale, vertical eddy exchange as being predominantly confined to a comparatively thin layer above the ground.

The influence of vertical eddy exchange may be expressed in a prediction equation through a term of the form,

$$\frac{\partial}{\partial z} \left(K \frac{\partial \Theta}{\partial z} \right) , \qquad \text{(III-11)}$$

where Θ represents an arbitrary atmospheric property, and K is the mixing coefficient appropriate to that property. The product of K and the derivative of Θ represents the eddy flux of the property.

This term may be expanded by carrying out the indicated differentiation:

$$\frac{\partial}{\partial z} \left(K \frac{\partial \Theta}{\partial z} \right) \equiv \frac{\partial K}{\partial z}\frac{\partial \Theta}{\partial z} + K\frac{\partial^2 \Theta}{\partial z^2} . \qquad \text{(III-12)}$$

The second term on the right hand side of this equation is of a form encountered in the molecular theory of heat transfer. The action of K in this term is restricted to reducing (increasing) local maxima (minima) in the vertical distribution of Θ at a rate dependent upon the magnitude of K. In the first term on the right hand side of Eq. III-12, we see a form suggestive of that associated with convective transfer of the property Θ by non-eddy vertical air currents. Suppose, for concreteness, that Θ is a property which increases with z. Then, if $\partial K/\partial z$ is negative, this term will contribute to a local decrease in Θ in the same way as would an upward wind current.

If one reflects on the mixing-length concept of turbulent exchange [20], it seems reasonable to anticipate that the coefficient K would tend toward a limiting value with increasing distance from the ground. The size of this value is expected to depend upon the two factors, intensity of the turbulent motion induced at the ground, and the distribution of the property being transferred. Additionally, the possibility of the atmospheric static-stability structure being such as to inhibit the vertical extent of ground-produced eddy motion can be expected to influence the vertical distribution of K.

We do not possess an adequate theory for prescribing the precise behavior of the mixing coefficient in the transition layer. Nonetheless, we have attempted a formulation of its variation based on the ideas outlined above.

To begin with, a basic value of the coefficient is prescribed at the base of the transition layer in accordance with the value derived from the contact-layer formulas. This value gives an estimate of the intensity of the mixing process active in the contact layer, and has been used to specify in two ways the coefficient, K, throughout the remainder of the transition layer.

First, it was assumed that this value remains unchanged. It is this assumption that was used in the simplified equations of horizontal motion. The second assumption allowed for a linear decrease of this coefficient with height to a residual value of 10^3 cgs units at the top of the transition layer. In order to allow for the influence of atmospheric stability, we introduced a weak dependence upon thermal stability from 500 m above the ground to the top of the transition layer. The restriction to elevations above 500 m was prompted by the results of some initial experiments.

Using idealized data with a two-component, sinusoidal, diurnal ground-temperature wave, and permitting the stability dependence to extend down to the base of the transition layer resulted in considerable distortion of the diurnal temperature wave. This second assumption on the mixing coefficient was not introduced into the horizontal wind computation because of the difficulty and computation time involved in computing a numerical solution of the governing equations.

Denoting the value of the mixing coefficient at the top of the contact layer by $\hat{K}$, the second assumption on the distribution of K may be expressed as,

$$K = 10^3 + \hat{K}\,[(H - z)/(H - h)], \qquad h \leq z < 500\ \text{m}, \tag{III-13a}$$

$$K = 10^3 + \hat{K}\,[(H - z)/(H - h)]\,(0.88 - 0.20 \cdot 10^{+4}\,\frac{\partial T}{\partial z}), \quad 500\text{m} \leq z \leq H. \tag{III-13b}$$

We also imposed an upper limit of 10^6 cgs units on the value of K.

7. The heat Transfer Equation

If the only diabatic energy source is the convergence of the vertical-eddy heat flux, the first law of thermodynamics and the equation of the state for an ideal gas may be combined to yield the equation,

$$\frac{\partial \Theta}{\partial t} = - u\frac{\partial \Theta}{\partial x} - v\frac{\partial \Theta}{\partial y} - w\frac{\partial \Theta}{\partial z} + \frac{\partial}{\partial z}\left(K_H \frac{\partial \Theta}{\partial z}\right), \tag{III-14}$$

where Θ is the potential temperature and K_H is the mixing coefficient for sensible heat. The potential temperature is related to the temperature, T, and the pressure, p, through the expression:

$$\Theta = T \left(\frac{p}{P}\right)^{-\kappa}, \tag{III-15}$$

where P is a standard pressure and κ is the ratio of the gas constant for dry air, R, to the specific heat at constant pressure for dry air, c_p. The hydrostatic equation,

$$\frac{\partial p}{\partial z} = - \frac{gp}{RT}, \tag{III-16}$$

where g is the acceleration of gravity, may be used to rewrite Eq. III-14 as

$$\frac{dT}{dt} = \frac{\kappa T}{p}\frac{dp}{dt} + \frac{\partial}{\partial z}\left[K_H \frac{\partial T}{\partial z} + \frac{g}{c_p}\right] + \frac{g}{c_p T} \cdot K_H \left[\frac{\partial T}{\partial z} + \frac{g}{c_p}\right] \tag{III-17}$$

The first term on the right can be approximated (see Appendix I) by the relation,

$$\frac{\kappa T}{p}\frac{dp}{dt} \cong \frac{\kappa T}{p}(w + \hat{w})\frac{\partial p}{\partial z} = -\frac{g}{c_p}(w + \hat{w}). \qquad \text{(III-18)}$$

The last term on the right of Eq. III-17 is negligibly small except in cases of extreme instability, which we will not expect to encounter in application of the model. By introducing these approximations, Eq. III-17 may be put into the form,

$$\frac{\partial T}{\partial t} = -u\frac{\partial T}{\partial x} - v\frac{\partial T}{\partial y} - w\left(\frac{\partial T}{\partial z} + \frac{g}{c_p}\right) - \frac{g}{c_p}\hat{w} + \frac{\partial}{\partial z}\left(K_H\frac{\partial T}{\partial z} + \frac{g}{c_p}\right) + \left(\frac{d}{dt}T\right)_w. \qquad \text{(III-19)}$$

In addition to the diabatic influence of the eddy heat flux, we have incorporated into Eq. III-19 a term, $(dT/dt)_w$, representing the heat exchange associated with water substance phase changes. The procedure for computing this diabatic effect is discussed in Subsection 9.

8. Water Substance Prediction

We will consider water to be present in the atmosphere in two phases: liquid and vapor. The ratio of the mass density of water vapor to the total mass density of moist air (vapor, dry air, and liquid water) is defined as the specific humidity and denoted by the letter, q. We will similarly define a quantity, r, as the ratio of the mass density of water substance (vapor plus liquid) to the total mass density of moist air. This quantity will be referred to as the specific moisture.

If we imagine a parcel of moist air to move in space, then the specific moisture will be invariant following such a movement under the following conditions:

(a) no molecular or eddy diffusion occurs, and

(b) no precipitation enters or leaves the parcel.

The water may change phase during the motion of the parcel, but the total moisture will be invariant. Thus, the equation governing r may be written

$$\frac{dr}{dt} = 0. \qquad \text{(III-19)}$$

The specific humidity of the parcel may, of course, change under these conditions in response to water-phase variations. If we denote the depletion rate of water vapor in response to condensation by, $(dq/dt)_c$ we may write the following equation for specific humidity:

$$\frac{dq}{dt} = - \left(\frac{dq}{dt} \right)_c . \tag{III-20}$$

Because the atmospheric motion is turbulent, eddy diffusion of water substance will occur. It will be assumed that the eddy mixing coefficients for both vapor and liquid are equal and that the liquid and vapor follow the air motion [27]. Equations III-19 and III-20 then become, upon expansion of the particle derivatives and the introduction of the eddy exchange mechanisms,

$$\frac{\partial q}{\partial t} = - u \frac{\partial q}{\partial x} - v \frac{\partial q}{\partial y} - w \frac{\partial q}{\partial z} + \frac{\partial}{\partial z} \left[K_w \frac{\partial q}{\partial z} \right] - \left[\frac{dq}{dt} \right]_c \tag{III-21}$$

and

$$\frac{\partial r}{\partial t} = - u \frac{\partial r}{\partial x} - v \frac{\partial r}{\partial y} - w \frac{\partial r}{\partial z} + \frac{\partial}{\partial z} \left[K_w \frac{\partial r}{\partial z} \right] . \tag{III-22}$$

The coefficients K_W in Eqs. III-21 and 22, and K_H in Eq. III-19 are computed from Eqs. III-13a and 13b. This procedure is followed because of its simplicity and the unavailability of any theoretically sound alternative within the framework of this model.

9. Computation of Water Phase Changes and Diabatic Heating

The equation governing specific humidity contains a term, $(dq/dt)_c$, which represents the source or sink of water vapor associated with phase changes in the water content of the air parcel. Similarly, the heat release associated with these phase changes appears in the thermodynamic energy equation as the diabatic source term $(dT/dt)_w$. In order to compute these two terms, we must introduce approximating assumptions. The scheme employed is based on the method used by Fisher [15] and modified by McDonald [27].

If the parameters, q, r, and T, and the other model variables are known at a given time, the equations governing q, r, and T, omitting the source terms

$(dq/dt)_c$ and $(dT/dt)_w$, may be used to obtain a first approximation of the values q^0, r^0, and T^0 at the next time step. The saturation value of specific humidity at a given point can be regarded as a function of the temperature alone if the pressure dependence is appropriately approximated. Thus, with the value T^0 we may associate a saturation value of specific humidity, q_s^0. An analysis of the relative values of the four quantities — q^0, r^0, T^0 and q_s^0 — must be made to decide if the values should be adjusted to account for the occurrence of phase changes and associated diabatic temperature changes. Before discussing the logic of the adjustment procedure, we first derive the equations for evaluating the approximate value of the adjustment.

For a change of water between the liquid and vapor phases, the Clausius-Clapeyron equation may be written to good approximation [33] as

$$d(\ln e_s) = m_w L\, d(T)/(R^* T^2), \tag{III-23}$$

where e_s is the saturation pressure of the water vapor in equilibrium with a plane water surface at a temperature of T degrees absolute, m_w is the molecular weight of water vapor (18), L is the latent heat of vaporization (cal gm^{-1}), and R* is the universal gas constant (1.986 cal deg^{-1}). The latent heat, L, is a function of the vapor temperature. This equation may be used to derive an approximate relationship between the saturation specific humidity, q_s, and the temperature. The value of q_s is closely given by

$$q_s = \frac{m_w}{m_d}\frac{e_s}{p}, \tag{III-24}$$

where m_d is the molecular weight (~ 29) of the gas mixture referred to as "pure dry air", and p is the partial pressure of this mixture in the parcel. It follows from Eqs. III-23 and 24 that

$$d(\ln e_s) = d(\ln q_s) + d(\ln p) = m_w L\, d(T)/(R^* T^2), \tag{III-25}$$

which, for normal atmospheric conditions may be written to good approximation as

$$dq_s = \left[\frac{m_w L q_s}{R^* T^2}\right] dT. \tag{III-26}$$

Equation III-26 is one of the two equations which will be employed in the saturation adjustment computation.

For an adiabatic-isobaric, water phase change (liquid ⟷ vapor) in a moist air parcel, the first law of thermodynamics may be written in approximate form as

$$c_p dT = -Ldq, \tag{III-27}$$

where c_p is the specific heat at constant pressure of dry air and L is the latent heat of vaporization. This is the second of the two equations which are required for the computation of the saturation adjustment.

We may now indicate the computational form of these two equations. Recalling that a superscript, 0, implies that the symbol stands for the first approximation to the value of the parameter (obtained as outlined earlier), and using an unscripted symbol to stand for the value of the parameter after the saturation adjustment has been applied to it, we may write Eq. III-26 as

$$q - q_s^0 = \frac{aq_s^0}{(T^0)^2}(T - T^0) \tag{III-28}$$

and Eq. III-27 as

$$b(T - T^0) = -(q - q^0), \tag{III-29}$$

where a and b are the quantities $(m_w \frac{L}{R^*}$ and (c_p/L) respectively.

Equation III-28 may be regarded as a straight-line, tangent approximation at the point (q_s^0, T^0) to the curve representing the solution of the Clausius-Clapeyron equation in a (q, T) plane. The parameters a and b will be taken to be constants; consequently, Eq. III-29 is a linear approximation to the general curvilinear solution to Eq. III-27.

One may now regard Eqs. III-27 and 28 as a pair of simultaneous linear equations in the two unknowns, T and q. Using Eq. III-29 in Eq. III-28, one may obtain,

$$T = T^0 + \frac{q^0 - q_s^0}{\left[\frac{aq_s^0}{(T^0)^2} + b\right]}. \tag{III-30}$$

Similarly, using Eq. III-28 in Eq. III-29, one finds that

$$q = q^0 - b \frac{q^0 - q_s^0}{\frac{a q_s^0}{(T^0)^2} + b} \tag{III-31}$$

The parameters a and b have the values

$$a = 5.393 \times 10^3 \text{ (deg)}, \tag{III-32}$$

$$b = 4.017 \times 10^4 \text{ (deg}^{-1}\text{)}. \tag{III-33}$$

The logic for applying the adjustment Eqs. III-30 and 31 will now be presented using the symbols

$$c_T = \frac{(q^0 - q_s^0) T_0^2}{a q_s^0 + b T^{0\,2}} \tag{III-34}$$

and

$$c_q = - b\, c_T. \tag{III-35}$$

The first step is to compare q^0 and q_s^0. If q^0 is equal to q_s^0, no adjustment is required and one simply writes

$$\begin{aligned} T &= T^0 \\ q &= q^0 \\ r &= r^0. \end{aligned} \tag{III-36}$$

If q^0 is greater than q_s^0, condensation should take place and an examination of the availability of water vapor must be included. If q^0 is greater than $|c_q|$, one writes

$$\begin{aligned} q &= q^0 + c_q \\ T &= T^0 + c_T \\ r &= r^0. \end{aligned} \tag{III-37}$$

Note in this case that $c_q < 0$ and $c_T > 0$, and that $|c_q|$ refers to the absolute value of c_q. If however, $|c_q|$ is greater than or equal to q^0, one writes the adjusted values as

$$\begin{aligned} q &= 0 \\ r &= r^0 \\ T &= T^0 + (q^0/b). \end{aligned} \tag{III-38}$$

The alternative which leads to Eq. III-38 is not likely to occur, as it implies the complete condensation of all the vapor in the air. We include it here for logical completeness alone.

Finally, if q^0 is less than q_s^0, one may expect evaporation of the liquid water in the air parcel. If $(r^0 - q^0)$ is zero (or negative for programming purposes) there is no liquid water in the air parcel and consequently no saturation adjustment is called for. One simply writes Eq. III-36 again. But if $(r^0 - q^0)$ is positive, there is liquid water available for evaporation. (Note that in this case $c_q > 0$ and $c_T < 0$). One must then inquire if c_q is greater than $(r^0 - q^0)$; if it is not, one writes

$$\begin{aligned} T &= T^0 + c_T \\ q &= q^0 + c_q \\ r &= r^0, \end{aligned} \tag{III-39}$$

but if it is greater, then one can only permit the evaporation of the liquid water which is available. Consequently, the adjustment equations are

$$\begin{aligned} q &= r^0 \\ r &= r^0 \\ T &= T^0 - (r^0 - q^0)/b. \end{aligned} \tag{III-40}$$

The examination of these alternatives exhausts the possible situations and leads finally to the specification of values of temperature and specific humidity that have been appropriately modified for the possibility of water phase changes.

As a final point in this section, we indicate the formula used to evaluate q_s^0 from T^0. In order to avoid the necessity for integrating the hydrostatic equation for the sole purpose of evaluating this relationship, we have assumed that the pressure at a point is an invariant function of the elevation of that point above mean sea level. Using the ICAO standard atmosphere, we found that this dependence could be written to good approximation as,

$$p(x, y, z) = \{1013 - 1.065 \times 10^{-3} (z + E(x, y)\} \text{ [mb]}, \qquad \text{(III-41)}$$

in where z is the elevation in cm of the point above the ground and E is the elevation in cm of the ground above mean sea level. Then, using Tetens approximating formula for saturation vapor pressure quoted in [20], and Eq. III-24, we obtained the formula,

$$q_s^0 = \frac{3.8 \times 10^{-3}}{[1.013 - 1.065 \times 10^{-6} (z + E)]} \exp \left\{ 17.25 \left[\frac{T^0 - 273}{T^0 - 35.7} \right] \right\} \qquad \text{(III-42)}$$

10. Cloud Specification

The prediction equations derived above provide the basis for forecasting the distribution of the relative humidity and liquid water content of the air. Although one might wish to assign to these predicted quantities a unique interpretation in terms of cloud occurrence, such a procedure is not apt to give very accurate results.

In view of the experience obtained in large-scale dynamical and statistical cloud prediction studies [1, 6, 37] it seems likely that superior results will be obtained by developing a probabilistic interpretation of the forecast parameters in terms of cloud occurrence. In Smagorinsky's paper, the problem of specifying a cloud amount—relative humidity relationship is discussed. The results of a limited study indicate that a linear relation between these parameters could explain a significant proportion of the observations. For low clouds, cloud amount in tenths, denoted by c, was related to the ratio of q to q_s by the linear expression,

$$c = 3.25 (q/q_s) - 1.95, \qquad (q/q_s) \geq .6. \qquad \text{(III-43)}$$

The problem of specifying this relationship occurs not only in the interpretation of forecasts, but also in the analysis of the initial data. Continuing research into these analyses and forecast-interpretation problems will eventually lead to an adequate solution, but an account of these efforts is beyond the scope of this paper. We have employed techniques which are in general agreement with Eq. III-43 in discussing forecasts made with this model and in performing the analysis of initial data for these forecasts.

11. Radiative-heat Flux and Precipitation

Two significant physical processes were omitted in formulating the equations governing the atmosphere in the transition layer. It is a priori desirable to incorporate a treatment of radiative-heat transfer and precipitation into a physical model of the atmospheric boundary layer. The neglect of these processes within our model is therefore deserving of some comment.

We shall restrict our discussion in this section to the radiative-heat transfer in the transition layer. The topic will be discussed separately as it affects our treatment of the contact-layer equations.

The boundary-layer models developed by Estoque [11] and Pandolfo, Cooley, and Atwater [32] incorporate procedures for computing the convergence of the infrared radiative flux. Neither model has as yet been tested on a case in which clouds were present within the boundary layer. The basic treatment of the radiation process follows the work of Elsasser [10, 11]. In Estoque's model, a numerical procedure developed by Brooks [4] and adapted by Elliott and Stevens [9] is used. In Pandolfo's model, the Elsasser tables [11] are stored in the computer, and the flux computed by a numerical integration analogue of the area-measuring graphical technique.

It must be emphasized that both of these sub-synoptic scale models are oriented toward single-station forecasting. This permits the inclusion of the rather lengthy computations required for the radiation calculation to be carried out without exceeding the high-speed storage capacity of an IBM 7090. The synoptic scale model presented in this document would have to carry out such computations through the use of slower access storage.

The computation of the infrared, radiative-flux convergence within the boundary layer is not independent of the distribution of water vapor, temperature, and cloudiness in the free air. For short-period, single-station forecasts, relatively accurate estimates of these free air distributions are obtained by assuming that the initially observed state does not vary appreciably during the forecast interval. This assumption would not be very appropriate in a synoptic scale prediction scheme. Moreover, presently available numerical prediction models for the free air, in their current form, do not provide predictions of the required parameters.

In summary, we can point to the availability of procedures for computing the influence of the infrared radiative flux which present no formal obstacle for incorporation in our model. On the other hand, the unavailability of certain required data and the existence of computational limitations put an adequate treatment of this process beyond our scope at present.

With reference to the precipitation process, and more explicitly, with regard to the evaporation of precipitation falling into the boundary layer from above, we again are handicapped by the absence of suitable predictions from free air models. Studies by Noguchi [29], Caplan [5] and Syono and Takeda [40] might be worked into a suitable basis for modeling this phenomena if large-scale precipitation rates were provided by a free-air model. In conclusion, we point out the potential for improving our current treatment of the physics of the transition layer. These improvements may be achieved if a suitable (i.e. moist) free-air, prediction model is developed.

IV

THE CONTACT-LAYER EQUATIONS

12. Introduction

The transition-layer equations require for their solution the specification of the heat and moisture flux at the lower boundary of the transition layer. Also required at that level are the horizontal wind components and the mixing coefficients. These conditions are provided in this model by means of a series of relations which are derived from a number of assumptions regarding the structure of the air layer in close proximity to the ground. This layer is referred to in this document as the contact layer. It corresponds to Lumley and Panofsky's surface-boundary layer [25], and Estoque's constant-flux layer [13]. There are two cogent reasons for introducing this layer into a synoptic-scale, boundary-layer model.

First, from the computational viewpoint, the accurate use of linear interpolation in approximating derivatives requires that the parameter being differentiated be distributed almost linearly between information levels. Near the ground, atmospheric variables tend to be non-linearly distributed with height[3]. Thus, if the prediction equations derived in Section III were to be applied down to the ground, considerations of numerical accuracy would require the use of a large number of information levels in this region, e.g., Fisher and Caplan [15] applied their prediction equations (which are similar to those in Section III within the contact layer, and this required using a vertical grid-mesh length as small as 2 m, and concentrating within the lowest 100 m, twelve of the total of twenty-three grid points used to cover the full depth of 1078 m. Such a disposition of information levels is disproportionate for use in the study of synoptic-scale, boundary-layer processes. When the contact-layer hypotheses are introduced [13, 30], one may employ the consequent saving in information levels to achieve greater refinement within the transition layer or in a variety of other ways. In our case, this

---

[3] For example, consider the validity of the logarithmic wind profile in a neutrally stratified boundary layer.

saving has been used to study the boundary-layer in three space dimensions.

The second reason for introducing the contact layer into the model involves physical considerations. The principal objective sought in application of the model derived here is improved accuracy in the prediction of large-scale, low-cloudiness. We anticipated the likelihood that turbulent heat and vapor exchange between the air and ground would play a part in achieving this goal. However, it was considered unnecessary to achieve great accuracy in computing these quantities. Indeed, if it were true that great accuracy was required, there would be little hope for success in the application of the model. One of the most difficult aspects of the micrometeorology of the surface-contact layer is in the specification of the surface temperature. In a recent study, Elliott [8] raises a question as to the existence of a unique, ground-air interface temperature. This question, and others which arise in a detailed study of the interface, are of considerable importance, but must be considered beyond the scope of our present investigation. The contact-layer hypotheses provide a means for circumventing the requirement for a detailed prediction in this region of very complex physical interactions, and for obtaining, at least qualitatively, correct estimates of the quantities needed to solve the transition-layer equations.

13. The Contact-layer Hypotheses

By analyses such as those given by Lumely and Panofsky [25], one can demonstrate the rationale for expecting the region near the ground to be characterized by a small variation in magnitude of the vertical flux of momentum and heat. To the extent possible with instruments of limited accuracy, micrometeorological observations of the eddy flux of heat and momentum support these analyses. Thus the experimental background is present for the working hypothesis that, within a thin layer of air adjacent to the ground, the eddy flux may be considered invariant with respect to height.

This assumption is a basis for the development of a similarity theory for the structure of the atmosphere within this layer. Accounts of the derivation of such theories are given in Monin [28], Priestley [34], and Lumley and Panofsky [25]. Our use of the results of these theoretical investigations centers in the derivation of formulas for evaluating the heat and vapor flux at the upper boundary

of the contact layer[4]. We will employ the Richardson's number as the stability parameter, and neglect the difference between the mixing coefficients for heat, momentum, and vapor.

The assumption that the vertical-eddy fluxes of momentum, heat, and vapor are independent of height in the contact layer permits one to write

$$K \frac{\partial s}{\partial z} = \frac{\tau}{\rho} = (u_*)^2, \tag{IV-1}$$

$$K \left[\frac{\partial T}{\partial z} + \gamma\right] = \frac{-H}{c_p \rho} = u_* \theta_*, \tag{IV-2}$$

$$K \frac{\partial q}{\partial z} = \frac{-Q}{\rho} = u_* q_*, \tag{IV-3}$$

where:

K is the mixing coefficient for momentum, heat and vapor ($cm^2\ sec^{-1}$),

s is the horizontal wind speed ($cm\ sec^{-1}$),

τ is the eddy shear stress ($gm\ cm^{-1}\ sec^{-2}$),

ρ is the air density ($gm\ cm^{-3}$),

T is the air temperature (deg),

γ is the adiabatic lapse rate of temperature (1°C/100 m),

H is the eddy heat flux ($cal\ cm^{-2}\ sec^{-1}$),

c_p is the specific heat of air at constant pressure ($0.239\ cal\ gm^{-1}\ deg^{-1}$),

q is the specific humidity,

Q is the eddy vapor flux ($gm\ cm^{-2}\ sec^{-1}$),

and the quantities u_*, θ_*, and q_* are constants with the dimensions of velocity, temperature, and specific humidity respectively.

The results of similarity theory and numerous empirical studies indicate that there are two principal regimes which occur in the contact layer. These are

---

[4] A unique upper boundary does not exist. It is our practice to choose 50 m as the depth of the contact layer which is a value suggested by Lumley and Panofsky [25].

denoted by the names; forced convection, and free convection. In the forced-convective regime, the energy of the turbulent motions is derived principally from the kinetic energy of the mean flow. In the free-convective regime, the energy of the turbulence arises principally from the bouyancy forces associated with the unstable density stratification produced in the layer by surface heating.

For the forced-convective regime, it follows [30] from the work of Monin and Obukhov that the mixing coefficient may be expressed in terms of the parameters of the mean flow by

$$K = [kz(1 - \beta R_i)]^2 \frac{\partial s}{\partial z} , \qquad \text{(IV-4)}$$

where:

k is von Karman's Constant,

β is a constant, and

R_i is the Richardson's number.

The Richardson's number is a dimensionless ratio between the actions of bouyancy and inertia and is defined by the relation,

$$R_i = \frac{g}{\overline{\theta}} \left[\frac{\partial T}{\partial z} + \gamma \right] \Big/ \left[\frac{\partial s}{\partial z} \right]^2 \qquad \text{(IV-5)}$$

where the ratio $g/\overline{\theta}$ is the coefficient of thermal expansion, g is the acceleration of gravity, and $\overline{\theta}$ is a mean temperature of the fluid. The term $(1 - \beta R_i)$ is the analytic representation (by the first terms of a power-series expansion) of the universal stability function which is postulated to exist in similarity theory.

In the free-convective regime, the mixing coefficients no longer depend upon the stress. Again, a combination of similarity theory and numerous empirical investigations indicates that, in the free-convective regime, the mixing coefficients may be expressed as functions of the mean state by the relation

$$K = \lambda z^2 \left[\frac{g}{\overline{\theta}} \left| \frac{\partial T}{\partial z} + \frac{g}{C_p} \right| \right]^{1/2} \qquad \text{(IV-6)}$$

The absolute value signs are used because the existence of the free-convective regime depends upon the existence of a negative static stability. The coefficient, λ, is found to have a value near 0.9 [34].

Examination of observations (made under conditions with differing Richardson's numbers) of the heat flux indicates that a relatively sharp transition between free- and forced-convective regimes occurs about the Richardson-number value of -.03 [34]. The importance of modeling such a transition lies in the different values of the heat flux computed by means of the formulas derived for the alternate regimes. This point will subsequently be elaborated.

If we introduce the value for the forced-convective, K from Eq. IV-4, into Eqs. IV-1, 2, and 3, we may write

$$\frac{\partial s}{\partial z} = \frac{u_*}{kz}\left[1 + \frac{\beta g}{\overline{\theta}}\,\frac{kz\theta_*}{u_*^2}\right], \tag{IV-7}$$

$$\frac{\partial T}{\partial z} = -\gamma + \frac{\theta_*}{kz}\left[1 + \frac{\beta g}{\overline{\theta}}\,\frac{kz\theta_*}{u_*^2}\right] \tag{IV-8}$$

$$\frac{\partial q}{\partial z} = \frac{q_*}{kz}\left[1 + \frac{\beta g}{\overline{\theta}}\,\frac{kz\theta_*}{u_*^2}\right] \tag{IV-9}$$

Now consider the integration of these equations. The wind speed, s, should vanish at z = 0 if the no-slip boundary condition is applied. The irregularity of natural terrain does not admit of a unique level of no slip and, in accordance with aerodynamic practice, a roughness length, z_0, has been introduced by micrometeorologists to account for this fact [39]. The wind speed is then assumed to vanish at that level. Integration of Eq. IV-7 then yields

$$s(z) = \frac{u_*}{k}\ln\left(\frac{z}{z_0}\right) + \frac{\theta_*}{u_*}\frac{\beta g}{\overline{\theta}}(z - z_0), \tag{IV-10}$$

where we note that for neutral stratification, θ_* is zero and thus, Eq. IV-10 reduces to the well-known logarithmic wind-profile formula. The linear term in this expression will produce the typical concavity or convexity of the wind-speed profile (plotted on a logarithmic height scale) associated with non-neutral thermal stratification [39].

As pointed out by Lumley and Panofsky [26], the constant-flux hypothesis as expressed in Eq. IV-8 is of doubtful validity below z = 1 m due to the relatively

strong convergence of the radiative flux below that height. Consequently, denoting the level of the instrument shelter as $z = z_i \geq 1$ m, we integrate Eq. (IV-8) using the boundary condition $T = T_i$ at $z = z_i$. The result is

$$T(z) = T_i - \gamma(z - z_i) + \frac{\theta_*}{k} \ln\left(\frac{z}{z_i}\right) + \frac{\beta g}{\bar{\theta}} \left(\frac{\theta_*}{u_*}\right)^2 (z - z_i) \qquad \text{(IV-11)}$$

For the sake of compatibility with Eq. IV-11, we will specify the boundary condition for Eq. IV-9 at $z = z_i$ also. The integration yields

$$q(z) = q(z_i) + \frac{q_*}{k} \ln\left(\frac{z}{z_i}\right) + \frac{\beta g}{\bar{\theta}} \frac{q_* \theta_*}{u_*^2} (z - z_i) \qquad \text{(IV-12)}$$

An analogous set of profile equations may be derived from the equations of constant flux by use of the free-convective-regime formula for the mixing coefficient (Eq. IV-6). The boundary conditions are applied at the same levels as in the case of forced convection. One finds that the profile equations may be written as

$$s(z) = -\frac{3u_*^2}{\lambda^{2/3}[u_*|\theta_*|]^{1/3}} \left(\frac{g}{\bar{\theta}}\right)^{-1/3} \left[z^{-1/3} - z_0^{-1/3}\right], \qquad \text{(IV-13)}$$

$$T(z) = T_i - \gamma(z - z_i) - \frac{3u_*\theta_*}{\lambda^{2/3}[u_*|\theta_*|]^{1/3}} \left(\frac{g}{\bar{\theta}}\right)^{-1/3} [z^{-1/3} - z_i^{-1/3}], \qquad \text{(IV-14)}$$

$$q(z) = q_i - \frac{3u_* q_*}{\lambda^{2/3}[u_*|\theta_*|]^{1/3}} \left(\frac{g}{\bar{\theta}}\right)^{-1/3} [z^{-1/3} - z_i^{-1/3}]. \qquad \text{(IV-15)}$$

14. The Empirical Formulas

Estoque and Pandolfo, in their previously cited work with boundary-layer prediction models, have employed the contact-layer profile relations derived above. Their use of them differs in an important respect from ours. The difference is necessitated by our omission of a prediction equation for the horizontal wind in the transition layer. This omission results from our conviction that it would have been inadvisable to embark on this investigation with a dynamically active model, especially in view of the well-known inadequacy of current synoptic wind observa-

tions for specifying the geostrophic deviation[5].

The use of the profile formulas in our work will be spelled out in the next two sections. In this section we will discuss the empirical formulas for the stress and geostrophic-deviation angle which form the basis upon which the subsequent formulation is constructed.

The empirical evidence which is employed here is taken from a paper presented by Prof. A. K. Blackadar [3] before a national meeting of the American Meteorological Society. This paper deals with the steady-wind distribution in a neutral, baroclinic boundary layer. In presenting his results, Blackadar used observational data on the relations between the friction velocity u_*, the geostrophic-wind speed, G, the surface Rossby number (G/fz_0) and the angle of deviation between the surface wind and the surface geostrophic wind. The sources of these observational data are identified in his paper.

We found that the following expressions could be used to approximate the principal characteristics of these relations:

$$u_* = G\,[0.07625 - 0.00625\,r], \tag{IV-16}$$

$$\psi = 0.625\,r^2 - 12.750\,r + 80.625, \tag{IV-17}$$

where

$$r = \log_{10}\left(\frac{G}{fz_0}\right), \tag{IV-18}$$

u_* is the friction velocity, G is the surface geostrophic wind speed, f is the Coriolis parameter, and z_0 the surface roughness. The quantity ψ is the angle (in degrees) between the surface wind and the surface geostrophic wind. Blackadar's theoretical results indicate that the wind direction does not vary appreciably through the lowest 50 m, and this is consistent with our use of the constant-flux hypothesis.

These empirical formulas are not dependent upon the static stability of the air in the contact layer. There is some theoretical evidence quoted in Haltiner and

---

[5] In this connection, simply recall the fact that the majority of wind reports are based on pilot balloon runs followed visually.

Martin [19] that the geostrophic-deviation angle should tend to be greater in inversion conditions and smaller in lapse conditions. According to Blackadar's theoretical results, the baroclinicity of the boundary layer also accounts for a tendency toward larger deviation angles when the thermal wind direction is opposite to the surface geostrophic wind direction and vice versa. Thus, we note that Eq. IV-17 does not take into account two of three relevant physical factors. However, there seemed to be little point in trying to model these refinements until some basic evaluations of the model are carried out. This is especially true because the geostrophic wind is not predicted by this model; it must be obtained from an independent, free-air prediction model.

The friction-velocity computation based on Eq. IV-16 may also require modification to take into account the existence of thermal enhancement (suppression) of the turbulent exchange in lapse (inversion) conditions. In some initial idealized experiments, analogous to those quoted earlier, we found that use of Eq. IV-16 tended to yield as large a negative heat flux values as positive. This seemed sufficiently unrealistic to require modification of Eq. IV-16 even in our basic model. We therefore replaced Eq. IV-16 with the following pair of equations:

$$u_* = 1.2\ G\ [0.07625 - 0.00625\, r], \quad \frac{\partial \theta}{\partial z} \leq 0$$

$$u_* = 0.8\ G\ [0.07625 - 0.00625\, r], \quad \frac{\partial \theta}{\partial z} > 0 \qquad \text{(IV-19)}$$

Repetition of the idealized experiments supported the use of these formulas. In practical application of a model similar to this one, we will have to recognize again the importance of having available an accurate prediction of the geostrophic wind.

15. Eddy-flux Evaluation

The technique employed in the computation of the eddy fluxes of heat and vapor at the interface ($z = h$) of the transition and contact layers will be explained in this section. The transition-layer prediction equations are applied at the level

$z = h$ to obtain values of temperature and specific humidity at this level[6]. These quantities, together with the time-dependent boundary conditions at $z = z_i$, are used in the profile formulas to transform them to equations in the quantities θ_* and q_*. The empirical calculation of u_* permits us to consider it as a known quantity in the profile equations for temperature and vapor.

The equations for the fluxes will be evaluated for the forced-convective regime. We will show that these formulas fail when the value of Richardson's number is nearly equal to the critical Richardson's number discussed by Priestly [34]. A transition to the free-convective formulas is then indicated, and, therefore, the flux formulas for free convection are derived. We conclude this section with a summary of the computational formulas.

We denote the values of temperature and specific humidity predicted at the level $z = h$ by the subscripted quantities, T_h and q_h, respectively. Consider first Eq. IV-11, the equation for the temperature profile in forced convection. If it is evaluated at $z = h$, the equation becomes a quadratic in θ_*. The two roots of this equation are readily obtained. Upon inspection, and realizing that θ_* must vanish when the lapse rate is neutral, the appropriate root, or solution, is found to be

$$\theta_* = -\frac{u_*^2}{2\beta} \cdot \frac{\overline{\theta}}{g} \cdot \frac{\ln (h/Z_i)}{k(h - Z_i)} \left\{ 1 - \left[1 - \frac{4\beta}{u_*^2} \cdot \frac{g}{\overline{\theta}} \left(\frac{T_i - T_h}{h - Z_i} - \frac{g}{C_p} \right) \left(\frac{\ln h/Z_i}{k(h - Z_i)} \right)^{-2} \right]^{1/2} \right\}. \qquad \text{(IV-20)}$$

Consideration of Eq. IV-11 evaluated at $z = h$ shows that it is readily evaluated for q_*. The result is

$$q_* = (q_h - q_i) \left[\frac{\ln h/Z_i}{k} + \frac{\beta\theta_*}{u_*^2} \frac{g}{\overline{\theta}} (h - Z_i) \right]^{-1}. \qquad \text{(IV-21)}$$

---

[6] We do not believe that any real problem arises from the dual character of the level $z = h$ in our use of both contact- and transition-layer formulas at this level. Estoque [13] uses a device to circumvent this question, but the quantitative calculations are sensibly unmodified.

The heat flux and vapor flux within the contact layer in forced convection are then obtained straight-forwardly by multiplying θ_* and q_* (computed by the formulas above) by u_* (computed from the empirical formulas). We then note that Eq. IV-20 yields a complex value of θ_* whenever the temperature gradient satisfies the following inequality;

$$\frac{T_i - T_h}{h - Z_i} - \frac{g}{C_p} > \frac{u_*^2}{4\beta} \frac{\overline{\theta}}{g} \left[\frac{\ln h/Z_i}{k(h - Z_i)} \right]^2 . \tag{IV-22}$$

Thus, Eq. IV-20 can only be applied with a temperature gradient at least as stable as the limiting value given by

$$\frac{T_h - T_i}{h - Z_i} + \frac{g}{C_p} = - \frac{\overline{\theta}}{g} \frac{u_*^2}{4\beta} \left[\frac{\ln h/Z_i}{k(h - Z_i)} \right]^2 \tag{IV-23}$$

At this limiting-temperature distribution, the heat flux, H, computed from the forced-convective formula is

$$H = - \rho C_p u_* \theta_* = \frac{\overline{\theta} C_p \rho u_*^3 \ln h/Z_i}{g 2\beta k (h - Z_i)} . \tag{IV-24}$$

In the forced-convective regime, the Richardson's number can be written as

$$R_i = \frac{1}{\beta} \left[1 - \left(1 + \frac{\beta g k z \theta_*}{\overline{\theta} u_*^2} \right)^{-1} \right] . \tag{IV-25}$$

Now, at the limiting-temperature gradient given in Eq. IV-23, the Richardson's number may be evaluated using Eq. IV-24. The result is

$$R_i = \frac{1}{\beta} \left[1 - \left(1 - \frac{z}{2} \frac{\ln h/Z_i}{(k - Z_i)} \right)^{-1} \right] . \tag{IV-26}$$

This Richardson's number may be evaluated for various heights, z, and values of the parameter β (See Table I). According to Priestley [34], the transition from forced-to free-convection is associated with a Richardson number of -0.03 or -0.02, measured at z = 1.5 m. Pandolfo [30] (also see Estoque [13] recommends the use of β = 3.0 in the forced-convective formulas on the basis

of his analysis of profiles in inversion conditions. From Table I we see that at z = 1.5 m with β = 3, the Richardson's number associated with the limiting temperature distribution, Eq. IV-23, agrees with Priestley's value.

TABLE I
RICHARDSON'S NUMBER
(associated with limiting temperature distribution between 1 and 50 meters for forced-convective heat flux equation) as a function of the parameter, β, and the height z(m) at which R_i is measured in a layer of constant-flux of total depth 50 m.

β \ z (m)	.5	1.0	1.5	2.0	2.5	3.0
1	-.021	-.039	-.063	-.087	-.111	-.135
2	-.010	-.019	-.032	-.044	-.056	-.007
3	-.007	-.013	-.021	-.029	-.037	-.045
4	-.005	-.009	-.016	-.022	-.028	-.034
5	-.004	-.008	-.012	-.017	-.022	-.027
10	-.002	-.004	-.006	-.009	-.011	-.014

Because the forced-convective heat-flux formula fails to supply a useful result on the lapse side of the limiting temperature distribution, one may there apply the free convective formulas. It is of some interest to examine the possibility of enforcing continuity in the heat flux computed from the forced-and free-convective equations at the limiting temperature distribution. In the first instance, the profile formula, Eq. IV-14, may be evaluated at z = h and solved for the heat flux, H, to give

$$H = -\rho C_p u_* \theta_* = +\rho C_p \left\{ \frac{\lambda^{2/3}}{3} \left(\frac{g}{\theta}\right)^{1/3} \frac{h - Z_i}{h^{-1/3} - Z_i^{-1/3}} \left[\frac{T_h - T_i}{h - Z_i} + \frac{g}{C_p} \right] \right\}^{3/2} \qquad \text{(IV-27)}$$

Now, at the limiting temperature distribution given by Eq. IV-23, the free-convective heat flux is given by Eq. IV-27 as

$$H = + \frac{\rho C_p \lambda u_*^3}{3^{3/2}} \left(\frac{g}{\theta}\right)^{-1} \left[Z_i^{-1/3} - h^{-1/3}\right]^{-3/2} \left[\frac{(\ln h/Z_i)^2}{4\beta k^2 (h - Z_i)}\right]^{3/2} . \qquad \text{(IV-28)}$$

For continuity in the computed heat flux at the limiting temperature distribution, Eqs. IV-28 and 24 should be equal. This equality then implies a relationship between β and λ, which after some manipulation may be solved for λ to give

$$\lambda = k^2 \frac{4(3)^{3/2} (Z_i^{-1/3} - h^{-1/3})^{3/2} (h - Z_i)^{1/2}}{(\ln h/Z_i)^2} \beta^{1/2} \qquad \text{(IV-29)}$$

Again, using $Z_i = 1$ m, $h = 50$ m and $k = 0.38$, we find that

$$\lambda = 0.85 \sqrt{\beta} \qquad \text{(IV-30)}$$

Priestley [34] quotes 0.9 as the most likely value of λ, whereas, according to Eq. IV-30, we note that for $\beta = 1$, $\lambda = .85$; for $\beta = 2$, $\lambda = 1.2$; and for $\beta = 3$, $\lambda = 1.5$. The values $\beta = 2$ and $\lambda = 1.2$, although not the precise values indicated by the experimental evidence, are considered to be sufficiently accurate for our work. If the heat flux in free convection is computed from Eq. IV-27, it is simple to evaluate the vapor flux from Eq. IV-15. We will next recapitulate the procedure for computing the heat and vapor fluxes in the contact layer.

The first step is to compute u_* from the appropriate formula of the pair denoted as Eq. IV-19. One may then determine if the free- or forced-convective formulas are appropriate by evaluating the left- and right-hand sides of Eq. IV-23.

If forced convection is indicated, one solves Eq. IV-20 for θ_*, and then solves Eq. IV-21 for q_*. The forced-convective fluxes are then computed from u_*, θ_*, and q_*.

If free convection is indicated, the heat flux is computed from Eq. IV-27. Knowing $u_*\theta_*$, Eq. IV-15 may be evaluated for the vapor flux.

16. Formulas for the Horizontal Wind Components and Mixing Coefficients

In Subsection 13 we presented the following expressions for the mixing coefficient in forced and free convection, respectively,

$$K = [kz(1 - \beta R_i)]^2 \frac{\partial s}{\partial z}, \qquad \text{(IV-31)}$$

$$K = \lambda z^2 \left[\frac{g}{\theta} \left| \frac{\partial T}{\partial z} + \frac{g}{C_p} \right| \right]^{1/2} \tag{IV-32}$$

In order to evaluate Eq. IV-31 at z = h, it is convenient to derive the two relations

$$\frac{K}{u_*} = kz\,(1 - \beta R_i)\,, \tag{IV-33}$$

$$(1 - \beta R_i) = \left[1 + \frac{\beta g}{\theta} kz \frac{\theta_*}{u_*^2} \right]^{-1} \tag{IV-34}$$

It follows from these relations that K may be written as

$$K = \frac{kzu_*}{1 + \frac{\beta g}{\theta} \frac{\theta_*}{u_*^2} kz} \tag{IV-35}$$

Consequently, the value of K at z = h under forced convection is given by

$$\hat{K} = K(h) = \frac{ku_*h}{1 + \frac{\beta g}{\theta} \frac{\theta_*}{u_*^2} kh}\,. \tag{IV-36}$$

The evaluation of Eq. IV-32 requires the introduction of the constant-flux relation,

$$K \left[\frac{\partial T}{\partial z} + \frac{g}{C_p} \right] = u_* \theta_*\,, \tag{IV-37}$$

into the equation. Then the value of K at z = h is

$$\hat{K} \equiv K(h) = [\lambda h^2]^{2/3} \left\{ \frac{g}{\theta} |u_* \theta_*| \right\}^{1/3} \tag{IV-38}$$

The boundary values, U and V, required for computing the horizontal wind in the transition layer are derived as follows.

In forced convection, Eq. IV-10 yields

$$s(h) = \frac{u_*}{k} \ln \left(\frac{h}{Z_0} \right) + \frac{\theta_*}{u_*} \frac{\beta g}{\theta} (h - Z_0) \tag{IV-39}$$

For free convection Eq. IV-13 yields

$$s(h) = -\frac{3u_*^2}{\lambda^{2/3}[u_*|\theta_*|]^{1/3}}\left(\frac{g}{\theta}\right)^{-1/3}\left[h^{-1/3} - Z_0^{-1/3}\right] \qquad \text{(IV-40)}$$

Let the geostrophic wind components at z = h (evaluated from Eqs. III-4a and b) be denoted by U_g and V_g. One may then fix the angle

$$\phi_g = \tan^{-1}\left[\frac{V_g}{U_g}\right] \qquad \text{(IV-41)}$$

in degrees. Combining ϕ_g and the deviation angle, ψ computed from Eq. IV-17, we have

$$\phi = \phi_g + \psi, \qquad \text{(IV-42)}$$

and

$$U = s(h)\cos\phi \qquad \text{(IV-43)}$$

$$V = s(h)\sin\phi.$$

17. Contact-layer Boundary Conditions

This model has been designed so that for the transition-layer prediction equations the lower-boundary conditions are derived from formulas obtained from the equations valid in the contact layer. The latter set of equations also requires the availability of boundary conditions for their evaluation. One set of these conditions is supplied by requiring continuity in the dependent variables at the interface between the two layers. There remains the need to provide a means for computing the temperature and specific humidity at the level of the instrument shelter, $z = z_i$.

We will consider first the procedure for obtaining the temperature at the instrument shelter. The primary cause for variations in this temperature is the variation in the solar radiation received at the ground. Secondary factors involve terrestrial and atmospheric radiation. All of these factors are influenced by the constitution of the atmosphere (clouds, water vapor, carbon dioxide, etc.) and by the ground characteristics (albedo, thermal conductivity, etc.). Because of this complex interaction, it did not seem realistic to attempt in this model to specify

deterministically the temperature at the level of the instrument shelter. One might achieve adequate accuracy through the use of a combination of statistical prediction methods and physical climatology. This is one of the problems we plan to study during the coming year. In the experiments reported in this paper (see Section VII), we neglected the change in temperature due to radiation.

In addition to radiation processes, the temperature at the level of the instrument shelter may be expected to change in response to the advection process. Because the instrument-shelter level is within the contact layer, we decided to omit advective-temperature changes from consideration unless they were greater than the temperature change which would be produced by a convergence within the contact layer of some 20 percent of the heat flux passing through the layer. The procedure used in the experiments (see Section VII) estimated the temperature change due to advection at the top of the contact layer and applied this change to the instrument shelter whenever it exceeded the criterion given above.

In determining the specific humidity at the level $z = z_i$, we assumed the relative humidity was specified a priori. This value, coupled with the scheme given above for obtaining the temperature and an assumption that the air pressure was known at $z = z_i$, is sufficient for determining the specific humidity at $z = z_i$. Here again we believe that statistical prediction methods utilizing those predictors available within the model could provide an improved technique for prescribing the relative humidity.

V

COMPUTATIONAL FORMULATION OF MODEL

In the preceding sections, the various equations which govern the behavior of our model of the atmospheric planetary-boundary layer were formulated. We now describe the computational scheme by which the model equations are to be applied to the prediction problem. The differential equations, region of integration, and time are made discrete by the introduction of a grid mesh of points.

The region of integration will be of limited horizontal extent. For simplicity, we will assume that the grid points in the (x, y)-plane are equally spaced a distance d apart. The grid points along each vertical will be spaced at unequal distances, $(\Delta z)_i$, apart. The density of grid points in the vertical will diminish with increasing distance above the ground. The time coordinate will be divided into increments of equal duration, Δt. We will assume that the region may be covered by (L + 1) grid points in the x-coordinate, (M + 1) grid points in the y-coordinate, and K grid points in the z-coordinate. We will use the following notation to represent a function's value at a grid point:

$$f^{l,n}_{m,k} = f(x=x_l,\ y=y_m,\ z=z_k,\ t=t_n), \qquad \text{(V-1)}$$

where

$$x_l = (l-1)\,d, \qquad l = 1, \ldots, L+1;$$

$$y_m = (m-1)\,d, \qquad m = 1, \ldots, M+1;$$

$$z_k = \sum_{i=1}^{k} (\Delta z)_i, \qquad k = 1, \ldots, K;$$

$$t_n = \tau + (n-1)\,\Delta t, \qquad n = 1, \ldots, N+1;$$

and τ is the time of the initial data measured from some suitable reference time.

If we wish to refer to the value of a function at some particular, but unspecified value of x, y, z, or t, we will use a Greek letter in place of a Roman symbol. Thus, the value of a function at a particular time step may be denoted by $f^{l,\nu}_{m,k}$.

18. The Difference Equations

The prediction equations for the transition layer will be put into a partially-implicit difference form. This partially-implicit scheme has the major advantage of being computationally stable for relatively large time-step increments. One must pay for this advantage by solving the set of simultaneous linear equations which result from the difference equations. A simple computer-oriented solution of these algebraic equations may be obtained by the method of Gaussian Elimination. Before presenting the difference equations, we discuss the form taken by the various differential terms.

The time derivative in all the equations is approximated by a forward difference over an interval, Δt. We write

$$\frac{\partial f}{\partial t} \cong \frac{f^{l,n+1}_{m,k} - f^{l,n}_{m,k}}{\Delta t} \qquad \text{(V-2)}$$

It is to be noted that computational stability is insured by the partially-implicit difference scheme for relatively large values of (Δt) (see subsection 19), but that in order to insure a good approximate solution, the value chosen for Δt must not be too large.

The horizontal advection terms are approximated by the upwind technique used by Fisher [14] and discussed in Forsythe and Wasow [16]. This procedure is outlined in Appendix II for the various advection quantities. The one-sided derivative approximation is theoretically of lower-order accuracy than that obtainable with a centered difference approximation, but from a practical viewpoint the method is in better accord with the concept of advection as a transport process dependent only upon upstream values of the transported quantity, and will frequently involve smaller truncation errors.

The diffusion terms and the vertical advection terms are approximated by centered space derivatives. The mixing coefficients and vertical velocities are evaluated at the current time step, whereas the quantities being diffused and advected are evaluated at the subsequent time step. This procedure introduces the so-called implicit character into the difference equations. The vertical coordinate index on the mixing coefficients is that of the grid point at the top of

the interval for which the coefficient is evaluated.

The difference equations approximating the prediction equations are written out in Appendices III, IV, and V. In order to demonstrate the method of solution of the difference equations, it is adequate to treat just one equation; the heat transfer equation has been selected for this purpose. Using the equations outlined in Appendix III, one may rewrite these equations in the form

$$a^{\lambda,\nu}_{\mu,k}\, T^{\lambda,\nu+1}_{\mu,k-1} + b^{\lambda,\nu}_{\mu,k}\, T^{\lambda,\nu+1}_{\mu,k} + c^{\lambda,\nu}_{\mu,k}\, T^{\lambda,\nu+1}_{\mu,k+1} = d^{\lambda,\nu}_{\mu,k}. \quad (k=1, \ldots, K-1) \tag{V-3}$$

The various coefficients in Eq. V-3 are spelled out in Appendix VI.

The system of (K-1) algebraic equations represented by Eq. V-3 may be solved for the (K-1) values of $T^{\lambda,\nu+1}_{\mu,k}$ (k=1, ..., K-1) by the method of Gaussian Elimination which does not involve any iteration. The various coefficients in Eq. V-3 are all computed from quantities known at $t = t_\nu$. The upper-boundary temperature $T^{\lambda,\nu+1}_{\mu,k}$ is known at $t = t_\nu$, because it is a prescribed boundary condition. The other prediction equations are susceptible to an identical solution procedure.

19. Analysis of Computational Stability

The choice of difference equations, indicated in Appendices III, IV, and V, was made to permit the use of a relatively long time step. It is well known that the solution of a difference equation may exhibit an improper exponential growth if the ratio of the time and space intervals does not satisfy certain criteria. These computational stability criteria are derived from consideration of linearized versions of the difference equations in which the coefficients are assumed to be constants. The intuitive justification for regarding such criteria as applicable to the more general difference equations is presented in Section IV of the paper by Richtmyer [36].

Because the various equations employed in this model are of similar form, we will derive the computational stability criteria for a generic case. For simplicity, only the principal steps in the analysis are presented here, and we retain only one of the horizontal coordinates.

Let the difference equation be

$$q^{n+1}_{l,k} - q^{n}_{l,k} = -\frac{U\Delta t}{\Delta x}\left[q^{n}_{l,k} - q^{n}_{l-1,k}\right] - \frac{w\Delta t}{2\Delta Z}\left[q^{n+1}_{l,k+1} - q^{n+1}_{l,k-1}\right] - \frac{K\Delta t}{(\Delta Z)^2}\left[q^{n+1}_{l,k+1} + q^{n+1}_{l,k-1} - 2q^{n+1}_{l,k}\right]. \tag{V-4}$$

We have assumed for simplicity that U is positive. It is also required that K be positive. The coefficient w may be either positive or negative. Let us replace the coefficients by the symbols

$$\sigma = \frac{U\Delta t}{\Delta x} > 0,$$

$$\rho = \frac{w\Delta t}{2\Delta Z}, \tag{V-5}$$

$$\gamma = \frac{K\Delta t}{(\Delta Z)^2} > 0.$$

Because Eq. V-4 is linear with constant coefficients, a solution may be sought in the form of a series of terms [16, Section 29] of the type

$$q^{n}_{l,k} = Ae^{cn\Delta t}\, e^{i[\gamma l\Delta x + \kappa k\Delta Z]}, \tag{V-6}$$

where A, λ, κ are real constants, and c is a complex constant.

If Eq. V-6 is substituted into Eq. V-4, one obtains

$$[e^{c\Delta t} - 1] = -\sigma\,[1 - e^{-i\lambda\Delta x}] - \rho\,[e^{c\Delta t}(e^{ik\Delta z} - e^{-ik\Delta z})] - \gamma\,[e^{c\Delta t}(e^{ik\Delta z} + e^{-ik\Delta z} - 2]. \tag{V-7}$$

Solving for $e^{c\Delta t}$, one gets

$$e^{c\Delta t} = \left[\frac{1 - \sigma(1 - e^{-i\lambda\Delta x})}{1 + \rho(e^{ik\Delta z} - e^{-ik\Delta z}) + \gamma(e^{ik\Delta z} + e^{-ik\Delta z} - 2)}\right]. \tag{V-8}$$

Referring to the form of Eq. V-6, it is clear that the solution will show exponential growth with time (increasing n) if the amplitude of $e^{c\Delta t}$ is greater than unity. Using this, one may replace Eq. V-8 by the inequality

$$\left| \frac{1 - \sigma[1 - e^{-i\lambda\Delta x}]}{1 + \rho[e^{i\kappa\Delta z} - e^{-i\kappa\Delta z}] + \gamma[e^{i\kappa\Delta z} + e^{-i\kappa\Delta z} - 2]} \right| \leq 1, \qquad \text{(V-9)}$$

which is a necessary condition for the difference equation to possess bounded solutions of the form of Eq. V-6 for $n \rightarrow \infty$[7].

$$\sigma(\sigma - 1)(1 - \cos\gamma\Delta x) \leq 2\gamma(1 - \cos\kappa\Delta z) + 2\gamma^2(1 - \cos\kappa\Delta z)^2 + 2\rho^2 \sin^2\kappa\Delta z \qquad \text{(V-10)}$$

Inspection shows that the right hand side of Eq. V-10 is non-negative, whereas the left hand side will be non-positive if $\sigma \leq 1$. Thus, we conclude that the difference equation will have computationally-stable solutions provided that,

$$\Delta t \leq \left(\frac{\Delta x}{U}\right). \qquad \text{(V-11)}$$

This requires that the time step not exceed the space-grid mesh divided by the largest horizontal velocity which is likely to occur. If we assume that Δx is 100 km and U_{max} is 40 m sec^{-1}, then Δt may be as large as 40 minutes.

A theorem, due to Lax, which states the equivalence of stability and convergence for properly posed initial-value difference equations is proven in Richtmyer's book [36]. This implies for our problem that, if Δt is taken sufficiently small while the condition Eq. V-11 is maintained, the solution obtained from the difference equation will be close to the solution of the differential equation. This difference between the solutions of the difference and differential equations can be ascribed to truncation error. It would seem necessary then, to experiment with various choices of Δt which satisfy Eq. V-11 to arrive at an optimum value relative to the two desirable features:

(a) Minimal computation time for a forecast of fixed duration,

(b) Minimal truncation error relative to the observational accuracy of the data employed.

---

[7] $n \rightarrow \infty$ implies either (a) for Δt fixed, the duration of the prediction, T, $\rightarrow \infty$, or (b) for T fixed, Δt approaching zero.

Such experiments may be carried out in conjunction with investigation of the relationships among stability, convergence and/or truncation error for finite values of Δt, and the space increments Δz and Δx.

20. Specification of Boundary Conditions

In Section III, the boundary conditions necessary for the solution of the differential equations were enumerated. These conditions apply equally to the difference equations and are of two kinds. At the upper boundary, the values of the temperature, specific humidity, specific moisture, geostrophic wind components, and thermal wind components are required. At the lower boundary, the fluxes of heat and vapor, together with the components of the horizontal wind, are required.

The first kind of data is to be provided independently of the boundary layer model. It is our present plan to specify these values in tests of the boundary-layer model by use of the predictions made with an Air Weather Service multi-level model or, when such are not available, from observed data. More particularly, the predicted values of temperature, specific humidity, and geopotential height for 850, 700, and 500 mb at six-hour intervals are used with linear interpolation to provide the needed quantities at 2000 meters above the ground at each time step.

In order to provide the lower-boundary conditions, we make use of the various formulas outlined in Section IV. These require for their evaluation the predictions made by the boundary-layer model at $z = h$, as well as the surface temperature and relative humidity which are currently provided by the schemes discussed in subsection 17.

VI

EXPERIMENTAL BACKGROUND

21. Preliminary Experiments

The initial experiments conducted with the model equations were simplified by using only two space dimensions (one vertical and one horizontal) and the use of idealized initial and boundary conditions. The variety of results obtained in this manner is not presented here, but these results were used to modify the various equations of the model. Some of these instances of model modification were pointed out in the preceding text. In this sense, the results presented in Section VII of this report have also led us to modify certain parts of the model. The section dealing with the use of the free-convective formulas is an example of such a change. Unfortunately, we did not have time to re-program this change into the model and, consequently, the experiments reported in Section VII do not permit us to evaluate its significance. This state-of-flux in the model formulation indicates that the model should be considered a base model, similar to a electronic engineer's breadboard design. In the following subsections, we will discuss the subsidiary analysis techniques used to process the observed data and to specify the exterior factors involved in the model.

22. The Analysis of Initial-Temperature and Humidity Data

We collected the synoptic upper-air and surface data (received via teletype) at the weather station of the TRC Service Corp. during the five-day period, 6 February—10 February, 1964. In order to process the radiosonde observations, we first used linear interpolation between the significant-level reports to obtain the temperature and dew points at the levels required in the model. This step was accomplished through the use of the computer program, "Sounding Construction," written at the UAC Computation Laboratory.

These data were available at the various radiosonde observing stations located within the geographical region to which the model was to be applied. In order to start the numerical computation of the forecast, these data must be available on a regular array of grid points. With the intention of automating, and

making objective, the analysis of the initial data, we had programmed a routine for interpolating from the data at the radiosonde stations onto the horizontal grid point array. The Successive Approximation Technique (SAT) system [41] for performing such an analysis was used. This technique requires the preliminary specification of a first guess to a grid-point analysis. We attempted to use this method with two types of initial guess[8]. The results were not satisfactory, principally due to the absence of a means of enforcing vertical consistency in the resulting grid-point data analysis. We therefore decided to abandon, for the time being, the attempt to completely automate the analysis.

The method finally adopted involved subjective analysis. The difference in temperature between successive levels in the vertical was computed for each reporting station. These numbers were then plotted on a base map. On each map, isopleths were drawn for the values of the vertical-temperature difference (proportional to the static stability of the layer). These isopleths were then used to interpolate the temperature differences onto the grid points. The data at the grid points on each map were then used in conjunction with a surface-temperature analysis to reconstruct the temperature, at each level, for every grid point.

In analyzing the humidity field, we used the results of the "Sounding Construction" program to compute the dew-point depression at each level. These were then analyzed in the manner used for the temperature difference. The final dew point distribution resulted from a combination of the independent analyses of temperature and dew-point depression.

23. The Analysis of the Geostrophic Wind

In Subsection 5, we noted that the geostrophic wind was assumed to vary linearly with the height through the boundary layer. It is rather straight forward to compute the geostrophic wind at the surface under the assumption that it is equivalent to that computed from sea-level pressures. Similarly, the computation

---

[8] These methods are given in the monthly progress report for July, 1964. (External Monthly Progress Report, Contract No. 11910, The Travelers Research Center, Inc.)

of the geostrophic wind in the upper-air surfaces of constant pressure may be computed directly. In practice, we interpolated the surface pressure and upper-air geopotential analyses into grid-point values, and evaluated, by finite difference approximation, the geostrophic-wind components at mean sea level, 850 mb and 700 mb. The sea-level components were used to evaluate u_g^0 and v_g^0 in Eqs. III-4a and b. The determination of the geostrophic-wind components, u_g^H and v_g^H, valid at the upper boundary of the model-boundary layer, was done by linear interpolation between the 850- and 700-mb geostrophic-wind components. This interpolation was based on the reported height of these pressure levels above the station.

24. Terrain Height and Surface Roughness

Figure 1 presents the distribution of the height above mean sea level of the grid points used in the computation discussed in Section VII. The heights are plotted in meters, with isopleths drawn at 100 meter intervals. The data used in arriving at these figures were taken from Berkofsky and Bertoni's report [2], and from several other sources. Where possible, we chose the grid-point values so as to preserve the large-scale gradients of height.

In Figure 2, the distribution of the surface-roughness coefficient used in the model experiments is given. These values were subjective estimates made with the help of some characteristic values of this quantity for various ground-cover characteristics presented by Kung and Lettau [23]. These values and their distribution are of course open to considerable criticism. One is not displeased, therefore, by the result of the subsequently reported experiment, which indicates that this coefficient's variation may not be overly significant for large-scale boundary-layer processes.

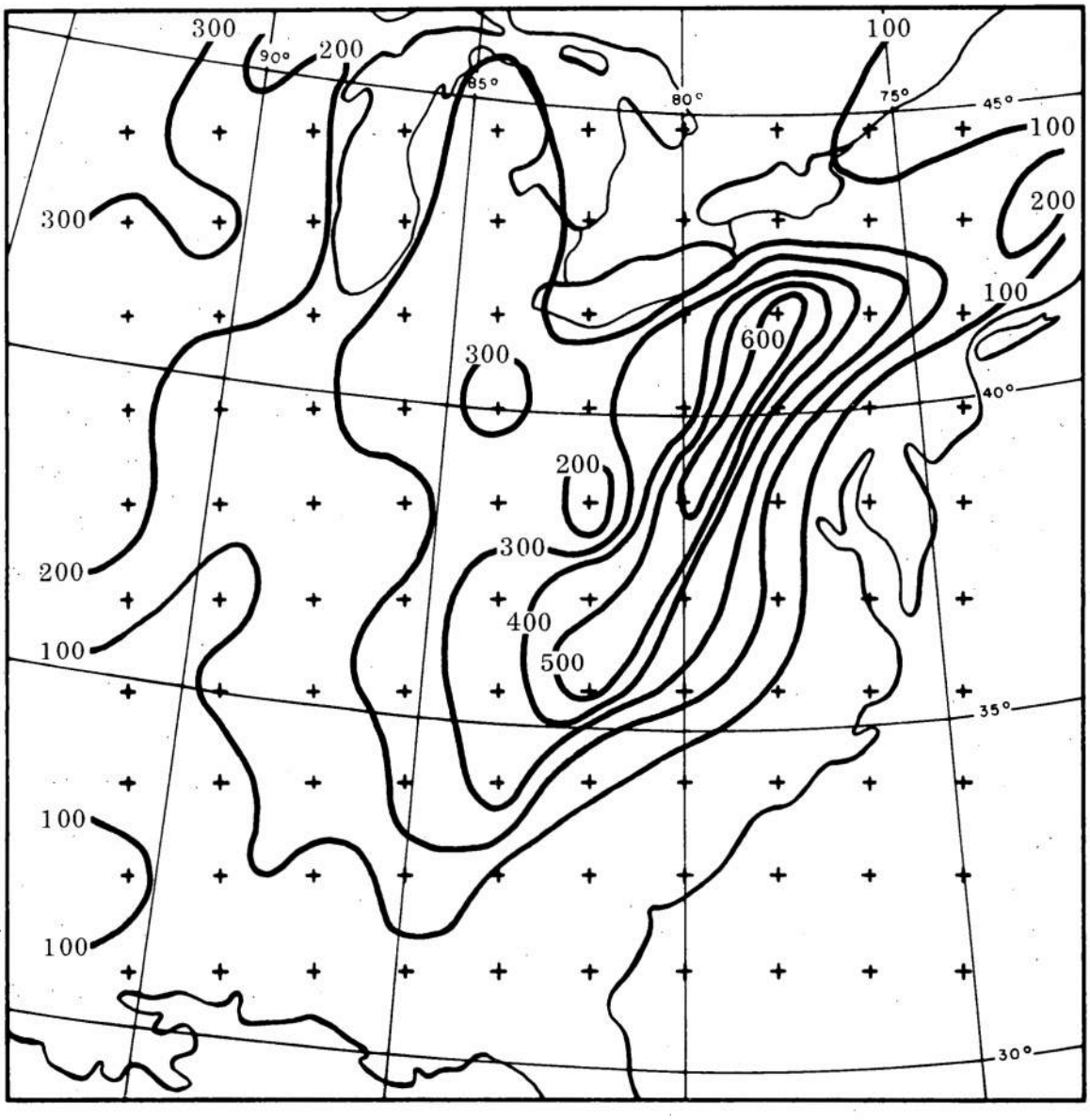

Figure 1. Distribution of terrain height (m).

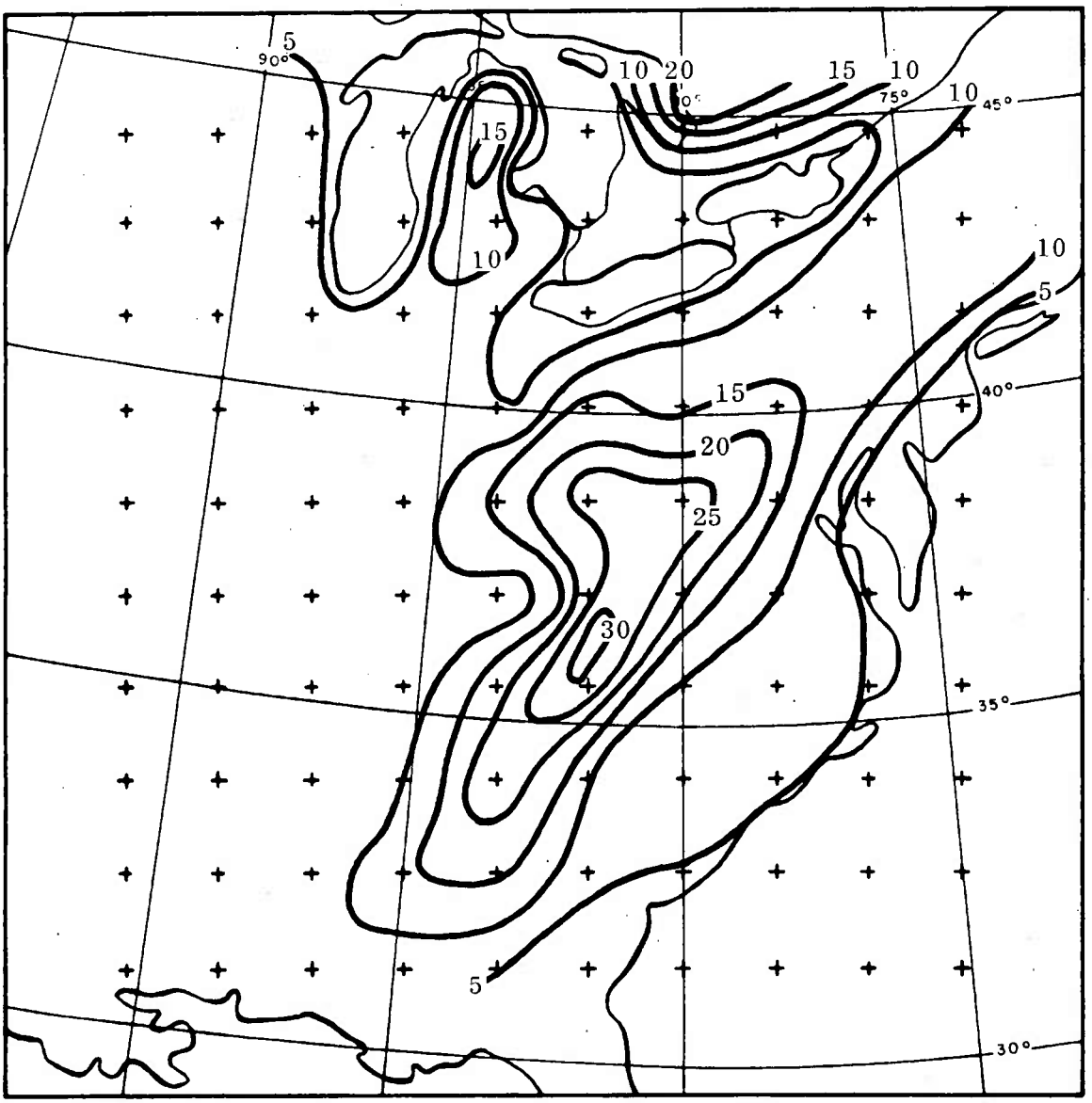

Figure 2. Distribution of surface roughness coefficient (m).

VII

EXPERIMENTAL RESULTS

25. The Synoptic Case and the Experiments Conducted

According to our original plans, we were to use for boundary conditions at the top of the boundary layer the temperature, relative humidity, and geopotential fields predicted by the cloud-forecasting technique being developed by the Computer Techniques Division at Headquarters, Air Weather Service (AWS)[9]. We were notified by AWS that this model would be run during the period, 6 February—11 February, 1964. Consequently, we collected synoptic data for this period and determined that the synoptic case studied would be selected from this time interval. The most interesting weather phenomena occurred at the beginning of this period in the region indicated in Figure 1. The experiments discussed in this section were all twelve-hour forecasts for the period 1200Z, 6 February—0000Z, 7 February, 1964.

Synoptic charts for the initial and final times of this period are presented in Figures 3 and 4. Throughout this forecast period, low cloudiness covered the greater part of the region of interest. At the initial time, precipitation was occurring in a large, crescent-shaped area. By the end of the period, the precipitation was confined predominantly within the northeastern quadrant of the region, with a southward-oriented tongue along the Appalachian Mountains. This development was associated with a rapid (25 knots) eastward displacement of the low-pressure system and the northeastward movement of a cyclogenetic area originally located in eastern North Carolina.

The basic prediction obtained with the model is denoted here as experiment number two. (An error in the specification of the input data was made in the first experiment.) Additional experiments were made with the modifications

---

[9] Refer to the monthly progress report for June, 1964 for the reasons for changing this plan. (External Monthly Progress Report, Contract No. 11910, The Travelers Research Center, Inc.).

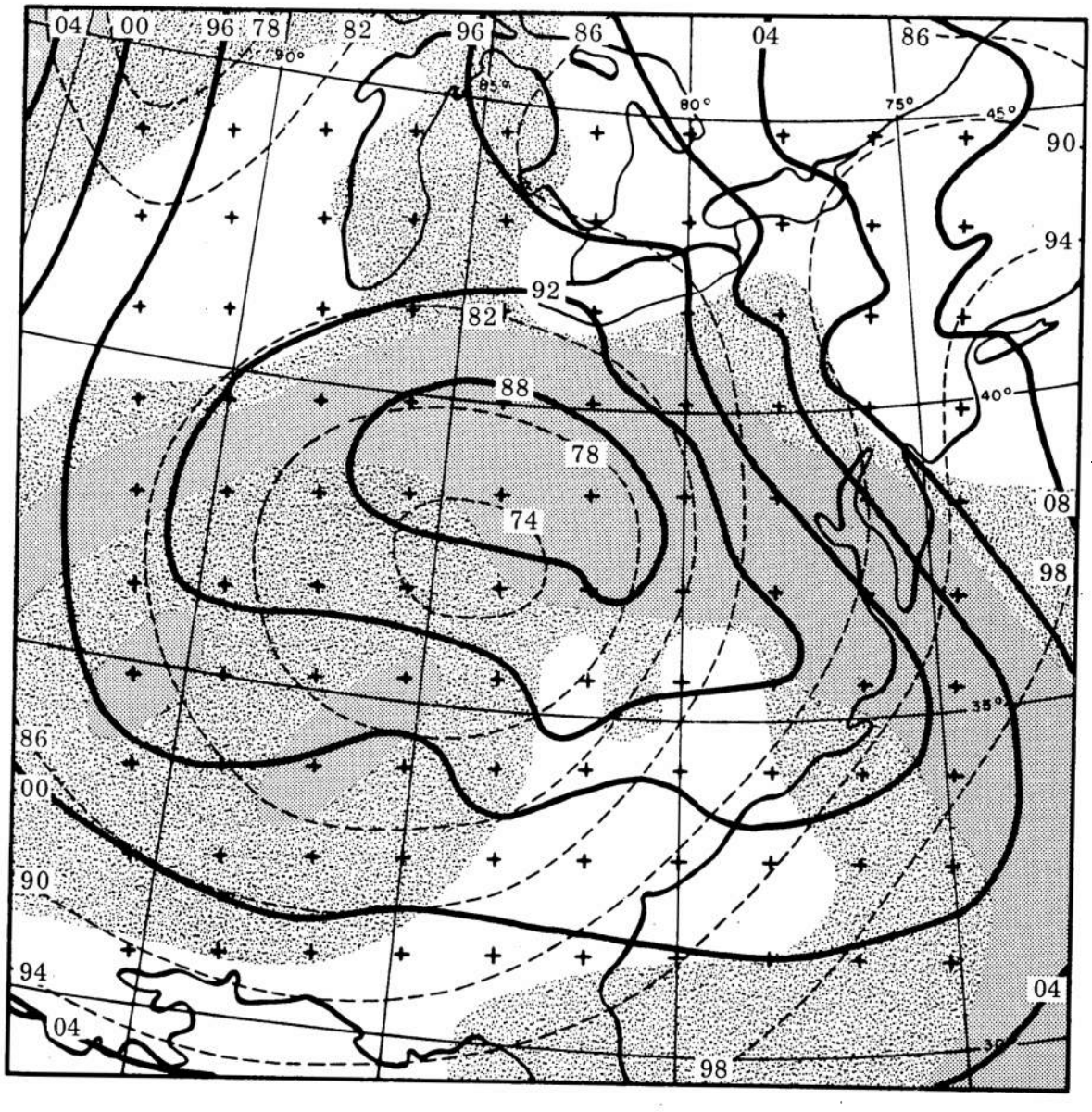

Figure 3. Synoptic chart; 1200Z, 6 Feb. 1964. ━ Sea level isobars
--- 700 mb geopotential contours ▭ Broken to overcast ▭ Precipitation

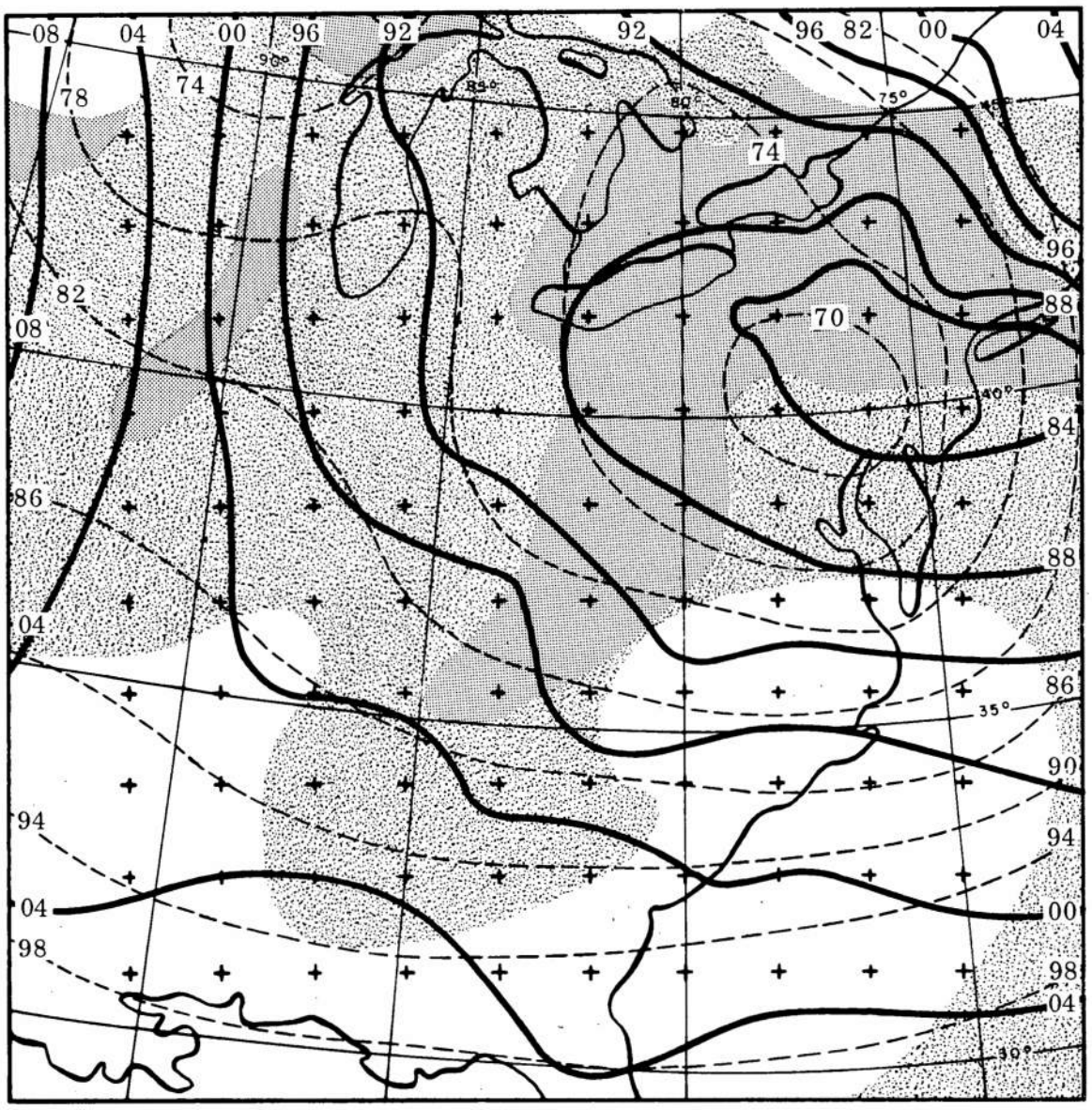

Figure 4. Synoptic chart; 0000Z, 7 Feb. 1964. ▬ Sea level isobars
--- 700 mb geopotential contours ▭ Broken to overcast ▭ Precipitation

indicated in Table II. All the experiments utilized thirteen grid points in the vertical. They were located at 50, 100, 150, 220, 300, 400, 500, 650, 850, 1150, 1550 and 2000 m above the terrain at the grid point. A total of one hundred grid-points was used in the horizontal. There are ten columns, numbered from L = 1 to L = 10, from west to east and ten rows, numbered from M = 1 to M = 10, from south to north.

The objective of these experiments was to estimate the general predictive capability of the model and to determine if it might be simplified by various modifications without affecting its predictive accuracy. In what follows, we discuss our analysis of these experiments. As may be easily visualized, the output from such a series of experiments is voluminous. The approach adopted for our analysis of results is basically subjective. It must be clear that we cannot reproduce here more than a few selected figures. We hope that these will be suggestive of the results obtained and serve to illustrate some of our remarks.

26. The Basic Experiment and its Verification

Experiment 2 was based on the complete model outlined in the preceding text. The only significant differences between the model outlined there and that used are as follows.

First, the procedure for computing the various eddy fluxes did not include the free-convective formulas. Whenever θ_* was computed to be complex, we set the radical in Eq. IV-20 equal to unity. This should have the effect of underestimating the heat flux in unstable conditions.

Secondly, the boundary conditions at the top of the transition layer were taken from our analysis of observations at the initial and final times of the forecast interval. The intermediate values were specified by assuming a linear variation in time.

The prediction made in experiment two is indicated in Figure 5, which is a constant-level chart showing the temperature and relative humidity forecast at the level 1500 m above mean sea level. Figures 6 and 7 are similar charts showing the analysis of the initial and verifying data.

Consider first Figures 5 and 6. The cloudiness at this level may be associated with the shaded regions, where the heavier shaded region is an area of maximum

TABLE II
SYNOPSIS OF EXPERIMENTS CONDUCTED

Exp. no.	Factor varied	Expression of variation
3	Time step	Δt varied from 15 min in Exp. 2 to 30 min
4	Surface roughness coefficient	z_0 set equal to uniform, constant value of 1 cm
5	Terrain induced vertical velocity	$\hat{w}$ was set equal to zero
6	Lateral boundary condition	Normal component of advection neglected on the lateral boundaries
7	Mixing coefficient	Neglected variation of K with height and stability
8	Lateral boundary condition	Both components of advection neglected on lateral boundary points at which inflow exists
9	Lateral boundary condition	Both components of advection neglected on lateral boundaries

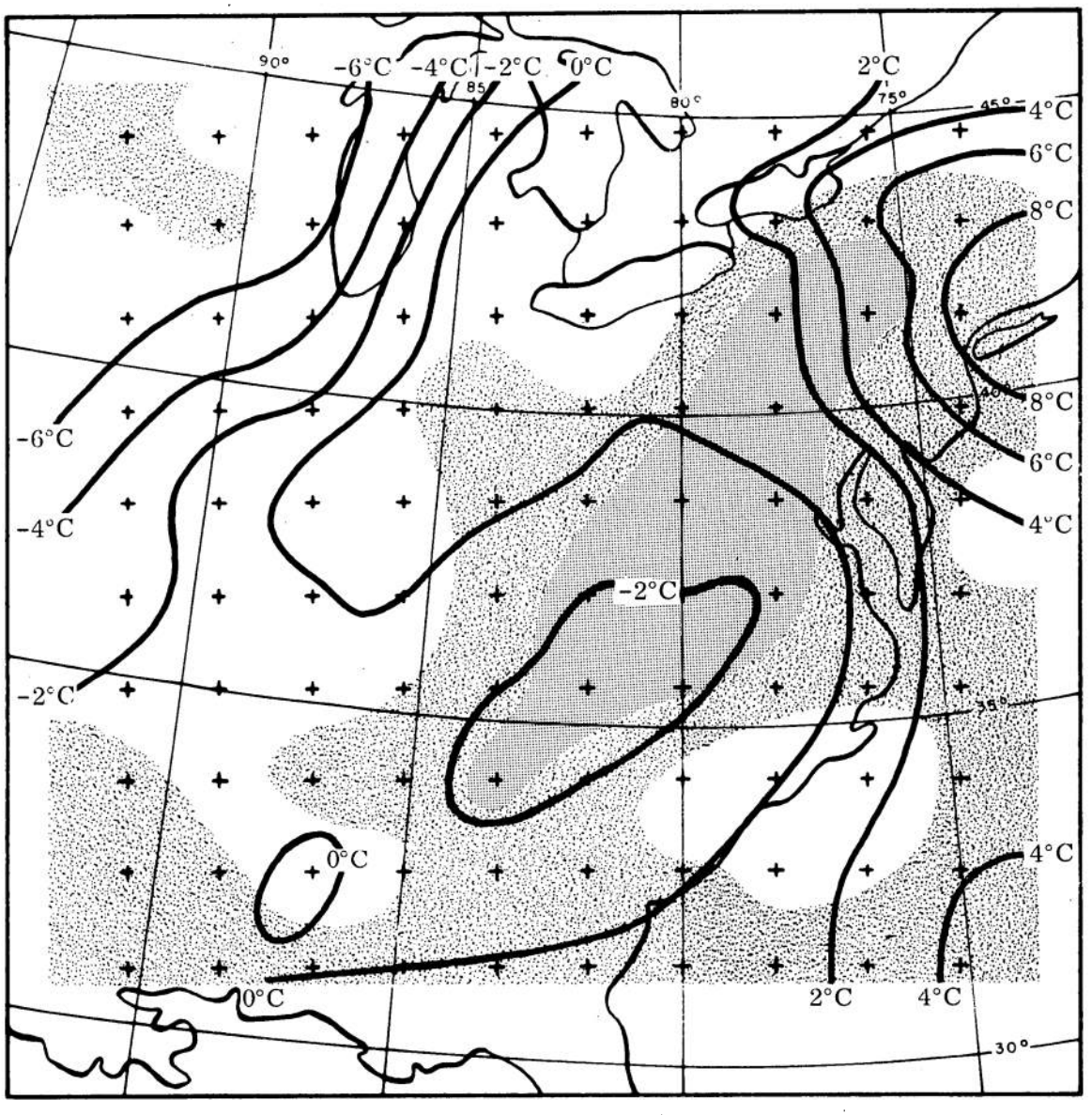

Figure 5. Constant level analysis (z = 1500 m); Experiment no. 2 forecast; 0000Z, 7 Feb. 1964. RH < 77% RH > 77% RH > 93%

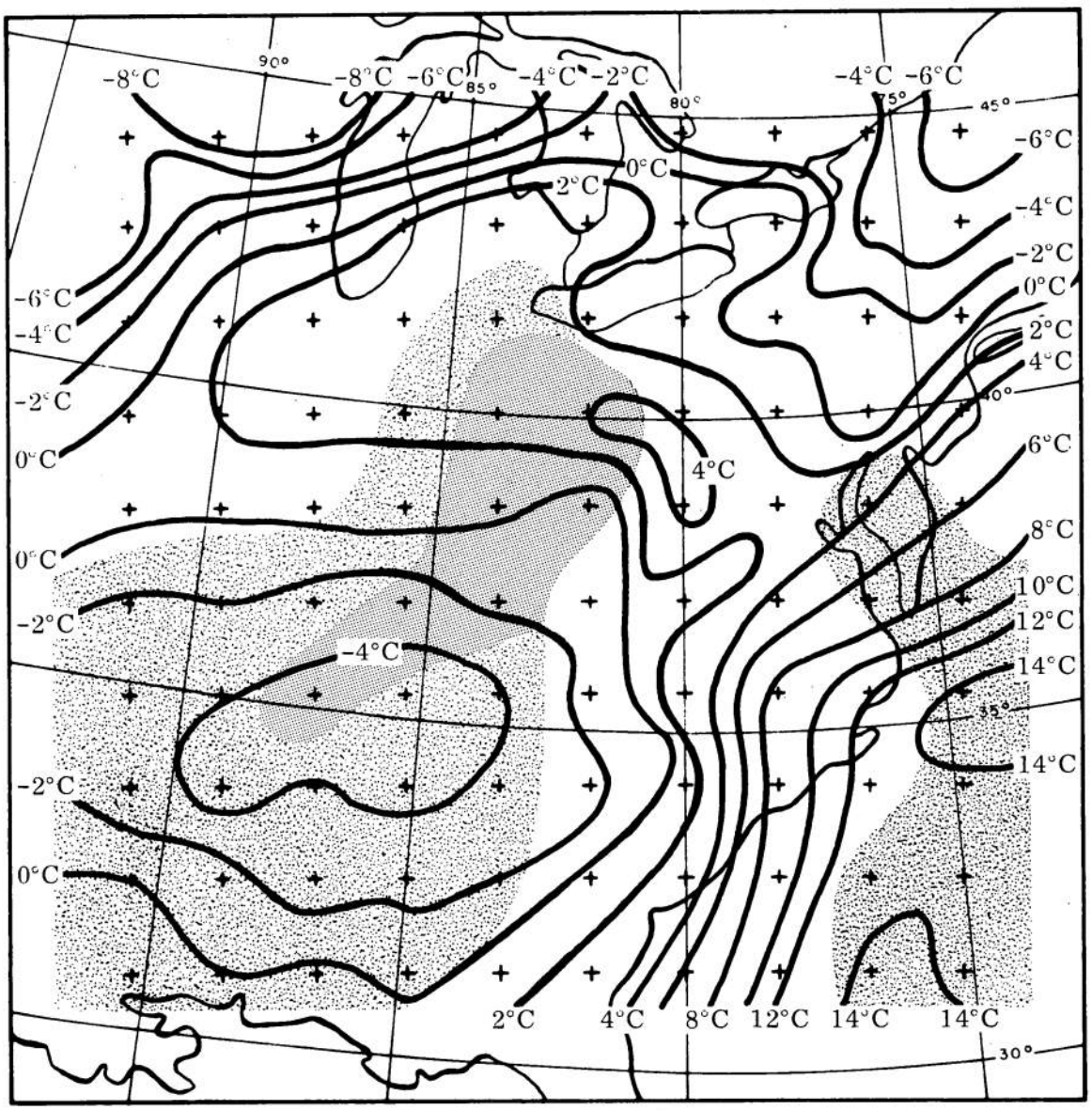

Figure 6. Constant level analysis (z = 1500 m); 1200Z, 6 Feb. 1964.
$T-T_d > 3°C$ $T-T_d \leq 3°C$ $T-T_d \leq 1°C$

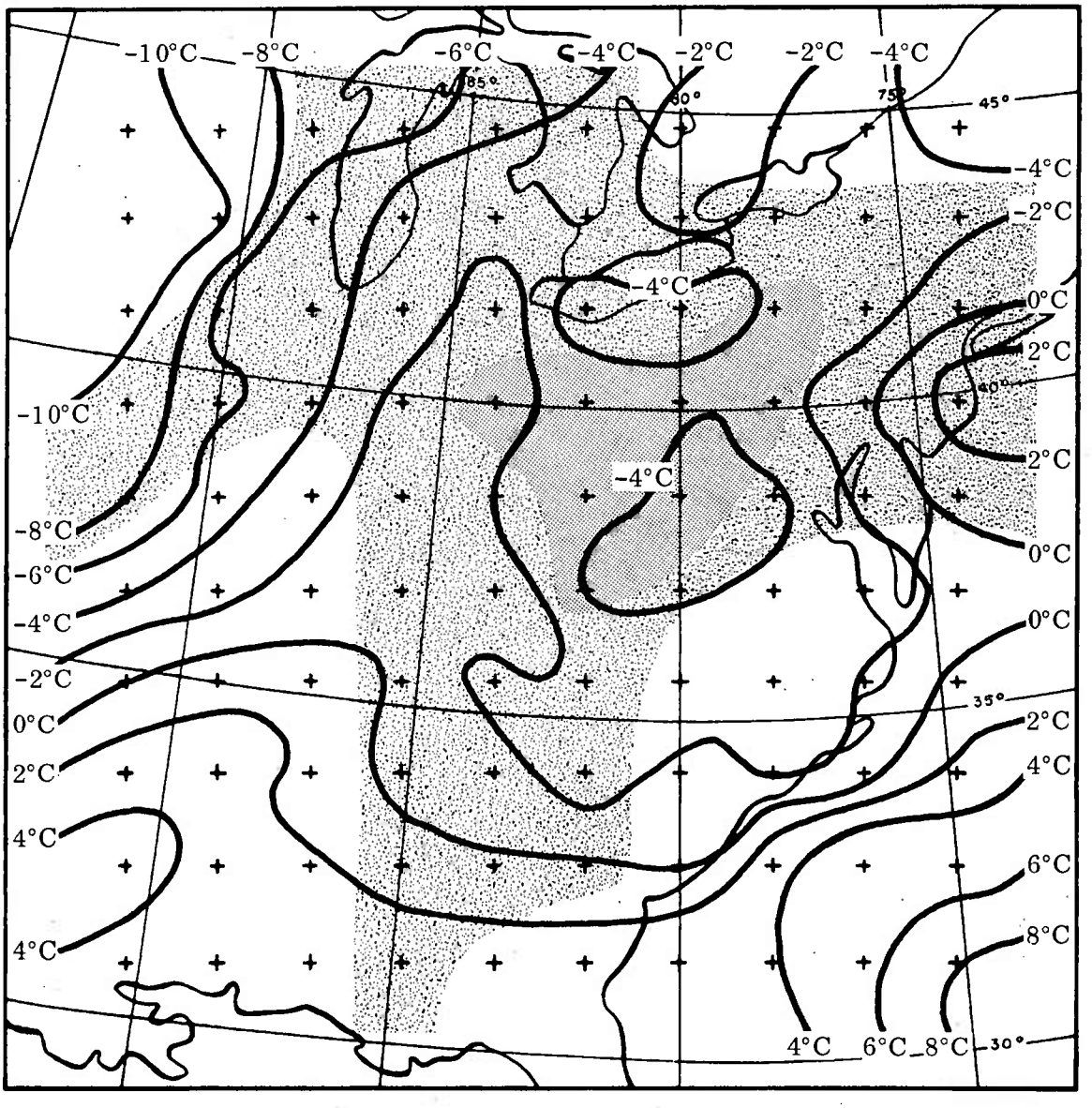

Figure 7. Constant level analysis (z = 1500 m); 0000Z, 7 Feb. 1964.

$T-T_d > 3°C$ $T-T_d \leq 3°C$ $T-T_d \leq 1°C$

likelihood of overcast cloud. The forecast displacement and enlargement of this area agrees broadly with the observed change in cloudiness and precipitation (see Figures 4 and 7). The temperature forecast in the central portion of the map is also commensurate with the observed-temperature variation. Near the boundaries of the region, the forecast-temperature field is in considerable error. This is discussed in more detail in Subsection 31.

Figures 8 and 9 depict vertical cross-section analyses along the sixth grid row (counting from one at the southern-most grid row). Again, except for the region near the left- and right-hand boundaries, the temperature and humidity forecasts agree well with the observed distributions.

In Tables III and IV, the predicted vertical velocities are given. The units are cm sec^{-1}, and positive values indicate upward moving air. The terrain-induced velocities ($\hat{w}$) are relatively large compared with the frictionally-induced velocities (w). Note that it is the large value of $\hat{w}$ at L = 7 and M = 6 which is associated with the column of maximum shading in Figure 10. Additionally, we may note the large negative value of $\hat{w}$ at grid point, L = 8, M = 6. The importance of this terrain-induced velocity field will be discussed in subsection 29.

Table V presents the error in the temperature forecast at three different levels in Experiment 2. In view of our use of linear interpolation in time between observed temperatures as the upper-boundary condition, the errors in temperature appear to be quite large. Tables VI, VII, and VIII present the grid-point distribution of the differences between observed and predicted temperatures. The largest differences are noted near the lateral boundaries. This result was expected (see Section IV). The errors and their distribution may be accounted for in part by the distribution of the observations used to specify the initial and final distributions of data. In addition, the linkage between the upper-boundary conditions (2000 m above ground) and the interior grid points is predominantly associated with vertical advection. The somewhat greater magnitude of the error at 1550 m indicates that this process is not overly effective in forcing the interior temperatures to follow those applied at the upper boundary. We plan to follow up this implication in future experiments to determine the possibility of

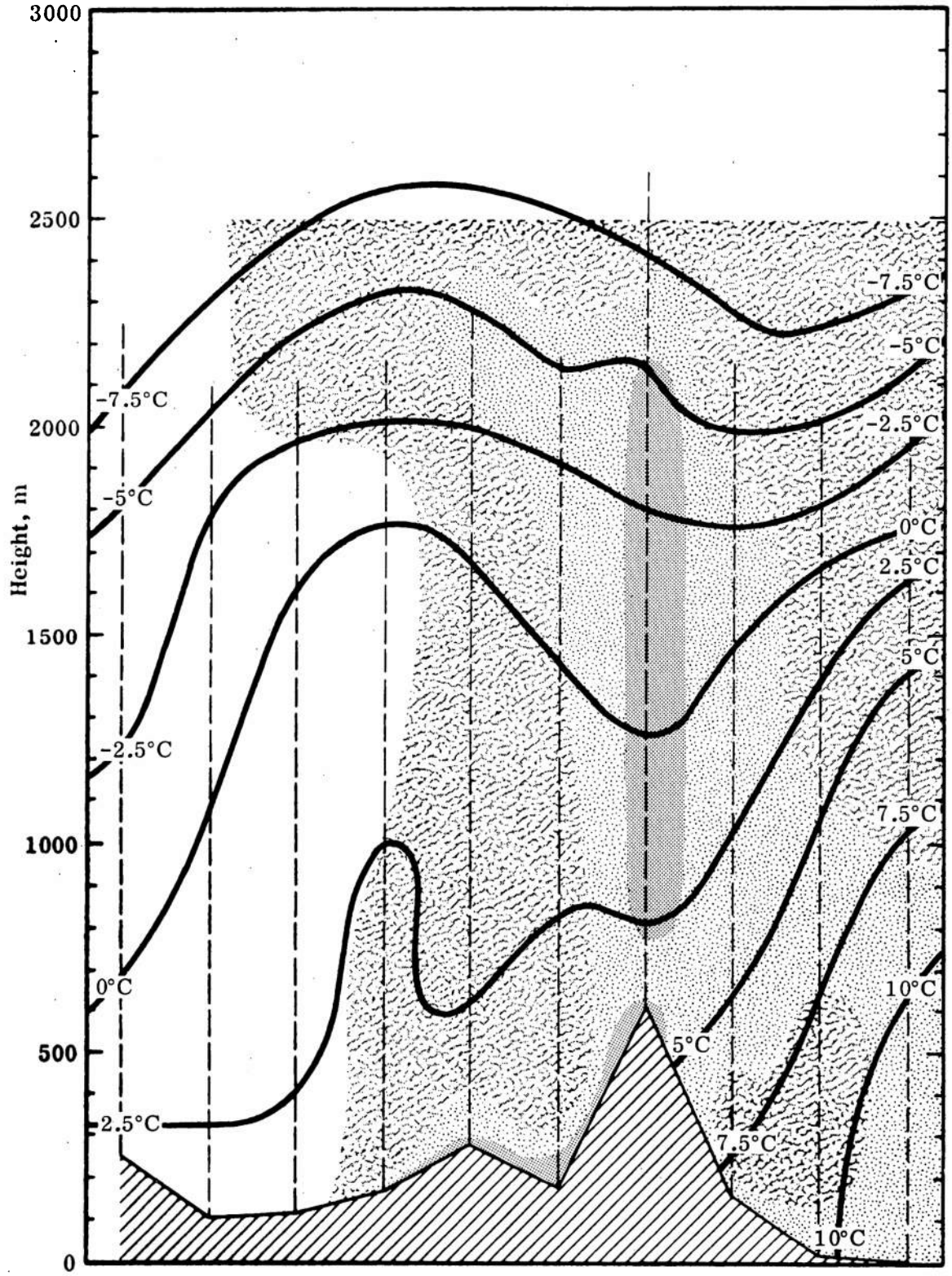

Figure 8. Vertical cross section (M = 6); Experiment no. 2 forecast; 0000Z, 7 Feb. 1964. RH ≥ 100% RH ≥ 93% RH ≥ 77% RH < 77%

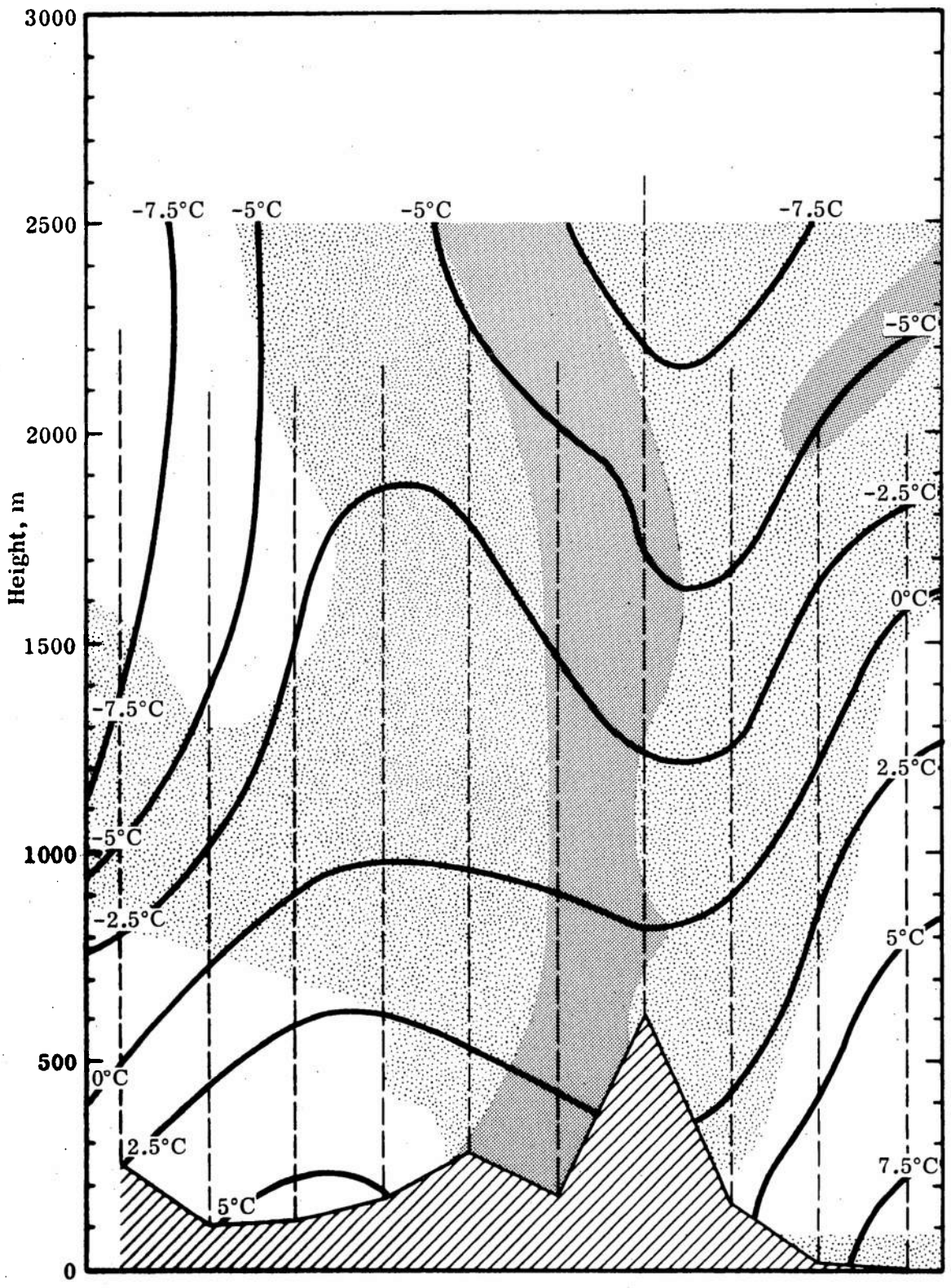

Figure 9. Vertical cross section (M = 6); observed; 0000Z, 7 Feb. 1964.

$T-T_d > 3°C$ $T-T_d \leq 3°C$ $T-T_d \leq 1°C$

TABLE III

DISTRIBUTION OF w (cm sec^{-1}) FROM EXPERIMENT NO. 2 (frictionally induced)
AT z = 1000 m ABOVE MSL

M \ L	1	2	3	4	5	6	7	8	9	10
10	-	-	-	-	-	-	-	-	-	-
9	-	-0.2	0.4	0.7	0.2	0.0	-0.1	0.1	1.4	-
8	-	-0.4	0.2	0.6	0.6	~ 0.5	0.6	0.9	1.7	-
7	-	-0.3	0.3	0.5	0.7	1.1	1.1	1.3	1.1	-
6	-	0.3	0.4	0.4	-0.4	0.6	1.0	0.4	0.5	-
5	-	1.0	0.3	-0.5	-0.4	1.0	1.0	-0.2	0.2	-
4	-	0.1	-0.1	-0.8	0.4	0.9	-0.2	-0.5	-0.5	-
3	-	-0.8	-0.6	0.1	0.1	-0.9	-1.1	-0.7	-0.7	-
2	-	-0.3	-1.0	-0.5	0.2	-0.5	-0.2	-0.7	0.3	-
1	-	-	-	-	-	-	-	-	-	-

TABLE IV

DISTRIBUTION OF $\hat{w}$ (cm sec^{-1}) FROM EXPERIMENT NO. 2 (terrain induced)
AT z = 1000 m ABOVE MSL

M \ L	1	2	3	4	5	6	7	8	9	10
10	-	-	-	-	-	-	-	-	-	-
9	-	1.4	-0.6	-0.1	0.1	0.0	0.1	0.4	-2.0	-
8	-	-1.2	-0.2	0.4	0.1	-0.3	0.1	2.6	3.2	-
7	-	-0.3	-0.1	0.3	0.6	0.7	0.5	-1.0	-0.5	-
6	-	-0.6	-0.4	-0.3	0.7	-1.8	5.3	-6.2	-1.6	-
5	-	-0.2	0.5	1.0	1.2	2.9	-1.4	-3.1	-1.8	-
4	-	0.4	0.7	0.1	1.0	2.8	-4.1	-1.9	-0.8	-
3	-	0.1	0.9	0.1	1.2	-2.8	-1.3	-0.6	-0.2	-
2	-	-0.1	-0.6	0.6	-1.2	-0.6	-0.2	-0.2	0.0	-
1	-	-	-	-	-	-	-	-	-	-

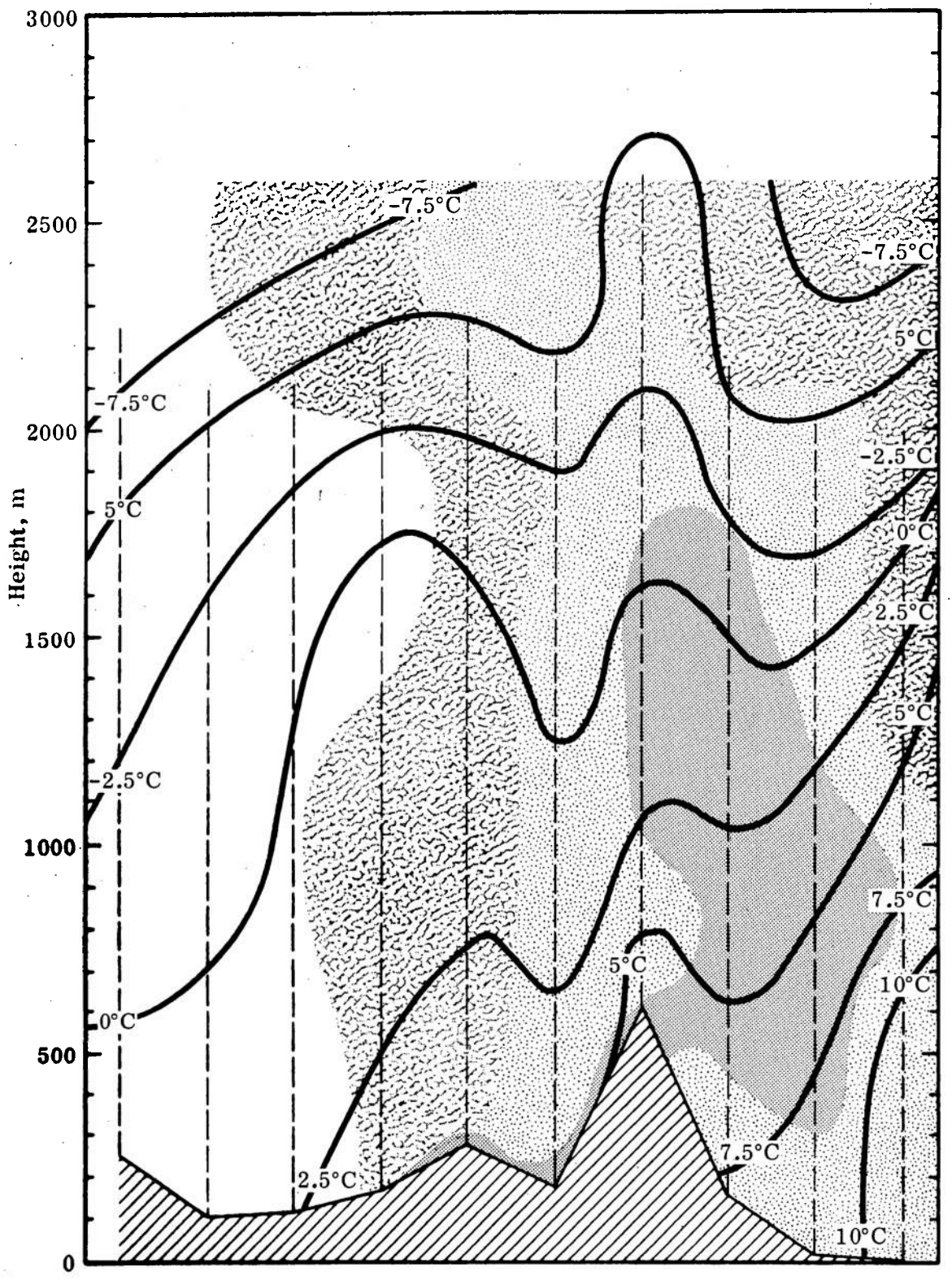

Figure 10. Vertical cross section (M = 6); Experiment no. 5 forecast; 0000Z, 7 Feb. 1964. RH ≥ 100% RH ≥ 93% RH ≥ 77% RH < 77%

TABLE V

DISTRIBUTION OF ERROR (observed less forecast) IN TEMPERATURE PREDICTED IN EXPERIMENT NO. 2 OVER 100 GRID POINTS AT THREE LEVELS IN THE VERTICAL (measured above local terrain), AND OBSERVED TEMPERATURE CHANGES (persistence)

Temperature error (°C)	Class Mean (°C)					
	Experiment no. 2			Persistence		
	1550 m	1150 m	500 m	1550 m	1150 m	500 m
-14	—	—	—	2	1	—
-13	—	—	—	—	1	—
-12	—	—	—	1	2	—
-11	—	1	—	1	1	1
-10	1	1	—	3	2	1
-9	2	1	—	2	9	4
-8	1	2	—	6	6	4
-7	4	1	2	10	3	10
-6	3	3	—	9	7	6
-5	5	4	4	4	8	10
-4	7	17	9	5	8	8
-3	14	9	12	9	8	8
-2	16	9	9	7	6	5
-1	10	12	16	8	2	6
0	5	9	2	4	7	8
+1	7	6	4	4	11	12
+2	3	9	12	3	6	5
+3	14	7	15	7	4	6
+4	6	7	7	4	4	—
+5	1	—	5	5	1	3
+6	1	1	3	3	1	3
+7	—	1	—	2	2	—
+8	—	—	—	1	—	—
Avg.	3.09	3.02	2.84	4.40	4.60	3.90

TABLE VI

EXPERIMENT NO. 2 TEMPERATURE ERROR (observed less forecast) AT z = 500 m in °C

M \ L	1	2	3	4	5	6	7	8	9	10
10	-4.3	-1.5	2.0	-2.7	-7.1	-4.7	-0.7	-1.8	-2.8	-3.3
9	-4.4	-0.8	4.0	-0.6	-2.7	-3.2	-2.1	-3.2	-3.8	-5.4
8	-3.4	1.0	2.4	-0.9	-1.9	-4.5	-3.6	-1.2	-4.4	-7.2
7	-2.3	-0.7	0.4	-1.0	-0.5	-2.3	-2.1	-2.6	-3.4	-4.7
6	-2.1	-0.7	0.4	-0.7	-1.0	-1.7	-2.5	-3.5	-3.8	-4.4
5	2.7	1.4	1.5	1.6	2.0	-1.0	-0.6	-0.7	-2.7	-3.9
4	4.9	5.1	4.3	2.6	1.7	2.7	1.5	0.6	-0.7	-2.6
3	5.4	6.3	3.7	2.8	2.6	1.8	2.4	2.2	0.5	-0.6
2	5.8	4.3	2.6	2.7	2.8	2.8	2.8	5.6	5.1	1.6
1	4.8	3.7	2.9	2.4	3.2	4.3	4.3	3.4	3.0	2.8

TABLE VII

EXPERIMENT NO. 2 TEMPERATURE ERROR (observed less forecast) AT z = 1150 m in °C

M \ L	1	2	3	4	5	6	7	8	9	10
10	-4.8	-2.3	0.4	-1.3	-4.3	-4.3	-1.9	-2.7	-5.5	-7.5
9	-5.2	-2.4	1.7	-0.7	-3.5	-4.2	-2.9	-6.5	-8.8	-10.7
8	-4.1	-1.1	-0.3	-1.8	-3.2	-6.0	-6.1	-4.7	-7.9	-9.6
7	-3.6	-3.9	-2.9	-2.0	-1.1	-4.0	-4.0	-3.9	-4.8	-4.0
6	-4.2	-4.1	-3.1	-3.0	-2.4	-2.8	-3.8	-4.1	-3.6	-3.5
5	-0.6	-1.3	-1.2	-1.2	-0.1	-2.6	-2.2	-0.9	-2.0	-3.1
4	2.4	3.1	-0.7	0.1	-0.2	-1.2	0.4	-0.2	-0.7	-1.7
3	4.4	4.2	2.5	1.6	1.9	0.7	1.0	0.8	-0.2	-0.2
2	6.8	4.3	1.2	1.4	2.1	1.9	1.7	4.1	3.9	1.4
1	5.7	3.9	2.4	2.1	2.5	3.5	3.2	3.0	2.8	3.1

TABLE VIII

EXPERIMENT NO. 2 TEMPERATURE ERROR (observed less forecast) AT z = 1550 m in °C

M \ L	1	2	3	4	5	6	7	8	9	10
10	-3.1	-1.2	1.1	-0.8	-4.9	-6.0	-1.9	-3.3	-6.9	-8.3
9	-2.8	-0.3	3.3	-0.6	-5.7	-4.9	-2.3	-6.7	-8.8	-9.7
8	-2.5	0.9	0.9	-1.8	-5.1	-6.8	-6.3	-5.2	-7.0	-8.9
7	-3.1	-2.5	-1.9	-2.2	-1.9	-4.3	-4.3	-4.3	-5.0	-3.1
6	-4.3	-4.0	-2.6	-2.9	-1.8	-1.6	-2.5	-3.6	-3.2	-3.4
5	-1.5	-1.7	-1.4	-1.3	0.3	-2.1	-2.2	-1.4	-3.2	-3.9
4	1.6	3.0	2.5	0.0	-0.3	1.4	-0.5	-1.8	-2.3	-2.4
3	4.0	4.2	3.6	2.5	1.7	-0.4	-1.1	-2.5	-1.8	-0.9
2	5.8	4.8	3.1	2.6	2.2	0.9	-0.9	1.9	3.1	1.2
1	4.4	4.0	3.4	3.7	3.3	3.3	2.8	2.6	3.0	3.5

dispensing with independent forecasts of the upper-boundary temperature and humidity.

Tables IX, X, and XI present the observed-temperature changes during the forecast interval at the various grid points. A comparison of these observed changes with the errors in the forecast indicates that at many of the points with large observed-temperature changes the predictions are remarkably accurate.

It is our opinion that the results of this experimental forecast are quite encouraging. The synoptic case used did not lend itself to a detailed evaluation of the potential of the model for developing low cloudiness. The model does seem capable of translating cloud fields, and in some instances (see Subsection 29) of dissipating them.

27. Influence of the Time Step Used

In our analysis of the computational stability of the model in Section V, it was determined that linear stability was assured if the time step, Δt, did not exceed the time required for an air parcel to traverse one grid interval. It was indicated that the time step could be as long as forty minutes, if the grid interval was 100 km and the average wind 40 m sec^{-1}. A question remained as to the accuracy of the solution which would result if the time step was made relatively large.

To get an idea of this influence, we compared two forecasts which differed only in the time step. In experiment three, Δt was set to thirty minutes. These predictions were compared with those obtained in experiment two for which Δt was fifteen minutes. The largest temperature difference between the two forecasts was 0.6°C. At most grid points, the difference was ± 0.1°C. The humidity distributions were similarly unaffected by this change in time step.

The conclusion that the time step may be safely increased to thirty minutes must be examined further for cases in which turbulent exchange plays a greater role than in the synoptic case studied in this series of experiments. It does seem safe, however, to use the longer time step in those instances when advective processes predominate in the boundary layer.

TABLE IX

OBSERVED TEMPERATURE CHANGE AT z = 500 m in °C

M \ L	1	2	3	4	5	6	7	8	9	10
10	-5.2	-2.2	1.7	-2.6	-7.1	-6.0	-2.9	-4.5	-4.7	0.1
9	-4.6	-7.0	-3.3	-4.7	-5.5	-7.6	-7.2	-8.1	-0.6	1.0
8	-8.8	-6.8	-6.7	-4.6	-3.9	-5.3	-6.6	-1.4	-0.8	2.0
7	-8.7	-6.4	-6.5	-3.4	-2.7	-6.3	-6.6	-3.1	2.7	2.6
6	-7.0	-3.9	-2.8	-2.3	-2.4	-2.3	-7.7	-4.9	-1.5	-0.6
5	1.0	-0.3	1.1	1.1	0.3	-4.2	-3.8	-3.7	-3.9	-4.4
4	5.3	5.1	4.6	3.0	1.1	0.4	-4.8	-9.2	-9.8	-10.5
3	6.0	6.4	2.4	2.6	1.3	0.5	-0.1	-5.8	-8.9	-8.2
2	5.8	2.6	1.1	1.2	1.2	1.1	0.2	-1.0	-4.7	-6.7
1	2.6	1.8	-0.3	0.3	1.5	0.9	-0.5	-3.4	-6.2	-3.7

TABLE X

OBSERVED TEMPERATURE CHANGE AT z = 1150 m in °C

M \ L	1	2	3	4	5	6	7	8	9	10
10	-5.2	-2.3	1.6	-2.1	-0.4	-2.9	0.7	0.7	-0.8	-2.9
9	-5.1	-8.6	-4.9	-5.5	-5.3	-6.6	-3.1	-5.2	1.4	1.7
8	-9.4	-8.7	-8.6	-5.8	-4.7	-6.3	-5.9	-0.4	-1.6	1.0
7	-10.2	-9.5	-8.5	-4.3	-3.4	-7.5	-7.6	-3.8	1.3	-0.2
6	-8.9	-6.2	-4.3	-2.9	-2.6	-2.7	-8.8	-6.7	-4.3	-4.2
5	-1.8	-1.8	0.4	1.3	0.9	-4.1	-3.7	-6.2	-7.6	-8.3
4	3.5	4.7	2.0	3.7	2.5	0.5	-6.2	-12.3	-13.3	-13.9
3	5.8	7.1	3.3	3.6	1.9	0.5	-2.2	-9.0	-12.1	-10.5
2	7.0	3.9	2.0	1.5	1.0	-0.3	-2.7	-4.3	-7.7	-8.4
1	3.4	2.6	-0.3	0.9	0.3	-1.2	-3.6	-6.5	-8.6	-4.7

TABLE XI
OBSERVED TEMPERATURE CHANGE AT z = 1550 m in °C

M \ L	1	2	3	4	5	6	7	8	9	10
10	-2.4	-0.1	2.7	-2.1	-1.3	-3.3	1.4	1.2	-0.9	3.0
9	-1.8	-5.6	-3.2	-5.9	-7.2	-6.9	-1.3	-3.3	2.5	3.5
8	-7.0	-5.9	-7.0	-6.0	-6.3	-6.5	-4.9	0.0	-0.9	1.4
7	-8.9	-7.4	-5.8	-4.4	-3.7	-7.0	-6.7	-3.6	-0.8	-0.8
6	-8.1	-5.1	-2.8	-1.8	-1.5	-1.0	-7.6	-6.9	-5.2	-5.6
5	-1.8	-1.1	-1.8	-2.9	-2.9	-2.6	-4.0	-6.8	-9.5	-9.5
4	3.1	5.2	6.9	5.9	4.6	1.6	-5.9	-2.9	-14.2	-14.1
3	4.3	7.7	6.3	5.0	3.9	1.2	-2.9	-11.1	-12.4	-10.1
2	3.7	4.8	7.1	5.9	3.3	0.3	-4.8	-5.9	-7.9	-7.8
1	2.0	1.6	3.4	4.9	2.9	-0.3	-3.6	-7.6	-8.7	-7.5

28. Influence of the Roughness-coefficient Variation

The roughness coefficient, z_0, was assigned a constant value of 1.0 cm in experiment four. The principal influence of this modification might be expected to show up in the frictionally-induced vertical-velocity component, w. Table XII gives the distribution of w. Although the percent changes in this quantity are relatively large, they are almost negligible in comparison with the difference between w and $\hat{w}$ (see Tables III and IV). An examination of the temperature and moisture forecasts showed that this modification had negligible impact on the predicted values of temperature and relative humidity.

Tables XIII and XIV present the values of the friction velocity (cm sec^{-1}) and heat flux (millicals cm^{-2} min^{-1}) computed at 00Z, 7 February, 1964 in experiments two and four. Both quantities reflect the variation of z_0 between the experiments. The fact that such variations were not effective in modifying the predicted fields implies that, in this synoptic case, the eddy-transport mechanisms were of secondary importance.

29. Influence of the Terrain-induced Vertical Velocity

In experiment five, we deleted the terrain-induced vertical velocity, $\hat{w}$, from the prediction equations. Figure 11 displays the predicted temperature and humidity distribution at the constant level—1500 m above mean sea level. It is to be expected, of course, that these predictions will differ from those obtained in experiment two in the vicinity of the major terrain features (see Figure 1). That this is true is shown in Table XV, which gives the vertical average of the absolute value of difference in temperature forecast in the two experiments.

Figures 8, 9, and 11 display vertical cross-section analyses of the temperature and humidity as observed and forecast in these two experiments. The rather large value of $\hat{w}$ at gridpoint L = 8, M = 6 in Table IV, was associated with the dissipation of low cloudiness on the leeward side of the Appalachians. When $\hat{w}$ was neglected in experiment five, high humidities were predicted in this region. It seems quite clear that the inclusion of this process of terrain-induced vertical motion within the model is important.

TABLE XII

DISTRIBUTION OF w(cm sec^{-1}) FROM EXPERIMENT NO. 4 AT z = 1000 m ABOVE MSL

M \ L	1	2	3	4	5	6	7	8	9	10
10	-	-	-	-	-	-	-	-	-	-
9	-	-0.2	0.4	0.6	0.1	-0.1	-0.2	0.2	1.4	-
8	-	-0.3	0.1	0.5	0.4	0.4	0.5	0.8	1.4	-
7	-	-0.2	0.2	0.4	0.5	0.8	0.8	1.0	1.0	-
6	-	0.3	0.3	0.3	-0.3	0.5	1.2	0.4	0.6	-
5	-	0.8	0.3	-0.4	-0.4	0.8	1.2	0.1	-0.1	-
4	-	0.1	-0.1	-0.8	0.1	0.9	0.3	-0.3	-0.6	-
3	-	-0.8	-0.5	-0.1	0.1	-0.5	-0.8	-0.5	-0.4	-
2	-	-0.2	-1.2	-0.4	0.4	-0.3	0.1	-0.6	0.3	-
1	-	-	-	-	-	-	-	-	-	-

TABLE XIII

FRICTION VELOCITY (cm sec^{-1}) COMPUTED FOR 00Z, 7 FEB. 1964 BY EXPERIMENT NO. 2 (lower values) AND EXPERIMENT NO. 4 (upper values)

M \ L	1	2	3	4	5	6	7	8	9	10
10	40.6	50.9	50.7	23.4	12.6	9.2	30.6	39.2	61.6	69.3
	46.3	58.2	57.6	23.8	15.3	9.2	38.3	47.0	70.5	83.9
9	41.0	45.6	45.7	29.4	19.3	21.8	31.6	46.5	62.7	84.0
	46.7	52.1	52.2	29.4	22.9	21.8	31.6	46.5	75.9	102.1
8	35.7	40.6	45.4	35.3	29.4	29.7	33.7	29.0	23.8	51.5
	40.7	46.2	51.8	40.2	33.4	29.7	38.3	34.7	28.4	62.1
7	36.2	41.0	40.5	31.4	36.4	37.3	28.3	28.2	23.8	18.9
	41.2	46.7	46.2	35.7	41.4	46.0	34.8	34.6	28.4	18.9
6	41.2	32.2	31.9	32.4	41.8	50.0	33.9	44.3	48.7	39.2
	47.0	36.7	36.2	36.9	51.7	64.2	43.2	54.8	48.7	39.2
5	35.6	13.1	24.2	30.7	41.8	46.2	45.7	39.4	44.4	62.0
	40.5	14.8	27.5	34.8	47.6	58.4	57.7	70.9	50.7	62.0
4	30.1	24.6	32.0	29.8	40.0	51.1	51.1	40.0	59.5	59.6
	34.2	27.9	36.4	33.9	50.5	66.5	61.6	68.4	67.8	59.6
3	14.6	18.8	24.3	29.6	32.0	35.8	41.9	37.3	37.2	36.1
	16.5	21.2	27.6	35.4	40.2	42.9	47.8	42.4	37.2	36.1
2	18.8	19.9	14.2	29.9	29.6	22.4	19.8	30.0	40.5	37.8
	21.3	22.5	16.1	36.7	36.3	25.4	22.4	30.0	40.5	37.8
1	19.8	9.4	3.1	9.2	17.5	22.4	13.4	29.6	45.8	46.0
	22.4	10.5	3.4	10.4	19.8	22.4	13.4	29.6	45.8	46.0

TABLE XIV

HEAT FLUX (millical cm^{-2} min^{-1}, where positive value indicates downward heat transport) COMPUTED FOR 00Z, 7 FEB. 1964 IN EXPERIMENT NO. 2 (lower values) AND EXPERIMENT NO. 4 (upper values)

M \ L	1	2	3	4	5	6	7	8	9	10
10	24.4	47.1	79.6	35.8	14.7	7.5	47.4	70.4	150.6	184.1
	27.8	53.9	93.6	35.9	19.2	7.4	65.6	90.3	176.0	233.7
9	28.1	42.7	62.0	47.8	23.1	28.6	45.3	87.9	147.4	245.9
	33.0	49.0	70.8	47.6	30.2	28.0	43.2	84.9	191.7	316.5
8	26.0	41.5	63.3	57.3	40.1	37.5	41.0	36.9	29.0	119.6
	29.6	46.8	71.0	67.9	47.4	36.5	48.5	47.4	38.5	161.6
7	26.3	45.0	50.7	37.1	41.0	34.5	22.3	25.6	24.3	22.0
	28.5	50.1	56.6	43.1	46.6	42.6	27.6	33.9	32.4	22.0
6	30.5	27.4	29.0	29.5	39.1	44.0	10.6	23.0	62.0	55.2
	31.5	29.9	31.9	32.3	47.0	55.5	6.3	32.2	63.5	55.3
5	19.1	3.2	10.3	17.9	31.5	27.5	11.4	0.6	8.1	35.7
	19.8	3.6	11.9	21.0	34.9	29.7	7.4	-1.1	10.0	37.3
4	13.3	9.6	14.2	14.5	23.4	24.7	11.4	0.4	-30.7	-44.6
	16.0	11.4	16.2	16.7	30.3	28.0	8.3	-5.3	-40.2	-44.0
3	4.3	3.7	2.5	7.9	8.6	8.5	9.2	1.9	-16.3	-41.3
	5.3	4.4	2.8	9.8	9.6	9.5	10.2	1.0	-15.7	-40.0
2	2.5	2.9	3.6	11.0	11.4	7.5	4.4	3.4	-5.3	-26.9
	3.1	3.7	4.3	13.7	14.2	8.7	5.0	3.7	-4.5	-26.2
1	2.1	1.8	0.4	2.8	8.5	10.5	2.2	-0.2	-7.2	-15.2
	2.4	2.2	0.5	3.3	10.0	10.2	2.2	0.0	-7.3	-15.2

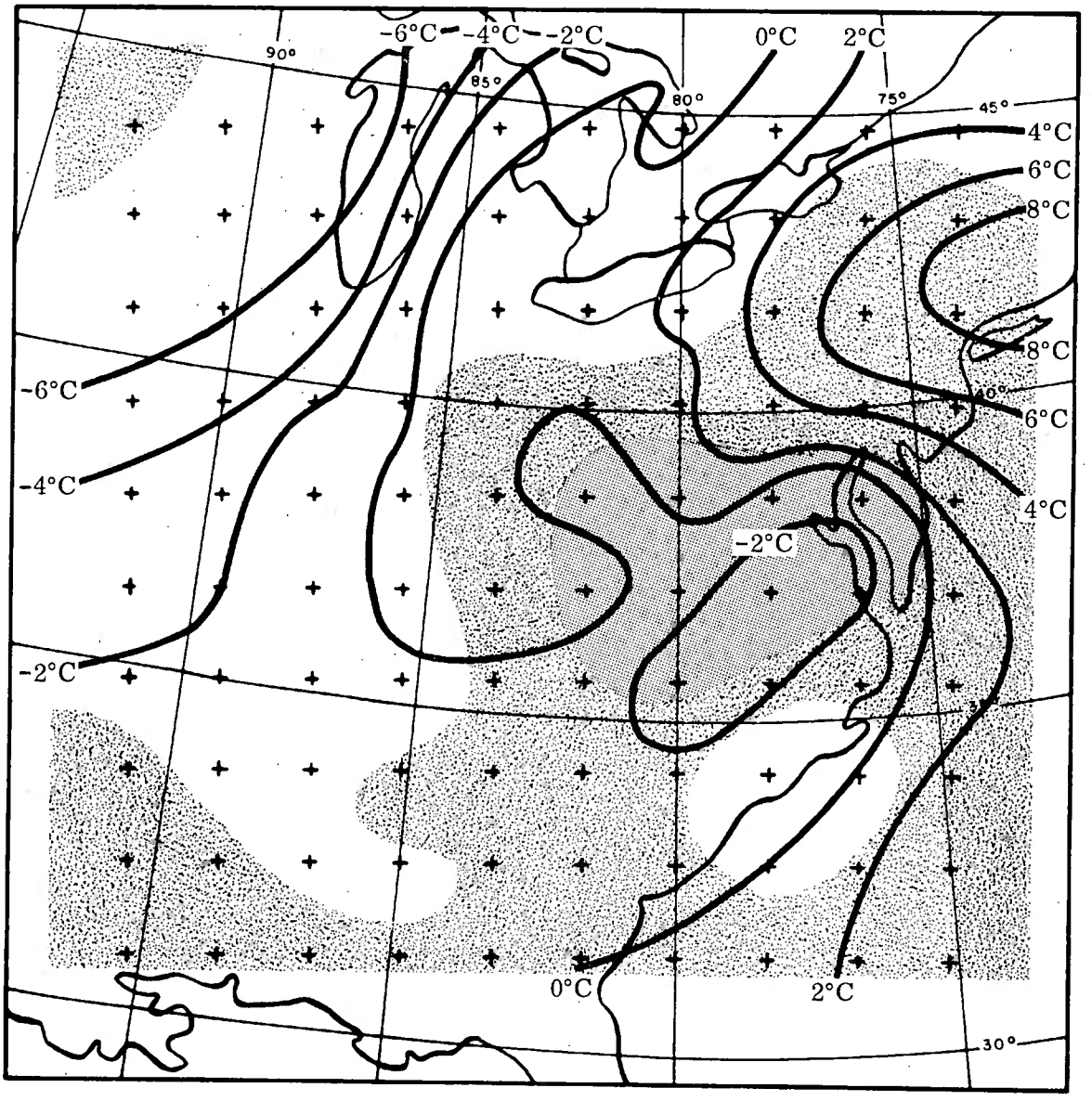

Figure 11. Constant level analysis (z = 1500 m); Experiment no. 5 forecast; 0000Z, 7 Feb. 1964. RH < 77% RH > 77% RH > 93%

TABLE XV

GRID POINT VALUES (°C) OF VERTICALLY AVERAGED ABSOLUTE VALUE OF THE DIFFERENCE IN TEMPERATURE PREDICTED IN EXPERIMENT NO. 2 AND EXPERIMENT NO. 5

M \ L	1	2	3	4	5	6	7	8	9	10
10	0.00	0.00	0.00	0.04	0.00	0.32	0.34	0.13	0.08	0.01
9	0.00	0.91	0.15	0.14	0.05	0.46	0.27	0.15	0.42	0.02
8	0.02	0.32	0.66	0.14	0.07	0.73	1.75	4.09	2.88	0.05
7	0.02	0.50	0.39	0.08	0.32	0.09	1.13	1.96	0.21	0.19
6	0.12	0.94	0.82	0.46	0.48	0.70	2.16	0.36	0.99	0.57
5	0.05	0.45	0.19	0.75	1.33	1.65	0.67	0.74	1.25	0.68
4	0.02	0.27	0.69	0.72	1.45	2.53	0.16	1.13	1.18	0.62
3	0.01	0.07	0.97	0.83	1.60	0.24	0.76	1.13	0.90	0.45
2	0.00	0.09	0.32	0.42	0.11	0.51	0.50	0.59	0.30	0.00
1	0.00	0.02	0.03	0.04	0.02	0.05	0.01	0.01	0.00	0.00

30. Influence of the Variation in the Mixing Coefficient

We neglected the dependence of the mixing coefficient upon height and stability in experiment seven. As in experiment four, this modification should influence the computed, frictionally-induced vertical velocity, w (see Table XVI). The remarks made in subsection 28 may be reiterated here. Figure 12 displays the predicted temperature and humidity fields at 1500 m above mean sea level obtained in this experiment. There are only minor differences between this forecast and that obtained in experiment two. This is shown more quantitatively in Table XVII, which gives the vertically-averaged absolute value of the difference in temperatures predicted in experiments two and seven.

The implication of this result is that our present formulation of the dependence of the mixing coefficient on stability and height is not reflecting any synoptically important processes. We had previously examined the effect of this dependence in an idealized, two-dimensional experiment, with the same result. It appears that we may do well in the future to neglect in the model the added complication of computing this dependence.

31. Influence of Lateral-boundary Conditions

Experiments six, eight, and nine differed from experiment two in only the procedure used for computing the horizontal advection on the lateral boundaries. The character of these differences is outlined in Table II.

Tables XVIII, XIX, and XX, give the vertical average of the absolute value of the difference in temperature predicted in experiment two and in these other forecasts.

In both Experiments 2 and 6, we computed the advection parallel to the lateral boundaries while neglecting, in certain instances, the component of advection normal to the boundary. A comparison of the signs of the errors on the boundary indicates that Experiment 6 has even larger errors on the eastern boundary than those found in Experiment 2.

In Experiment 8, we neglected both components of advection on inflow boundaries. It appears from a close examination of the boundary errors that the procedure used in Experiment 8 would have improved the accuracy of the fore-

TABLE XVI

DISTRIBUTION OF (cm sec^{-1}) FROM EXPERIMENT NO. 7 (frictionally induced) AT z = 1000 m ABOVE MSL

M \ L	1	2	3	4	5	6	7	8	9	10
10	-	-	-	-	-	-	-	-	-	-
9	-	-0.3	0.6	0.7	0.2	0.0	-0.2	0.2	1.6	-
8	-	-0.4	0.2	0.6	0.6	0.5	0.7	1.2	1.8	-
7	-	-0.3	0.3	0.5	0.7	1.1	1.1	1.3	1.1	-
6	-	0.4	0.4	0.4	-0.5	0.7	2.3	0.5	0.5	-
5	-	0.9	0.3	-0.5	-0.7	1.2	1.6	-0.2	0.0	-
4	-	0.1	-0.1	-1.0	0.3	1.5	0.2	-0.5	-0.9	-
3	-	-1.0	-0.6	0.0	0.1	-0.9	-1.1	-0.7	-0.6	-
2	-	-0.3	-1.2	-0.5	0.3	-0.4	-0.1	-0.7	0.3	-
1	-	-	-	-	-	-	-	-	-	-

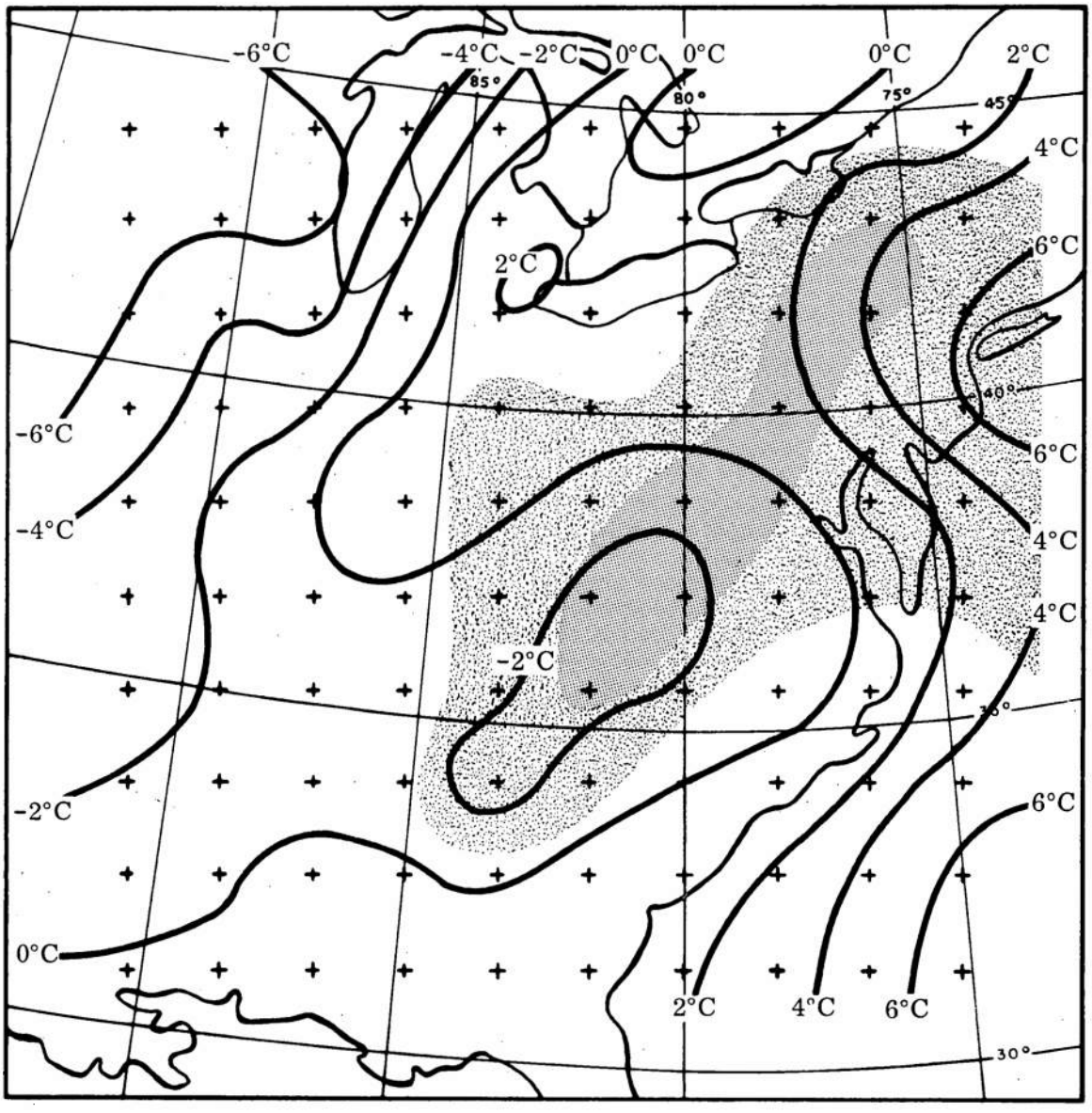

Figure 12. Constant level analysis (z = 1500 m); Experiment no. 7 forecast; 0000Z, 7 Feb. 1964. RH < 77% RH > 77% RH > 93%

TABLE XVII

GRID POINT VALUES (°C) OF VERTICALLY AVERAGED ABSOLUTE VALUE OF THE DIFFERENCE IN TEMPERATURE PREDICTED IN EXPERIMENT NO. 2 AND EXPERIMENT NO. 7

M \ L	1	2	3	4	5	6	7	8	9	10
10	0.40	0.39	0.32	0.12	0.12	0.22	0.42	0.64	0.88	1.00
9	0.36	0.35	0.42	0.15	0.18	0.23	0.46	0.74	0.93	1.02
8	0.34	0.34	0.28	0.14	0.23	0.28	0.40	0.35	0.39	0.58
7	0.29	0.31	0.28	0.22	0.23	0.30	0.32	0.21	0.21	0.23
6	0.32	0.32	0.28	0.30	0.27	0.27	0.09	0.17	0.20	0.21
5	0.32	0.25	0.26	0.29	0.29	0.15	0.14	0.28	0.25	0.25
4	0.26	0.25	0.26	0.28	0.30	0.20	0.42	0.55	0.52	0.45
3	0.28	0.29	0.35	0.37	0.38	0.42	0.44	0.46	0.52	0.45
2	0.39	0.40	0.33	0.32	0.38	0.35	0.28	0.40	0.61	0.64
1	0.39	0.31	0.21	0.16	0.15	0.18	0.19	0.31	0.52	0.64

TABLE XVIII

GRID POINT VALUES (°C) OF VERTICALLY AVERAGED ABSOLUTE VALUE OF THE DIFFERENCE IN TEMPERATURE PREDICTED IN EXPERIMENT NO. 2 AND EXPERIMENT NO. 6

M \ L	1	2	3	4	5	6	7	8	9	10
10	0.2	0.01	0.02	1.49	1.28	1.60	2.31	3.34	4.81	5.83
9	0.02	0.01	0.01	0.45	0.45	0.56	0.37	0.25	0.11	0.23
8	0.09	0.01	0.03	0.47	0.19	0.18	0.08	0.08	0.12	0.67
7	0.21	0.03	0.03	0.14	0.08	0.05	0.02	0.00	0.01	1.72
6	0.48	0.02	0.01	0.02	0.04	0.02	0.00	0.00	0.00	3.92
5	0.36	0.16	0.07	0.03	0.01	0.00	0.00	0.00	0.01	5.42
4	0.11	0.08	0.05	0.01	0.00	0.00	0.00	0.00	0.02	6.41
3	0.04	0.03	0.01	0.00	0.00	0.00	0.00	0.00	0.01	6.42
2	0.07	0.05	0.01	0.01	0.01	0.00	0.04	0.00	0.01	5.95
1	1.37	1.28	0.88	0.76	0.60	0.38	0.14	0.08	0.08	5.02

TABLE XIX

GRID POINT VALUES (°C) OF VERTICALLY AVERAGED ABSOLUTE VALUE OF THE DIFFERENCE IN TEMPERATURE PREDICTED IN EXPERIMENT NO. 2 AND EXPERIMENT NO. 8

M \ L	1	2	3	4	5	6	7	8	9	10
10	0.02	1.12	0.96	0.85	0.16	0.28	0.66	2.16	3.49	5.58
9	0.63	0.75	0.52	0.16	0.03	0.20	1.23	3.01	5.06	7.12
8	0.50	0.36	0.24	0.03	0.01	0.17	0.76	2.38	4.08	7.29
7	2.57	0.12	0.11	0.00	0.02	0.05	0.26	0.40	0.63	4.68
6	1.79	0.15	0.02	0.04	0.01	0.02	0.05	0.08	0.36	1.20
5	1.35	0.30	0.09	0.05	0.05	0.00	0.01	0.04	0.23	0.65
4	0.38	0.33	0.25	0.15	0.09	0.02	0.02	0.02	0.05	0.20
3	0.60	0.30	0.20	0.10	0.06	0.03	0.03	0.08	0.22	0.60
2	0.41	0.18	0.07	0.05	0.04	0.00	0.38	0.44	0.86	1.99
1	1.37	0.80	0.52	0.30	0.23	0.97	4.12	3.92	7.47	5.02

TABLE XX

GRID POINT VALUES (°C) OF VERTICALLY AVERAGED ABSOLUTE VALUE OF THE DIFFERENCE IN TEMPERATURE PREDICTED IN EXPERIMENT NO. 2 AND EXPERIMENT NO. 9

M \ L	1	2	3	4	5	6	7	8	9	10
10	0.02	1.12	1.00	1.00	0.94	1.15	1.00	1.08	1.82	5.82
9	1.10	0.85	0.59	0.71	0.30	0.38	1.43	3.12	5.40	7.56
8	3.48	0.16	0.26	0.37	0.10	0.18	0.88	2.42	4.29	7.82
7	4.22	0.25	0.08	0.11	0.05	0.06	0.28	0.41	0.63	5.01
6	2.50	0.21	0.02	0.03	0.04	0.02	0.05	0.08	0.37	3.42
5	1.35	0.30	0.08	0.05	0.05	0.00	0.01	0.04	0.25	2.45
4	0.38	0.33	0.25	0.15	0.09	0.02	0.02	0.02	0.06	6.04
3	0.60	0.30	0.20	0.10	0.06	0.03	0.03	0.08	0.22	5.87
2	0.41	0.19	0.08	0.05	0.03	0.12	0.38	0.45	0.87	6.55
1	1.37	0.83	1.87	0.98	0.83	2.58	4.12	5.86	7.47	5.02

cast only near the boundary in the northeast. On the other boundaries, the results are slightly inferior to those obtained in experiment two. Similar comments apply to the comparison of experiments nine and two; however, the complete neglect of advection on the boundary in experiment nine led to noticeably larger, overall boundary errors.

In spite of these differences, it is quite clear from the tabulated differences that the boundary influences were not propagated far into the interior of the region. None of the four methods used so far to specify lateral boundary advection can be highly recommended. It will be necessary to analyze alternative schemes as part of our future work.

APPENDIX I

COORDINATE SYSTEM

A natural coordinate system with which to represent the distribution of atmospheric processes is a spherical system fixed in the rotating earth.

Haurwitz [20] derives Newton's second law of motion in such a system. He then derives the simpler form of these equations under the tangent-plane coordinate transformation.

It is possible to simplify the equations of motion in spherical coordinates by the neglect of certain terms, and thereby arrive at a form analogous to that achieved by the tangent-plane transformation. We refer to this system as the quasi-Cartesian form of the equations.

In order to make clear the coordinate system used in this paper, we discuss the approximations necessary to derive the quasi-Cartesian form of the equations from their original form in spherical coordinates. We then introduce a modified spherical coordinate system and show that this leads to a modified quasi-Cartesian form of the equations.

The spherical system of coordinates, r', ϕ, and λ, has its origin at the center of the earth. The plane $\lambda = 0$ is a meridian fixed in the earth containing the axial vector, $\vec{\Omega}$, which represents the angular velocity of the earth's rotation. The plane, $\phi = 0$, is normal to $\vec{\Omega}$ and coincides with the equatorial plane of the earth. The coordinate, r', denotes the radial distance of the point from the center of the earth. Let $r' = a$ be the mean radius of the earth and therefore mean sea level. Let $r' = E(\lambda, \phi)$ be the equation representing the actual distance of the earth's surface terrain from the center of the earth.

Let u, v, and w' be the components of linear velocity of a fluid element at the point (r', ϕ, λ). Then

$$u = r' \cos\phi \frac{d\lambda}{dt}$$

$$v = r' \frac{d\phi}{dt} \qquad \text{(AI-1)}$$

$$w' = \frac{dr'}{dt} .$$

Let Φ be a scalar property of the fluid. The distribution in space and time of the property Φ defines a function,

$$\Phi = F(r', \lambda, \phi, t) \tag{AI-2}$$

The so-called particle derivative [7] of Φ may be expressed as,

$$\frac{d\Phi}{dt} = \frac{\partial \Phi}{\partial t} + \frac{\partial \Phi}{\partial \lambda}\frac{d\lambda}{dt} + \frac{\partial \Phi}{\partial \phi}\frac{d\phi}{dt} + \frac{\partial \Phi}{\partial r'}\frac{dr'}{dt}, \tag{AI-3}$$

or by using Eqs. AI-1 and 2, or

$$\frac{d\Phi}{dt} = \frac{dF}{dt} = \frac{\partial F}{\partial t} + \frac{u}{r' \cos \phi}\frac{\partial F}{\partial \lambda} + \frac{v}{r'}\frac{\partial F}{\partial \phi} + w'\frac{\partial F}{\partial r'}, \tag{AI-4}$$

The divergence of the fluid velocity may be written [18] as

$$\text{div } \vec{v} = \frac{\partial w'}{\partial r'} + \frac{1}{r'}\frac{\partial v}{\partial \phi} + \frac{1}{r' \cos \phi}\frac{\partial u}{\partial \lambda} + \frac{2w'}{r'} - \frac{v}{r'}\tan \phi. \tag{AI-5}$$

Newton's second law takes the form [19]

$$\frac{du}{dt} + \frac{uw'}{r'} - \frac{uv}{r'}\tan \phi - fv + cw' = F_\lambda \tag{AI-6a}$$

$$\frac{dv}{dt} + \frac{vw'}{r'} + \frac{u^2}{r}\tan \phi + fu = F_\phi \tag{AI-6b}$$

$$\frac{dw'}{dt} - \frac{u^2 + v^2}{r'} - cu = F_{r'} - g, \tag{AI-6c}$$

where

$$f = 2\omega \sin \phi \tag{AI-7a}$$

$$c = 2\omega \cos \phi. \tag{AI-7b}$$

The F's refer to the forces applied per unit mass, ω is the magnitude of the earth's angular velocity, and g is the apparent gravity acceleration.

These are the pertinent equations and relations necessary for deriving the physical model in the text. These may be put into quasi-Cartesian form if we assume that the curvature of the earth's surface is not physically significant for the processes being investigated.

One writes

$$\begin{aligned} dx &\equiv r' \cos \phi \, d\lambda \\ dy &\equiv r' \, d\phi \\ dz' &\equiv dr' \end{aligned} \tag{AI-8}$$

$$u \equiv \frac{dx}{dt}$$

$$v \equiv \frac{dy}{dt} \qquad \text{(AI-9)}$$

$$w' \equiv \frac{dz'}{dt}.$$

The various relations and equations derived above may now be written as

$$\frac{d\Phi}{dt} = \frac{\partial F}{\partial t} + u\,\frac{\partial F}{\partial x} + v\,\frac{\partial F}{\partial y} + w'\,\frac{\partial F}{\partial Z'} \qquad \text{(AI-10)}$$

$$\text{div}\,\vec{v} = \frac{\partial w'}{\partial z'} + \frac{\partial v}{\partial y} + \frac{\partial u}{\partial x} + \left[\frac{2w'}{r'} - \frac{v}{r'}\tan\phi\right] \qquad \text{(AI-11)}$$

$$\frac{du}{dt} - fv + \left[cw' + \frac{uw'}{r'} - \frac{uv}{r'}\tan\phi\right] = F_\lambda \qquad \text{(AI-12)}$$

$$\frac{dv}{dt} + fu + \left[\frac{vw'}{r'} + \frac{u^2}{r'}\tan\phi\right] = F_\phi \qquad \text{(AI-13)}$$

$$\frac{dw'}{dt}\left[-cu + \frac{u^2 + v^2}{r'}\right] = F_{r'} - g. \qquad \text{(AI-14)}$$

The terms enclosed in brackets in Eqs. AI-11 to 14 are neglected on order of magnitude and scale considerations [42] to arrive at the quasi-Cartesian form.

We will now rederive the relations given above in a modified spherical coordinate system (r, λ, ϕ) so as to obtain the equations in a modified quasi-Cartesian system.

Let $r' = r + E(\lambda, \phi)$

$$\lambda = \lambda \qquad \text{(AI-15)}$$

$$\phi = \phi.$$

The arbitrary scalar Φ introduced above may be represented in the r, λ, ϕ system as

$$\Phi = G(r, \lambda, \phi, t). \qquad \text{(AI-16)}$$

We may now use the relations [43]

$$\Phi = F(r', \lambda, \phi, t) = G(r, \lambda, \phi, t) \qquad \text{(AI-17)}$$

and

$$\frac{\partial G}{\partial \lambda} = \frac{\partial F}{\partial \lambda} + \frac{\partial F}{\partial r'}\frac{\partial E}{\partial \lambda} = \frac{\partial F}{\partial \lambda} + \frac{\partial G}{\partial r}\frac{\partial E}{\partial \lambda}$$

$$\frac{\partial G}{\partial \phi} = \frac{\partial F}{\partial \phi} + \frac{\partial F}{\partial r'}\frac{\partial E}{\partial \phi} = \frac{\partial F}{\partial \phi} + \frac{\partial G}{\partial r}\frac{\partial E}{\partial \phi} \qquad \text{(AI-18)}$$

$$\frac{\partial G}{\partial r} = \frac{\partial F}{\partial r'}$$

$$\frac{\partial G}{\partial t} = \frac{\partial F}{\partial t}.$$

The particle derivative has the same value in either coordinate system, i.e.,

$$\frac{d\Phi}{dt} = \frac{dF}{dt} = \frac{dG}{dt}, \qquad \text{(AI-19)}$$

and by definition,

$$\frac{dG}{dt} = \frac{\partial G}{\partial t} + \frac{\partial G}{\partial \lambda}\frac{d\lambda}{dt} + \frac{\partial G}{\partial \phi}\frac{d\phi}{dt} + \frac{\partial G}{\partial r}\frac{dr}{dt}. \qquad \text{(AI-20)}$$

From Eqs. AI-1 and 15 we may rewrite Eq. AI-20 as

$$\frac{dG}{dt} = \frac{\partial G}{\partial t} + \frac{u}{r' \cos\phi}\frac{\partial G}{\partial \lambda} + \frac{v}{r'}\frac{\partial G}{\partial \phi} + \left[w' - \frac{dE}{dt}\right]\frac{\partial G}{\partial r}. \qquad \text{(AI-21)}$$

It is convenient to define w as

$$w \equiv \frac{dr}{dt} = w' - \frac{dE}{dt}. \qquad \text{(AI-22)}$$

Consider next the transformation of the expression for the velocity divergence given by Eq. AI-5. It follows from Eq. AI-22 that

$$\frac{\partial w'}{\partial r'} = \frac{\partial w}{\partial r} + \frac{\partial}{\partial r'}\left(\frac{dE}{dt}\right) \qquad \text{(AI-23)}$$

but by using Eq. AI-20, this becomes

$$\frac{\partial w'}{\partial r'} = \frac{\partial w}{\partial r} + \frac{\partial u}{\partial r'}\frac{1}{r' \cos\phi}\frac{\partial E}{\partial \lambda} + \frac{\partial v}{\partial r'}\frac{1}{r'}\frac{\partial E}{\partial \phi} - \frac{u}{r'^2 \cos\phi}\frac{\partial E}{\partial \lambda} - \frac{v}{r'^2}\frac{\partial E}{\partial \phi} \qquad \text{(AI-24)}$$

or

$$\frac{\partial w'}{\partial r'} = \frac{\partial w}{\partial r} + \frac{\partial u}{\partial r'}\frac{1}{r' \cos\phi}\frac{\partial E}{\partial \lambda} + \frac{1}{r'}\frac{\partial v}{\partial r'}\frac{\partial E}{\partial \phi} - \frac{1}{r'}\frac{dE}{dt}. \qquad \text{(AI-25)}$$

Using Eq. AI-17, the other derivatives in Eq. AI-5 can be evaluated.

$$\text{div } \hat{\mathbf{v}} = \frac{\partial w}{\partial r} + \frac{1}{r' \cos \phi} \frac{\partial u}{\partial \lambda} - \frac{\partial u}{\partial r'} \frac{1}{r' \cos \phi} \frac{\partial E}{\partial \lambda} + \frac{\partial u}{\partial r'} \frac{1}{r' \cos \phi} \frac{\partial E}{\partial \lambda}$$

$$+ \frac{1}{r'} \frac{\partial v}{\partial \phi} - \frac{\partial v}{\partial r'} \frac{1}{r'} \frac{\partial E}{\partial \phi} + \frac{\partial v}{\partial r'} \frac{1}{r'} \frac{\partial E}{\partial \lambda} \qquad \text{(AI-26)}$$

$$+ \frac{2w'}{r'} - \frac{v}{r'} \tan \phi - \frac{1}{r'} \frac{dE}{dt}.$$

Noting the cancelation effect, Eq. AI-26 reduces to

$$\text{div } \hat{\mathbf{v}} = \frac{\partial w}{\partial r} + \frac{1}{r' \cos \phi} \frac{\partial u}{\partial \lambda} + \frac{1}{r'} \frac{\partial v}{\partial \phi} + \frac{1}{r'} \frac{dE}{dt} \qquad \text{(AI-27)}$$

$$+ \left[\frac{2w}{r'} - \frac{v}{r'} \tan \phi \right].$$

The equations of motion transform easily, of course, in view of the uniqueness of the particle derivative.

To recapitulate then, the coordinate system used in the text is essentially a modified spherical coordinate system. In the various equations, we have neglected the terms involving the spherical shape of the earth and other small terms.

We employ the notation

$$dx = r \cos \phi \, d\lambda$$

$$dy = r \, d\phi \qquad \text{(AI-28)}$$

$$dz = dr$$

and

$$u = r \cos \phi \frac{d\lambda}{dt}$$

$$v = r \frac{d\phi}{dt} \qquad \text{(AI-29)}$$

$$w = \frac{dr}{dt}$$

$$\hat{w} = \frac{dE}{dt}.$$

When r appears undifferentiated in Eqs. AI-28 and 29, the mean value, $r = a$, is to be used. We point out here, however, the assumption introduced in the derivation of the thermodynamic energy equation in Subsection 7 of the text. The

particle derivative of the fluid pressure is

$$\frac{dp}{dt} = \left[\frac{\partial}{\partial t} + \frac{u}{r' \cos \varphi} \frac{\partial}{\partial \lambda} + \frac{v}{r'} \frac{\partial}{\partial \phi} + w' \frac{\partial}{\partial r'} \right] p . \tag{AI-30}$$

Because the pressure field (in response to the gravity acceleration) is largely distributed with spherical symmetry about the earth, one may, to good approximation, write

$$\frac{dp}{dt} \cong w' \frac{\partial}{\partial r'} p , \tag{AI-31}$$

and in accordance with Eq. AI-22 this approximation yields

$$\frac{dp}{dt} \cong w \frac{\partial p}{\partial r} + \frac{dE}{dt} \frac{\partial p}{\partial r} . \tag{AI-32}$$

In the text, we have used the notation

$$\hat{w} \equiv \frac{dE}{dt} \tag{AI-33}$$

and the hydrostatic equation

$$\frac{\partial p}{\partial r} = - \frac{gp}{RT} \tag{AI-34}$$

to write

$$\frac{dp}{dt} \cong - \frac{gp}{RT} (w + \hat{w}) . \tag{AI-35}$$

APPENDIX II

UPWIND ADVECTION APPROXIMATION

We define $X(f)^{l,n}_{m,k}$, an approximation to $u\,\frac{\partial f}{\partial x}$, as follows.

For $l = 1$;

$$\text{if } u^{l,n}_{m,k} \geq 0, \text{ set } X(f)^{l,n}_{m,k} = 0,$$
$$\text{if } u^{l,n}_{m,k} < 0, \text{ set } X(f)^{l,n}_{m,k} = d^{-1}\, u^{l,n}_{m,k} \left[f^{2,n}_{m,k} - f^{l,n}_{m,k} \right]. \tag{AII-1}$$

For $l = L + 1$;

$$\text{if } u^{L+1,n}_{m,k} \leq 0, \text{ set } X(f)^{L+1,n}_{m,k} = 0,$$
$$\text{if } u^{L+1,n}_{m,k} > 0, \text{ set } X(f)^{L+1,n}_{m,k} = d^{-1}\, u^{L+1,n}_{m,k} \left[f^{L+1,n}_{m,k} - f^{L,n}_{m,k} \right]. \tag{AII-2}$$

For $1 < l < L + 1$;

$$\text{if } u^{l,n}_{m,k} \geq 0, \text{ set } X(f)^{l,n}_{m,k} = d^{-1}\, u^{l,n}_{m,k} \left[f^{l,n}_{m,k} - f^{l-1,n}_{m,k} \right],$$
$$\text{if } u^{l,n}_{m,k} < 0, \text{ set } X(f)^{l,n}_{m,k} = d^{-1}\, u^{l,n}_{m,k} \left[f^{l+1,n}_{m,k} - f^{l,n}_{m,k} \right]. \tag{AII-3}$$

We define $Y(f)^{l,n}_{m,k}$, an approximation to $v\,\frac{\partial f}{\partial y}$, as follows.

For $m = 1$;

$$\text{if } v^{l,n}_{1,k} \geq 0, \text{ set } Y(f)^{l,n}_{1,k} = 0,$$
$$\text{if } v^{l,n}_{1,k} < 0, \text{ set } Y(f)^{l,n}_{1,k} = d^{-1}\, v^{l,n}_{1,k} \left[f^{l,n}_{2,k} - f^{l,n}_{1,k} \right]. \tag{AII-4}$$

For $m = M + 1$;

$$\text{if } v^{l,n}_{M+1,k} \leq 0, \text{ set } Y(f)^{l,n}_{M+1,k} = 0,$$
$$\text{if } v^{l,n}_{M+1,k} > 0, \text{ set } Y(f)^{l,n}_{M+1,k} = d^{-1}\, v^{l,n}_{M+1,k} \left[f^{l,n}_{M+1,k} - f^{l,n}_{M,k} \right]. \tag{AII-5}$$

For $1 \leq m \leq M+1$;

$$\text{if } v^{l,n}_{m,k} \geq 0, \text{ set } Y(f)^{l,n}_{m,k} = d^{-1}\, v^{l,n}_{m,k} \left[f^{l,n}_{m,k} - f^{l,n}_{m-1,k} \right],$$

$$\text{if } v^{l,n}_{m,k} < 0, \text{ set } Y(f)^{l,n}_{m,k} = d^{-1}\, v^{l,n}_{m,k} \left[f^{l,n}_{m+1,k} - f^{l,n}_{m,k} \right]. \qquad \text{(AII-6)}$$

APPENDIX III

THE DIFFERENCE APPROXIMATION FOR THE HEAT-DIFFUSION EQUATION

Set $t = t_\nu$, $x = x_\lambda$, $y = y_\mu$.

For $k = 1$;

$$\frac{T^{\lambda,\nu+1}_{\mu,1} - T^{\lambda,\nu}_{\mu,1}}{\Delta t} = - X(T)^{\lambda,\nu}_{\mu,1} - Y(T)^{\lambda,\nu}_{\mu,1} - \frac{g}{C_p}\hat{w}^{\lambda,\nu}_{\mu,1} + \frac{2}{(\Delta z)_2}\left[K^{\lambda,\nu+1}_{\mu,2}\left[\frac{T^{\lambda,\nu+1}_{\mu,2} - T^{\lambda,\nu+1}_{\mu,1}}{(\Delta z)_2} + \frac{g}{C_p}\right] - u^{\lambda,\nu}_{*\mu}\ \Theta^{\lambda,\nu}_{*\mu}\right]. \tag{AIII-1}$$

For $k = 2, \ldots, K-1$;

$$\frac{T^{\lambda,\nu+1}_{\mu,k} - T^{\lambda,\nu}_{\mu,k}}{\Delta t} = - X(T)^{\lambda,\nu}_{\mu,k} - Y(T)^{\lambda,\nu}_{\mu,k} - \frac{g}{C_p}\left[w^{\lambda,\nu}_{\mu,k} + \hat{w}^{\lambda,\nu}_{\mu,k}\right] - \frac{w^{\lambda,\nu}_{\mu,k}}{(\Delta z)_{k+1} + (\Delta z)_k}\left[T^{\lambda,\nu+1}_{\mu,k+1} - T^{\lambda,\nu+1}_{\mu,k-1}\right] + \frac{2}{(\Delta z)_{k+1} + (\Delta z)_k}\left\{K^{\lambda,\nu}_{\mu,k+1}\left[\frac{T^{\lambda,\nu+1}_{\mu,k+1} - T^{\lambda,\nu+1}_{\mu,k}}{(\Delta z)_{k+1}} + \frac{g}{C_\rho}\right] - K^{\lambda,\nu}_{\mu,k}\left[\frac{T^{\lambda,\nu+1}_{\mu,k} - T^{\lambda,\nu+1}_{\mu,k-1}}{(\Delta z)_k} + \frac{g}{C_p}\right]\right\}. \tag{AIII-2}$$

APPENDIX IV

THE DIFFERENCE APPROXIMATION FOR THE VAPOR-DIFFUSION EQUATION

Set $t = t_{\nu}$, $y = y_{\mu}$, $x = x_{\lambda}$.

For $k = 1$;

$$\frac{q^{\lambda,\nu+1}_{\mu,1} - q^{\lambda,\nu}_{\mu,1}}{\Delta t} = - X(q)^{\lambda,\nu}_{\mu,1} - Y(q)^{\lambda,\nu}_{\mu,1} + \frac{2}{(\Delta z)_2}\left\{K^{\lambda,\nu}_{\mu,2}\left[\frac{q^{\lambda,\nu+1}_{\mu,2} - q^{\lambda,\nu+1}_{\mu,1}}{(\Delta z)_2}\right] - u^{\lambda,\nu}_{*\mu}\ q^{\lambda,\nu}_{*\mu}\right\}. \tag{AIV-1}$$

For $k = 2, \ldots, K - 1$;

$$\frac{q^{\lambda,\nu+1}_{\mu,k} - q^{\lambda,\nu}_{\mu,k}}{\Delta t} = - X(q)^{\lambda,\nu}_{\mu,k} - Y(q)^{\lambda,\nu}_{\mu,k} - \frac{w^{\lambda,\nu}_{\mu,k}}{(\Delta z)_{k+1} + (\Delta z)_k}\left[q^{\lambda,\nu+1}_{\mu,k+1} - q^{\lambda,\nu+1}_{\mu,k-1}\right] + \frac{2}{(\Delta z)_{k+1} + (\Delta z)_k}\left\{K^{\lambda,\nu}_{\mu,k+1}\left[\frac{q^{\lambda,\nu+1}_{\mu,k+1} - q^{\lambda,\nu+1}_{\mu,k}}{(\Delta z)_{k+1}}\right] - K^{\lambda,\nu}_{\mu,k}\left[\frac{q^{\lambda,\nu}_{\mu,k} - q^{\lambda,\nu+1}_{\mu,k-1}}{(\Delta z)_k}\right]\right\}. \tag{AIV-2}$$

APPENDIX V

DIFFERENCE APPROXIMATION TO THE MOISTURE DIFFUSION EQUATION

Set $t = t_{\nu}$, $x = x_{\lambda}$, $y = y_{\mu}$.

For $k = 1$;

$$\frac{r^{\lambda,\nu+1}_{\mu,1} - r^{\lambda,\nu}_{\mu,1}}{\Delta t} = - X(r)^{\lambda,\nu}_{\mu,1} - Y(r)^{\lambda,\nu}_{\mu,1} + \frac{2}{(\Delta z)_2}\left\{K^{\lambda,\nu}_{\mu,2}\left[\frac{r^{\lambda,\nu+1}_{\mu,2} - r^{\lambda,\nu+1}_{\mu,1}}{(\Delta z)_2}\right] - u^{\lambda,\nu}_{*\mu}\, q^{\lambda,\nu}_{*\mu}\right\}. \quad \text{(AV-1)}$$

For $k = 2, \ldots, K-1$;

$$\frac{r^{\lambda,\nu+1}_{\mu,k} - r^{\lambda,\nu}_{\mu,k}}{\Delta t} = - X(r)^{\lambda,\nu}_{\mu,k} - Y(r)^{\lambda,\nu}_{\mu,k} - \frac{w^{\lambda,\nu}_{\mu,k}}{(\Delta z)_{k+1} + (\Delta z)_k}\left[r^{\lambda,\nu+1}_{\mu,k+1} - r^{\lambda,\nu+1}_{\mu,k-1}\right] + \frac{2}{(\Delta z)_{k+1} + (\Delta z)_k}\left[K^{\lambda,\nu}_{\mu,k+1}\left(\frac{r^{\lambda,\nu+1}_{\mu,k+1} - r^{\lambda,\nu+1}_{\mu,k}}{(\Delta z)_{k+1}}\right) - K^{\lambda,\nu}_{\mu,k}\left(\frac{r^{\lambda,\nu+1}_{\mu,k} - r^{\lambda,\nu+1}_{\mu,k-1}}{(\Delta z)_k}\right)\right] \quad \text{(AV-2)}$$

APPENDIX VI

DEFINITION OF COEFFICIENTS IN EQUATION V-3

For $k = 1$;

$$a^{\lambda,\nu}_{\mu,1} = 0$$

$$b^{\lambda,\nu}_{\mu,1} = -\{(\Delta t)^{-1} + 2K^{\lambda,\nu}_{\mu,2} / [(\Delta z)^2_2]\}$$

$$c^{\lambda,\nu}_{\mu,1} = 2K^{\lambda,\nu}_{\mu,2} / [(\Delta z)^2_2] \qquad \text{(AVI-1)}$$

$$d^{\lambda,\nu}_{\mu,1} = -T^{\lambda,\nu}_{\mu,1} / (\Delta t) + X(T)^{\lambda,\nu}_{\mu,1} + Y(T)^{\lambda,\nu}_{\mu,1} + \frac{g}{C_p}\hat{w}^{\lambda,\nu}_{\mu,1} - 2gK^{\lambda,\nu}_{\mu,2} / [C_p(\Delta z)]$$

$$+ 2u^{\lambda,\nu}_{*\mu}\Theta^{\lambda,\nu}_{*\mu} / (\Delta z)_2 .$$

For $2 \le h \le (K-2)$;

$$a^{\lambda,\nu}_{\mu,k} = 2K^{\lambda,\nu}_{\mu,k} / \{(\Delta z)_k [(\Delta z)_{k+1} + (\Delta z)_k]\} + w^{\lambda,\nu}_{\mu,k} / [(\Delta z)_{k-1} + (\Delta z)_k]$$

$$b^{\lambda,\nu}_{\mu,k} = -\left[(\Delta t)^{-1} + \{2 / [(\Delta z)_{k+1} + (\Delta z)_k]\}[K^{\lambda,\nu}_{\mu,k+1} / (\Delta z)_{k+1} + K^{\lambda,\nu}_{\mu,k} / (\Delta z)_k]\right] \qquad \text{(AVI-2)}$$

$$c^{\lambda,\nu}_{\mu,k} = 2K^{\lambda,\nu}_{\mu,k+1} / \{(\Delta z)_{k+1}[(\Delta z)_{k+1} + (\Delta z)_k]\} - w^{\lambda,\nu}_{\mu,k} / [(\Delta z)_{k+1} + (\Delta z)_k]$$

$$d^{\lambda,\nu}_{\mu,k} = T^{\lambda,\nu}_{\mu,k} / (\Delta t) + X(T)^{\lambda,\nu}_{\mu,k} + Y(T)^{\lambda,\nu}_{\mu,k} + \frac{g}{C_p}[w^{\lambda,\nu}_{\mu,k} + \hat{w}^{\lambda,\nu}_{\mu,k}]$$

$$+ 2g[K^{\lambda,\nu}_{\mu,k+1} - K^{\lambda,\nu}_{\mu,k}] / \{C_p[(\Delta z)_{k+1} + (\Delta z)_k]\} .$$

For $k = K - 1$;

$$a^{\lambda,\nu}_{\mu,K-1} = 2K^{\lambda,\nu}_{\mu,K-1} / \{(\Delta z)_{K-1}[(\Delta z)_{K-1}]\} + w^{\lambda,\nu}_{\mu,K-1} / [(\Delta z)_K + (\Delta z)_{K-1}]$$

$$b^{\lambda,\nu}_{\mu,K-1} = -\left[(\Delta t)^{-1} + \{2 / [(\Delta z)_K + (\Delta z)_{K-1}]\}[K^{\lambda,\nu}_{\mu,k} / (\Delta z)_K + K^{\lambda,\nu}_{\mu,K-1} / (\Delta z)_{K-1}]\right] \qquad \text{(AVI-3)}$$

$$c^{\lambda,\nu}_{\mu,K-1} = 0 .$$

$$
\begin{aligned}
d^{\lambda,\nu}_{\mu,K-1} = & - T^{\lambda,\nu}_{\mu,K-1} / (\Delta t) + X(T)^{\lambda,\nu}_{\mu,K-1} + Y(T)^{\lambda,\nu}_{\mu,K-1} \\
& - w^{\lambda,\nu}_{\mu,K-1} \, T^{\lambda,\nu}_{\mu,K} / [(\Delta z)_K + (\Delta z)_{K-1}] \\
& + \frac{g}{C_p} [w^{\lambda,\nu}_{\mu,K-1} + \hat{w}^{\lambda,\nu}_{\mu,K-1}] - 2K^{\lambda,\nu}_{\mu,K} \, T^{\lambda,\nu+1}_{\mu,K} / \{(\Delta z)_K [(\Delta z)_K \\
& + (\Delta z)_{K-1}]\} .
\end{aligned}
\qquad \text{(AVI-4)}
$$

REFERENCES

1. Árnason, G., et al., (1963), Large-scale Cloud Prediction: A Survey and an Appraisal. Tech. Rpt. No. 3, 76 pp., Contract AF19(626)-16, The Travelers Research Center, Inc., Hartford, Conn.

2. Berkofsky, L. and E. A. Bertoni (1960), Topographic Charts at One-degree Intersections for the Entire Earth. GRD Res. Notes No. 42, 43 pp., AFCRC, Bedford, Mass.

3. Blackadar, A. F. (1963), The Vertical Distribution of Wind in a Baroclinic, Adiabatic Atmosphere Boundary Layer. Unpubl. Manuscript, Dept. of Meteorol., Penn. State Univ.

4. Brooks, D. L. (1950), A Tabular Method for the Computation of Temperature Change by Infrared Radiation in the Free Atmosphere. J. of Meteorol., 7, pp. 313—321.

5. Caplan, P. M. (1962), Evaporation of Falling Rain, Unpubl. Thesis, Dept. of Meteorol., New York Univ.

6. Cooley, D. S. et al., (1964), Combination of Initial and Prognostic Data in Statistical Cloud Prediction. Tech. Doc. Rpt., Contract AF19(626)-3357, The Travelers Research Center, Hartford, Conn.

7. Dryden, H. L., et al., (1956), Hydrodynamics, 634 pp., Dover Publications, N.Y.

8. Elliott, W. P. (1964), The Height Variation of Vertical Heat Flux Near the Ground. Quart. J. Roy. Meteorol. Soc., 90:385, pp. 260—265.

9. —, and D. W. Stevens (1959), A Numerical Method for Computing Radiative Temperature Changes Near the Earth's Surface. GRD Res. Notes, 69, pp. 1—21. AFCRC, Bedford, Mass.

10. Elsasser, W. M. (1942), Heat Transfer by Infrared Radiation in the Atmosphere. Harvard Univ., Blue Hill Meteorol. Observatory, Milton, Mass.

11. —, and M. F. Culbertson (1960), Atmospheric Radiation Tables. Meteorol. Monogr. 4, AMS, Boston, Mass.

12. Estoque, M. A. (1961), A Theoretical Investigation of the Sea Breeze. Quart. J. Roy. Meteorol. Soc., 87, pp. 136—146.

13. —, (1963), A Numerical Model of the Atmospheric Boundary Layer. J. Geophys. Res., 68:4, pp. 1103–1113.

14. Fisher, E. L., (1961), A Theoretical Study of the Sea Breeze. J. Meteorol. 17, pp. 645–660.

15. —, and P. Caplan (1963), An Experiment in Numerical Prediction of Fog and Stratus. J. Atmos. Sci. 20:5, pp. 425–437.

16. Forsythe, G. E. and W. R. Wasow (1960), Finite-Difference Methods for Partial Differential Equations, 444 pp., Wiley, N. Y.

17. Gerrity, J. P., Jr. (1963), Mechanisms Important to the Formation, Movement and Dissipation of Low Clouds. Tech. Memo 7045-92, Contract AF19(626)-16, The Travelers Research Center, Inc., Hartford, Conn.

18. Godske, C. L., et al., (1957), Dynamic Meteorology and Weather Forecasting. (800 + xvi pp.,) Am. Meteorol. Soc., Boston, Mass.

19. Haltiner, G. J. and F. L. Martin (1957), Dynamical and Physical Meteorology. (470 + xi pp.) McGraw-Hill Book Co., Inc., New York.

20. Haurwitz, B. (1941), Dynamic Meteorology, (365 + x pp.), McGraw-Hill Book Co., Inc., New York.

21. —, (1959), A Linear Sea Breeze Model. Quart. Prog. Rpt. No. 3, 33 pp., Contract DA 36-039 SC 78091, Res. Div., Coll. of Eng., New York Univ., N. Y.

22. Jensen, C. E. (1963), Prediction of Large-scale Cloudiness and Airframe Icing Conditions by Machine Methods. J. Appl. Meteorol. 2:3, pp. 337–344.

23. Kung, E. C. and H. H. Lettau (1961), Regional and Meridional Distributions of Continental Vegetation Cover and Aerodynamic Roughness Parameters. Studies of 3-Dimensional Structure of the Planetary Boundary Layer, Dept. of Meteorol., Univ. of Wisconsin.

24. Lewis, E. (1957), Forecasting 700-mb Dewpoint Depression by a 3-Dimensional Trajectory Technique. Mo. Weath. Rev., 85, pp. 297–301.

25. Lumley, J. L. and H. A. Panofsky (1964), The Structure of Atmospheric Turbulence, 239 + xi pp., Interscience Publ., New York.

26. Matveev, L. T. (1964), On the Formation and Development of Layer Clouds. Tellus, 16:2, pp. 139–146.

27. McDonald, J. E. (1963), The Saturation Adjustment in Numerical Modeling of Fog. J. Atmos. Sci., 20:5, pp. 476–478.

28. Monin, A. S. (1958), The Structure of Atmospheric Turbulence (Trans. R. A. Silverman). Theory of Probability and its Appl., vol. 111, No. 3, Moscow.

29. Noguchi, K. (1960), On the Relative Humidity of Condensation Layer in the Case of Falling Rain, J. of Meteorol. Res., Tokyo, 12(2), pp. 68–70.

30. Pandolfo, J. P., D. S. Cooley, and E. A. Newburg (1963), Preliminary Investigations of Numerical Models for the Short-period Prediction of Wind, Temperature, and Moisture in the Atmospheric Boundary Layer. Final Rpt. 7047-80, U.S. Weather Bureau Contract Cwb-10368, The Travelers Research Center, Inc., Hartford, Conn.

31. —, —, and M. Atwater (1964). Further Investigations of Numerical Models of the Atmosphere Boundary Layer. Final Rpt., Contract Cwb-10682, The Travelers Research Center, Inc., Hartford, Conn.

32. Pearce, R. P. (1955), The Calculation of the Sea Breeze Circulation in Terms of the Differential Heating Across the Coast Line. Quart. J. Roy. Meteorol. Soc., 81:349, pp. 351–381.

33. Planck, M. (1926), Treatise on Thermodynamics, (297 + xiv pp.), Dover Publ., New York.

34. Priestley, C. H. B. (1959), Turbulent Transfer in the Lower Atmosphere, (130 + vii pp.), The Univ. of Chicago Press, Chicago, Ill.

35. Richtmyer, R. D. (1957), Difference Methods for Initial Value Problems. Interscience Tracts in Pure and Applied Mathematics, No. 4, Wiley (Interscience), New York.

36. —, (1962), A Survey of Difference Methods for Non-steady Fluid Dynamics. NCAR Tech. Notes 63-2, Nat'l Ctr. for Atmos. Res., Boulder, Colo.

37. Smagorinsky, J. (1960), On the Dynamical Prediction of Large-scale Condensation by Numerical Methods, Physics of Precipitation, Am. Geophys. Un., pp. 71–78, Washington, D.C.

38. —, and G. Collins (1955), On the Numerical Prediction of Precipitation. Mo. Weath. Rev. 83, pp. 53–68.

39. Sutton, O. G. (1953), Micrometeorology, McGraw-Hill Book Co., New York, (333 + xii pp.).

40. Syono, S. and T. Takeda (1962), On the Evaporation of Raindrops in a Sub-cloud Layer. J. Meteorol. Soc. of Japan, 40:5, pp. 245–265.

41. Thomasell, A., Jr., and J. G. Welsh (1962), Objective Analysis of Sea-level Pressure and Surface Temperature, Dew-point, and Wind. Interim Rpt., Tech. Publ. 19, Contract FAA/BRD-363, The Travelers Research Center, Inc., Hartford, Conn.

42. Thompson, P.D. (1961), Numerical Weather Analysis and Prediction, (170 + xiv pp.), MacMillian Co., New York.

43. Wigley, T. M. L. (1964), Approximations in the Use of Pressure Coordinates. Tellus 16:1, pp. 26–31.

UNCLASSIFIED
Security Classification

DOCUMENT CONTROL DATA - R&D

(Security classification of title, body of abstract and indexing annotation must be entered when the overall report is classified)

1. ORIGINATING ACTIVITY (Corporate author)	2a. REPORT SECURITY CLASSIFICATION
United Aircraft Corporation The Travelers Research Center, Inc.	Unclassified
	2b. GROUP N/A

3. REPORT TITLE

A PHYSICAL MODEL FOR THE PREDICTION OF LARGE-SCALE LOW CLOUDINESS

4. DESCRIPTIVE NOTES (Type of report and inclusive dates)

Technical Report May 64—December 64

5. AUTHOR(S) (Last name, first name, initial)

Gerrity, Joseph P., Jr.

6. REPORT DATE	7a. TOTAL NO. OF PAGES	7b. NO. OF REFS
February 1965	112	43

8a. CONTRACT OR GRANT NO.	9a. ORIGINATOR'S REPORT NUMBER(S)
AF 19(628)-3437 (15107) b. PROJECT NO. 1.0 c. System No. 433L d. Task No. 1.2	7463-150 9b. OTHER REPORT NO(S) (Any other numbers that may be assigned this report) ESD-TR-65-3

10. AVAILABILITY/LIMITATION NOTICES

Availability Notice (1) and Legal Notice (1)

11. SUPPLEMENTARY NOTES	12. SPONSORING MILITARY ACTIVITY
	Electronic Systems Division Air Force Systems Command

13. ABSTRACT

This paper is a report on a continuing effort to develop a physical-numerical model suitable for use in predicting large-scale fields of low cloudiness.

The need to incorporate, within such a model, those physical processes which are characteristic of the atmospheric boundary layer has been noted in several recent studies. That the inclusion of such processes be effected without imposing a requirement for non-standard, observational data has been adopted as a restriction in the design of the prediction model. A further design specification is that the model will be used in conjunction with a fine-mesh, free-air prediction model. This specification relieves us from the need to consider the prediction of dynamical developments within the bulk of the atmosphere.

Included in this paper are a derivation of a basic prediction model and the results of a test series of 12-hr forecasts made with various versions of the model using synoptic data for the period: 12Z, 6 Feb.—00Z, 7 Feb. 1964. The tests were designed to assess the characteristics of the model and to indicate areas in which more study is required.

The model tested differs broadly from previous boundary layer models in its use of all three space dimensions, a horizontal space mesh of 150 km, and a time step of 15 min. The model incorporates the computation of: eddy fluxes of heat and vapor, the transport of heat, vapor, etc. by ageostrophic horizontal winds, the influence of terrain- and friction-induced vertical motion, and the heat and mass exchanges involved in water-substance phase changes.

DD FORM 1 JAN 64 1473

UNCLASSIFIED
Security Classification

14. KEY WORDS	LINK A		LINK B		LINK C	
	ROLE	WT	ROLE	WT	ROLE	WT
Low-cloud Forecasting Physical Cloud-prediction Model Synoptic-scale Boundary-Layer Model						

INSTRUCTIONS

1. ORIGINATING ACTIVITY: Enter the name and address of the contractor, subcontractor, grantee, Department of Defense activity or other organization *(corporate author)* issuing the report.

2*a*. REPORT SECURITY CLASSIFICATION: Enter the overall security classification of the report. Indicate whether "Restricted Data" is included. Marking is to be in accordance with appropriate security regulations.

2*b*. GROUP: Automatic downgrading is specified in DoD Directive 5200.10 and Armed Forces Industrial Manual. Enter the group number. Also, when applicable, show that optional markings have been used for Group 3 and Group 4 as authorized.

3. REPORT TITLE: Enter the complete report title in all capital letters. Titles in all cases should be unclassified. If a meaningful title cannot be selected without classification, show title classification in all capitals in parenthesis immediately following the title.

4. DESCRIPTIVE NOTES: If appropriate, enter the type of report, e.g., interim, progress, summary, annual, or final. Give the inclusive dates when a specific reporting period is covered.

5. AUTHOR(S): Enter the name(s) of author(s) as shown on or in the report. Enter last name, first name, middle initial. If military, show rank and branch of service. The name of the principal author is an absolute minimum requirement.

6. REPORT DATE: Enter the date of the report as day, month, year; or month, year. If more than one date appears on the report, use date of publication.

7*a*. TOTAL NUMBER OF PAGES: The total page count should follow normal pagination procedures, i.e., enter the number of pages containing information.

7*b*. NUMBER OF REFERENCES: Enter the total number of references cited in the report.

8*a*. CONTRACT OR GRANT NUMBER: If appropriate, enter the applicable number of the contract or grant under which the report was written.

8*b*, 8*c*, & 8*d*. PROJECT NUMBER: Enter the appropriate military department identification, such as project number, subproject number, system numbers, task number, etc.

9*a*. ORIGINATOR'S REPORT NUMBER(S): Enter the official report number by which the document will be identified and controlled by the originating activity. This number must be unique to this report.

9*b*. OTHER REPORT NUMBER(S): If the report has been assigned any other report numbers *(either by the originator or by the sponsor)*, also enter this number(s).

10. AVAILABILITY/LIMITATION NOTICES: Enter any limitations on further dissemination of the report, other than those imposed by security classification, using standard statements such as:

(1) "Qualified requesters may obtain copies of this report from DDC."

(2) "Foreign announcement and dissemination of this report by DDC is not authorized."

(3) "U. S. Government agencies may obtain copies of this report directly from DDC. Other qualified DDC users shall request through

_____."

(4) "U. S. military agencies may obtain copies of this report directly from DDC. Other qualified users shall request through

_____."

(5) "All distribution of this report is controlled. Qualified DDC users shall request through

_____."

If the report has been furnished to the Office of Technical Services, Department of Commerce, for sale to the public, indicate this fact and enter the price, if known.

11. SUPPLEMENTARY NOTES: Use for additional explanatory notes.

12. SPONSORING MILITARY ACTIVITY: Enter the name of the departmental project office or laboratory sponsoring *(paying for)* the research and development. Include address.

13. ABSTRACT: Enter an abstract giving a brief and factual summary of the document indicative of the report, even though it may also appear elsewhere in the body of the technical report. If additional space is required, a continuation sheet shall be attached.

It is highly desirable that the abstract of classified reports be unclassified. Each paragraph of the abstract shall end with an indication of the military security classification of the information in the paragraph, represented as *(TS)*, *(S)*, *(C)*, *or (U)*.

There is no limitation on the length of the abstract. However, the suggested length is from 150 to 225 words.

14. KEY WORDS: Key words are technically meaningful terms or short phrases that characterize a report and may be used as index entries for cataloging the report. Key words must be selected so that no security classification is required. Identifiers, such as equipment model designation, trade name, military project code name, geographic location, may be used as key words but will be followed by an indication of technical context. The assignment of links, roles, and weights is optional.